ADDIS ABABA UNIVERSITY

ADDIS ABABA INSTITUTE OF TECHNOLOGY

SCHOOL OF CIVIL AND ENVIRONMENTAL ENGINEERING

ANALYTICAL INVESTIGATION ON THE SEISMIC PERFORMANCE OF PARTIALLY PRESTRESSED CONCRETE BEAM-COLUMN JOINTS

A Thesis in Structural Engineering

By

Hilina Assega

GSR/7540/11

Advisor

Dr. Ing. Adil Zekaria

(May 2021)

Addis Ababa

A Thesis

Submitted to the School of Civil and Environmental Engineering in Partial Fulfillment of the Requirements for the Degree of Master of Science

The undersigned have examined the thesis entitled **'Analytical Investigation on the Seismic Performance of Partially Prestressed Concrete Beam-Column Joints'** presented by **HILINA ASSEGA**, a candidate for the degree of **Master of Science** and hereby certify that it is worthy of acceptance.

Dr. Ing. Adil Zekaria		
Advisor	Signature	Date
Professor Dr. Ing. Girma Zerayohannes		
Internal Examiner	Signature	Date
Dr. Esayas G/Yohannes		
External Examiner	Signature	Date
Dr. Mebruk Mohammed		
Chair person	Signature	Date

UNDERTAKING

I certify that research work titled "Analytical Investigation on the Seismic Performance of Partially Prestressed Concrete Beam-Column Joints" is my own work. The work has not been presented elsewhere for assessment. Where material has been used from other sources it has been properly acknowledged/referred.

Hilina Assega

ABSTRACT

Prestressed concrete concept was initially established to develop the performance of concrete members under flexure. But nowadays researchers are pointing out its satisfactory performance under seismic action. In this study, the seismic performance of partially prestressed concrete (PPC) exterior and interior beam-column joint (BCJ) is evaluated. Joint specimens are taken from a published experimental research program executed in Kyoto and Chiba University, Japan. Both joint types are subjected to a reverse cyclic loading at the beam ends and are designed to fail in shear at the joints. A 2D finite element software program, VecTor2, is used to validate the non-linear response of the joints. A total of three interior joint specimens and one exterior joint specimen with variable prestress have been validated. The software sufficiently captured the response of the PPC interior BCJs. While in the exterior BCJ, the software's capability in capturing the last cycle after peak response was questionable. Six PPC exterior BCJs with variable prestress levels and four PPC interior BCJs with variable column axial load ratio has been analyzed and assessed for further investigation of its performance. The hysteretic response of the PPC exterior BCJ specimens is evaluated based on the ultimate storey shear capacity, stiffness, ductility, strength degradation, energy absorption, and dissipation capacity. Furthermore, the premature failure, and pinching of the PPC interior BCJ specimens, subjected to high compressive stress from column axial load and prestressing force is studied. In the PPC exterior BCJs, Variation of prestressing force didn't encounter a significant effect on the ultimate shear capacity of the joints. Stiffness, and ductility increased significantly with prestressing force level before remarkable shear crack formation and prestress loss at the joint. Strength degradation was severe with the prestressing level. This phenomenon undermined the inelastic energy dissipation capacity of the highly prestressed joints at the later cycles. Since the software's capacity is questionable at the last loading cycles, further evaluation of results at this loading stages might be crucial to obtain a more reasonable value. The column axial load variation in the PPC interior BCJ resulted in a considerable effect on the pinching behavior. Premature failure due to concrete crushing at the joint was not observed in any of the specimens.

Keywords: Partially prestressed concrete, Beam-column joint, Prestress level, Column axial load ratio, VecTor2, hysteretic response, Storey shear capacity, Stiffness, Ductility, Strength degradation, Pinching, Energy absorption and dissipation capacity.

ACKNOWLEDGMENTS

First and foremost, I would like to thank God and his mother Mary for giving me the strength, patience, and wisdom to work on this thesis paper.

Next, I would like to give my deepest gratitude to Addis Ababa University (AAU) for awarding me a "Female Scholarship" to proceed my second degree. This wouldn't have been possible without this opportunity.

My next appreciation goes to my advisor, Dr. Ing. Adil Zekaria for always being there when I needed his support and for pushing me to do a better job. His advice was very constructive and motivational, which initiated me to not give up easily.

I would also like to give my deepest gratitude to Dr. Esayas G/Yohannes who responded to the questions I had while developing the thesis idea; Engineer Mohammed for giving me guidance regarding the finite element software and Engineer Naol Gebeyew for assisting me, and introducing me to people with similar expertise with my thesis. I sincerely would also like to thank Dr. Engr. Minehiro Nishiyama from Japan for his quick response whenever I had a question regarding one of the experimental studies that I validated on this paper.

Furthermore, I would also like to thank my family for being by my side until now; for supporting me in every decision I made, and for believing in me. Special thanks go to my father Assega Lemma, my mother Bayoush Ayalew, and my little sister Dagmawit Assega.

Last but not least I would like to expand my appreciation to all my friends for giving me insight, and always telling me that I got this. ☺

TABLE OF CONTENTS

LIST OF TABLES

LIST OF FIGURES

NOTATIONS

$\emptyset$	Diameter
γ_{xy}	Concrete shear strain
f_{cy}	Vertical concrete stress
f_{yp}	Prestressing steel yield stress
f_y	Reinforcement yield stress
f_c	Concrete compressive strength
f_u	Ultimate tensile stress of reinforcement
f_t	Split stress of concrete
f_{cd}	Design concrete compressive strength
ε_y	Yield strain
f_{cx}	Concrete stress in the x-direction
LS_i	Initial loading stage
LS_f	Final loading stage
V_{ED}	Storey shear force
d	Storey displacement
μ_Δ	Displacement ductility factor
Δ^+_{max}	Positive deformation at 75% of ultimate shear in the +ve loading direction
Δ^-_{max}	Negative deformation at 75% of ultimate shear in the -ve loading direction
Δ^+_y	Yield deformation in the +ve loading direction
Δ^-_y	Yield deformation in the –ve loading direction
K_i	Secant stiffness per cycle, i
$P_{max,i}$	Maximum storey shear capacity per cycle, i
$\Delta_{max,i}$	Maximum storey deformation per cycle, i
N_{ED}	Column axial load
A_c	Column cross-sectional area
σ_{pp}	Prestress in prestressing steel
ε_{pp}	Prestrain corresponding to σ_{pp}
E_c	Modulus of elasticity of concrete
E_p	Modulus of elasticity of prestressing steel
E_s	Modulus of elasticity of reinforcement
β	Confinement pressure factor

ρ_v	Transverse reinforcement ratio
ρ_x	In-plane transverse reinforcement ratio in the x-direction
ρ_y	In-plane transverse reinforcement ratio in the y-direction
ρ_z	Out-plane transverse reinforcement ratio in the z-direction
τ_r	Radial bond stress
τ_t	Tangential bond stress
Δ_r	Radial slip
Δ_t	Tangential slip
τ_s	Split bond stress
τ_p	Pull out bond stress
Δ_s	Split bond-slip
Δ_p	Pull out bond-slip

ABBREVIATIONS

MCFT	Modified compression field theory
DSFM	Disturbed stress field model
NSC	Normal strength concrete
R	Region
EN	Eurocode
FE	Finite element
BCJ	Beam-column joint
RC	Reinforced concrete
PPC	Partially prestressed concrete
ADE	Accumulated dissipated energy
PS	Prestressing steel
NZS	New Zealand Standard
CEB	Comité Euro-International du Béton
FIP	Fédération International de la Précontrainte
AIJ	Architectural Institute of Japan

CHAPTER 1 INTRODUCTION

1.1 Background of the study

Moment resisting frames of buildings are usually designed to provide the required seismic resistance for the building. These frames are often constructed by reinforced concrete elements or fully/partially prestressed concrete elements. Prestressing operation improves the performance of a concrete member under external load by resulting in a self-equilibrating system of internal stresses.

For many years, the use of prestressed concrete members has been accepted to be advantageous for structures under flexure since it counteracts externally applied gravity loads. However, after a while, their significance in primary seismic-resistant members such as frames and shear walls has created a substantial argument. R. W. G. Blakeley et al [1] reviewed the observation of prestressed concrete structures performance under actual earthquake which was reported by different countries. According to their report, most of the prestressed concrete members have encountered no or less damage. Especially, partially prestressed concrete elements (sections that incorporate both prestressing and mild steel) have exhibited satisfactory responses due to their good performance in preventing chronicle hazards that might occur as a result of moment reversal.

During an earthquake, mostly, drastic collapse of structures occurs due to failure at the beam-column joints. T. Paulay and M. J. N. Priestley [2] have stated that beam-column joints are very critical regions in reinforced concrete frames designed for inelastic response to seismic excitation. This is because they are located in an area, where shear and bond stresses are considerably high. They are subjected to both vertical and horizontal shear forces as a result of seismic reversal moments from columns and beams during an earthquake. During moment reversal, beam longitudinal reinforcements are required to be in compression on one side and tension on the other. These forces are sustained by the bond stresses between the concrete and reinforcement. Following excessive drift, bond failure and the corresponding degradation of moment capacity may occur. Since shear and bond mechanisms in beam-column joints exhibit poor hysteresis properties, their response is mostly restricted to an elastic domain.

According to T. Paulay and M. J. N. Priestley [2], the horizontal and vertical shear forces in the joint are resisted by diagonal compression strut mechanism and truss mechanism. The diagonal compression strut resistance mechanism is fully active before the stress transfer mechanism at the joint is demolished due to degradation in bond strength. After the formation of high bond stress, transverse reinforcements and small diagonal concrete compression field between cracks will be active in resisting shear. This mechanism is called truss mechanism. In the diagonal compression strut mechanism, beam and column longitudinal reinforcements transfer the adjacent moment to the joint in terms of compressive force. This compressive force is resisted by the equilibrium of concrete compressive strength and the bond strength between the reinforcement and concrete. Researches have shown that the performance of a diagonal compression strut mechanism can be improved by confining the joint. Usually, joint confinement is provided by adding more transverse reinforcements and/or column axial loads. As discussed in R. Park et al [3], provision of column axial load widens the diagonal strut region in the joint as a result of an enlarged compression block across the column region. Due to the formation of a wider diagonal compression strut, horizontal bond forces along the longitudinal beam bars can now be disposed of more easily. The demand for transverse reinforcements will then be reduced and their contribution is required only to enable bond forces to be introduced into the joint region outside the diagonal compressive strut region. Accordingly, the presence of prestressing subjects compressive stress inside the joint, which directly increases the confinement of the joint core.

Experimental investigations on partially prestressed concrete beam-column joints under static cyclic loading have been executed in different years of study. In M. Nishiyama's research [4], a PPC interior BCJ subjected to a reverse cyclic loading showed improved hysteretic performance than ordinary reinforced concrete joints. However, these joints were designed to fail in flexure with plastic hinge occurring at the beam-column interface thus the true shear behavior of the joint was not fully understood. T. Kashiwazaki and H. Noguchi [5] studied the effect of prestressing force level on PPC interior BCJs ultimate shear performance and no significant effect was obtained.

1.2 Problem Statement

Beam-column joints are the most critical part of a structural element in reinforced concrete frames under seismic excitation. The vertical and horizontal shear forces in a joint are sustained by diagonal compression strut mechanism and truss mechanism. In the diagonal compression strut mechanism, resistance is provided by an equilibrium of compressive strength and bond strength between longitudinal reinforcements and the surrounding concrete. Following high bond stress, the diagonal strut resistance mechanism deteriorates and results in significant degradation of strength and stiffness. Usually, to improve the performance of the strut mechanism confinement is provided in the joints through column axial load and/or transverse reinforcements. Adequate confinement of joints considerably improves bond performance by widening the diagonal strut region in the joint. This significantly reduces high bond stress in the joint region. In this study, the effect of introducing confinement in the joint in terms of prestressing force is studied and the hysteretic behavior of joint specimens with variable prestress level is evaluated. Concrete crushing in the joint core that might occur due to high confinement stress, obtained from column axial load and prestressing force must also be considered as a potential cause of failure and is covered in this study.

1.3 Objective of the study

General objective

- To evaluate the hysteretic performance of a PPC exterior BCJ with variable prestressing force level and to study premature failure of a PPC interior BCJ that might occur due to high confinement stress, obtained from column axial load and prestressing force.

Specific Objective

- To perform a 2D non-linear analysis of a PPC exterior and interior BCJs subjected to repeated reverse cyclic loading.
- To study the hysteretic response of a PPC exterior BCJ with variable prestressing force in terms of ultimate shear capacity, stiffness, ductility, strength degradation, energy absorption, and dissipation capacity.

- To study the combined stress distribution effect due to column axial load and prestressing force in a PPC interior BCJ to prevent premature failure of a joint.
- To investigate the performance of a PPC interior BCJ with variable column axial load in terms of ultimate shear capacity and pinching.

1.4 Scope of the study

- Due to the limitations of laboratory test equipment a 2D non-linear finite element analysis is performed.
- Only reversed cyclic loading analysis is carried out.
- The conclusions made in PPC exterior BCJs might not work for PPC interior BCJs and vice versa. Since resistance in the interior joint is provided by the two adjacent beams while an exterior joint resistance is provided at one side only.
- Only Post-tensioned concrete joints are evaluated in this study, thus the constructed conclusions might not represent Pre-tensioned concrete joints.
- Effect of variations in joint size; prestressing steel arrangement and location; fully prestressed beam-column joint and other detailing variations inside the joint is not considered in this paper.
- The effect of column axial load on the PPC exterior BCJ could not be evaluated due to flexural failure of the specimen as the axial load is increased.
- The contribution of the floor slab to the joint hysteretic response is not considered.
- The design of the PPC BCJ specimens is not covered in this paper since their design information is obtained from the experimental program made at Chiba and Kyoto University, Japan.

1.5 Methodology

Due to the lack of laboratory test equipment, a 2D non-linear analysis is carried out in the PPC interior and exterior BCJs using a finite element program called VecTor2. All data including reinforcement, prestressing steel, and concrete material definitions; cross-sectional dimension and size of the members; laterally applied displacement history curve; test setup and boundary conditions are taken from previously done experimental programs by T. Kashiwazaki et al [5] and M. Nishiyama et al [6]. Preferable models for reinforcement, prestressing steel, and concrete are selected and used in the finite element

program based on the provided information. Since bond stress-slip information was not provided by the author, the bond property between the reinforcement/prestressing steel, and the surrounding concrete is assumed while modeling the PPC exterior BCJ. A perfect bond is assumed while modeling the PPC interior BCJs due to high yield strength and closely spaced transverse reinforcements in the joint region. A prestressing force level of 0, $0.25f_{yp}$, $0.4f_{yp}$, $0.59f_{yp}$, $0.7f_{yp}$ and $0.8f_{yp}$ was applied in the PPC exterior BCJs to study the effect of prestressing force in the hysteretic behavior. A column axial load ratio ($\frac{N_{ED}}{A_C * f_{cd}}$) of 0, 0.1, 0.4, and 0.65 were applied on a highly prestressed ($0.8f_{yp}$) PPC interior BCJs to study its effect on crushing of concrete and pinching behavior. The storey shear force-storey displacement hysteretic response is studied to evaluate the joint performance. The hysteretic response curve, the ultimate shear capacity, crack information, reinforcement, prestressing steel, and concrete stress variation are determined from the finite element software model output (Augustus). Stiffness is calculated according to the method used in S. Eshghi and V. Zanjanizadeh study [7]. Ductility is computed according to the equation stated under A. S. Elnashai and L. Di Sarno's book [8]. Energy absorption and dissipation capacity are estimated based on the approach given under A. Sayed and A. Tawfik [9].

1.6 Organization of the study

This study consists of 6 chapters. The first chapter is the introduction part which discusses the background, the statement of the problem, the objective, scope, methodology, and organization of the thesis. Literature reviews around the areas of prestressed concrete structures and PPC BCJs shear demand and resistance mechanisms are discussed in detail in chapter 2. PPC BCJ performance under repeated loading along with previously done researches is also elaborated in this chapter. The third chapter reviews the material property, sectional detailing, test setup, and boundary conditions of the PPC exterior and interior BCJ specimens. Finite element modeling and validation of the finite element software (VecTor2) is discussed in chapter four. All the employed models for the reinforcement, prestressing steel, concrete, and bond are discussed in this chapter. The parametric analysis, analytical result, and discussion are presented in chapter five. Finally, the conclusion made in this thesis paper is organized and presented under chapter six along

with the recommendations for further study around the seismic performance of prestressed concrete.

1.7 Significance of the study

- This study contributes significant knowledge in understanding the hysteretic performance of Partially Prestressed Beam-Column Joints when subjected to different levels of prestressing force and column axial load.
- The outcome of this research will also provide practicing engineers with what to consider while using Partially Prestressed Concrete members as primary-seismic resistant elements.

CHAPTER 2 LITERATURE REVIEW

2.1 Earthquake response and hysteretic behavior of concrete structures

The term seismic response usually creates an image of a force-displacement relationship. But in a deeper understanding level, it is expressed in terms of energy. The net work done on a structure by ground motions at the time of earthquake is the seismic energy absorbed by the system and can be represented with Equation (2.1). The equation expresses the seismic energy absorbed by structures as the integral of the base shear multiplied by the ground velocity with a time interval from the beginning of ground shaking to the end. During earthquake excitation, the ground displaces under a flexible structure and induces base shear on the first-story columns. As the motion proceeds, the induced base shear and the ground velocity integrate and energy will flow into the structure when their sign agrees and flows out when it disagrees. (D. P. Clough [10])

$$W(t_1) = \int_0^{t_1} V(t)\dot{x}(t)dt \qquad \textbf{(2.1)}$$

Where $W(t_1)$ is work done, $V(t)$ is Base shear (Force), $\dot{x}(t)$ is ground velocity, dt is time and $(\dot{x}(t)dt)$ is displacement.

During energy transformation to the structure following the lateral action, some of the energy is dissipated in the concrete whilst the rest is stored as strain energy which can be recovered when the structure is completely unloaded. Energy can be dissipated either through structural damage or without involving damage. Energy dissipation mechanisms that do not involve structural damage are deformation within the elastic range, wracking of partitions, micro cracking of reinforced concretes, working of joints, and inelastic behavior of the soil/foundation interface. When the building response surpasses the elastic limit the non-linear behaviors of force-displacement relationships will be initiated and energy will be dissipated through deformation of an inelastic member, either in flexural-tension cracking or material nonlinearity and some by yielding of the steel reinforcement. This can be achieved only if a ductile response is possible in the system. However, if the

structure is brittle collapse is imminent after maximum strength is achieved. These concepts are summarized in Figure 2.1. (D. P. Clough [10])

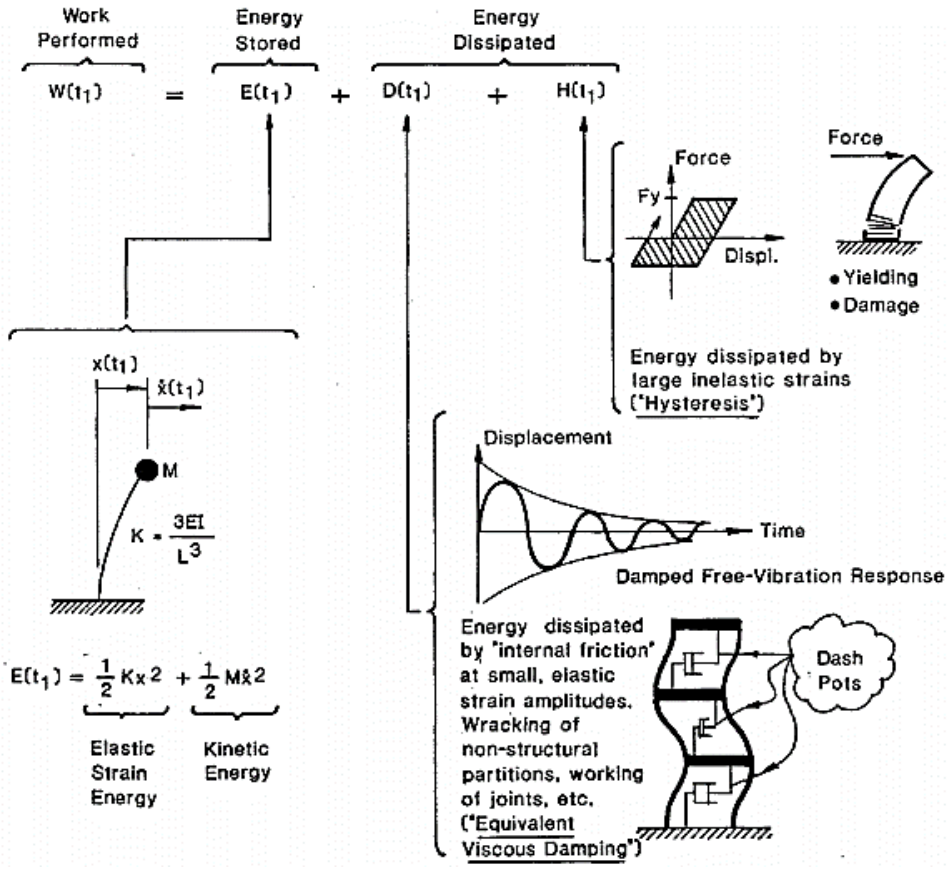

Figure 2.1 Earthquake energy balance in a structure [10]

Numerous hysteretic models are developed to simulate the response behavior of structures, that are subjected to seismic action. These models started from simple elasto-plastic models and developed into complex models. Simple elasto-plastic models do not take into account strength and stiffness degradation when subjected to cyclic loading, unlike the complex ones. When subjected to cyclic loading, reinforced concrete structures exhibit strength and stiffness degradation depending on the loading history and characteristics of the structure. Concrete cracking and loss of bond between the reinforcement and concrete are the main reasons for reinforced concrete structures to degrade in stiffness. Furthermore, in reinforced concrete structures subjected to reverse cyclic loading a large reduction in loading stiffness after unloading might occur. Such type of hysteretic phenomenon is called pinching. This behavior is experienced due to the opening of cracks during loading in one direction but as the loading reverses its direction the crack starts to close and partial

stiffness recovery will be achieved. Depending on the material property, level of ductile detailing, geometry, and connection type the level of pinching will differ. Structural components may also experience strength degradation when subjected to lateral reversed cyclic loading. Strength degradation or deterioration is a reduction in lateral strength due to either increasing inelastic displacement or repeated cyclic displacement located at the same level. (FEMA [11])

2.2 Prestressed concrete

According to ACI Committee, Prestressed concretes are concretes by which internal stress is introduced to it initially, which counteracts the given external loading to the desired degree. The prestressing action neutralizes the tensile strains and stresses caused by the external loads. This phenomenon minimizes or eliminates cracking of a section leading full concrete section to become active in resisting the load. In the case of reinforced concrete members, only the uncracked part of the section in the compression region participates in resisting the load, thus prestressed concretes are much more effective than non-prestressed concretes.

As an example, a simply supported beam made from an elastic material that is equally strong in tension and compression is shown in Figure 2.2. The stress distribution over the depth of the beam section and deflected shape of the beam, resulted from the uniformly distributed load, w, are shown in Figure 2.2 (a). The response is counteracted by applying an eccentric compression force P (prestressing force) to each end of the beam as shown in Figure 2.2 (b) along with the resultant stress distribution and deflected shape of the beam. The combined application of the prestressing force and distributed load, w, is shown in Figure 2.2 (c), which is obtained by superposition response of the load (Figure 2.2 (a)) and prestressing force, P, (Figure 2.2 (b)). As shown in the figure, both the compressive and tensile strains at the top and bottom reinforcements of the section are reduced and further the deflection of the member is minimized to a great extent. Furthermore, the shear capacity of members can also be enhanced by introducing a curved prestressing tendon. The inclined force induced by the prestressing force closes the inclined crack formed by shear stresses, therefore reducing the principal tension. Thus, in the presence of prestressing force, the length and crack width of both vertical and diagonal cracks are low. Thus, the aggregate interlock and zone of concrete under compression are larger as

compared to a non-prestressed beam under the same load. (J. M. Robberts and V. Marshall [12])

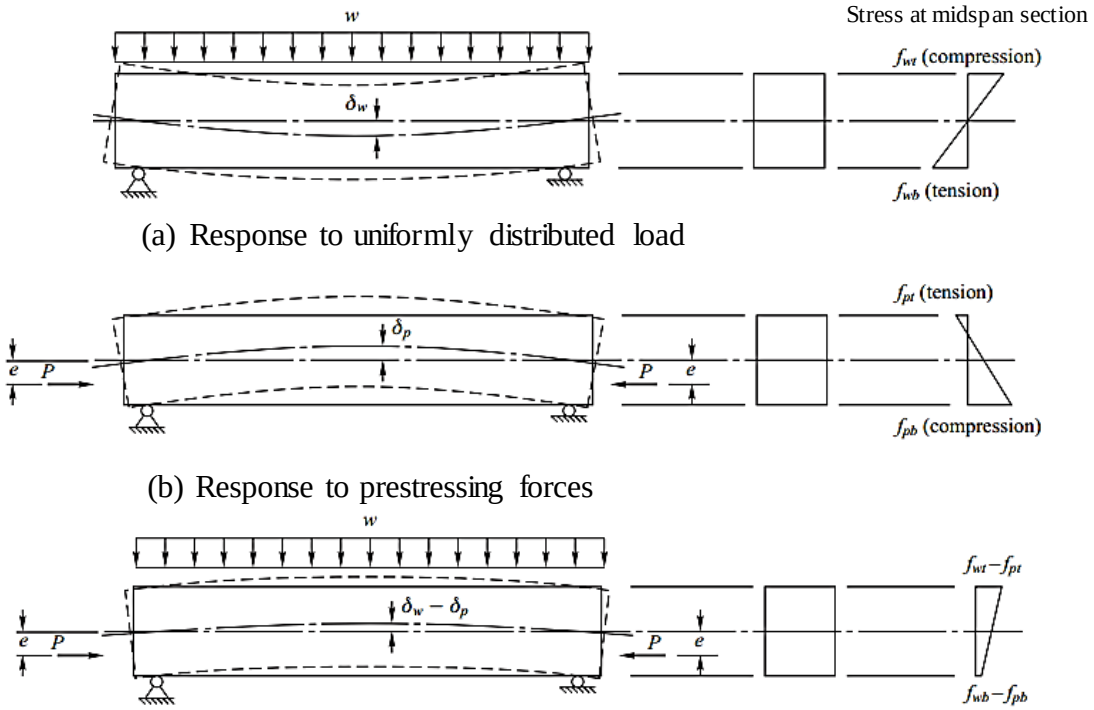

Figure 2.2 Effect of prestressing force [12]

Compared to reinforced concrete members, prestressed concrete member's compressive strength capacity is likely to be higher, and less permanent damage is expected since cracks are more likely to be closed again. (K. E. Williamson [13])

The steel used in prestressing has a strength that is approximately six times that of conventional reinforcing steel and it doesn't retain a well-defined yield point as the mild steel. Special bond and anchorage requirements are needed around joint regions, where complex stress patterns occur. (J. M. Robberts and V. Marshall [12])

2.2.1 Partially prestressed concrete members under earthquake

Prestressed concrete members are referred to as partially prestressed if the formation of flexural tensile cracks is allowed to occur at service load levels. Thus, a partially prestressed section incorporates both prestressed and non-prestressed (mild) steels, by which both contribute to the serviceability and ultimate strength of the member. While in

fully prestressed members, tension is not allowed to occur at service load levels, thus only prestressed steels are used in this section. (J. M. Robberts and V. Marshall [12])

The main advantage of using partially prestressed concrete members over fully prestressed ones, in earthquake-prone areas, is to prevent hazard which might occur due to reversal of moments. The carrying capacity of earthquake forces in structures is closely related to the location of the resultant compressive stress, C, before an earthquake. The resultant stress balances the moment before the earthquake. This stress, C, can be far from the neutral axis in two cases. The first case is when some of the dead loads and all of the live loads are not applied in the structural system (where C is at the lowest specified point as shown in Figure 2.3(a)). In this case, at the time of earthquake excitation, the positive moments produce no risk but the negative moments (when the direction of the seismic and prestressing moment is clockwise) may cause undesirable tensile stress. The second case is when all the design loads are applied (where C is at the highest specified point as shown in Figure 2.3(c)). In this case, the situation is the reverse and occurs when the direction of the seismic and prestressing moment is counterclockwise. Accordingly, these undesirable tensile stresses can be carried by reinforcing the top and bottom of the section. Thus, any reversal of moments, due to earthquake, cause no hazard in partially prestressed sections compared with fully prestressed ones. Since a fully prestressed section is designed for a certain value of the moment in a certain direction of the load, in the above-stated cases the section is prone to premature failure. (E. Arioglu [14])

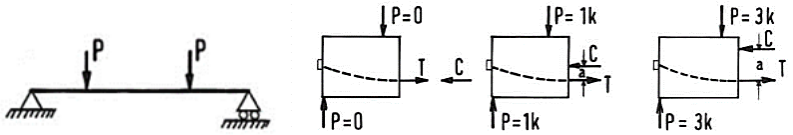

Figure 2.3 Variation of resultant compressive stress with increasing applied load in prestressed concrete [14]

2.2.2 Post-tensioned concrete

In concrete prestressing practice, different prestressing systems may be used to apply the required prestress. The high-strength prestressing steels are mostly tensioned by using hydraulic jacks. If tension is induced before concrete is cast it is called a pre-tensioned system. If it is induced after casting the concrete it is called a post-tensioned system. (R. Ian Gilbert [15])

Figure 2.4 shows the steps for post-tensioning a concrete element. First, the concrete is cast with the hollow duct inside which can be fixed to any desired profile as shown in Figure 2.4 (a). The hollow duct contains the prestressing steel which is unstressed at the time of concrete pouring. After the poured concrete regains its compressive strength, the prestressing steels will then be tensioned. The prestressing steel can be stressed from both sides of the member or one side by anchoring the other end of the member as shown in Figure 2.4 (b). After the prestressing operation, the prestressing steels are then anchored at each stressing end as shown in Figure 2.4 (c). During the stressing operation, the concrete is compressed and the applied prestress is maintained by the end anchorage plates bearing onto the concrete. Furthermore, whenever the direction of the prestressing steel changes, it can also induce a transverse force on the member. (R. Ian Gilbert [15])

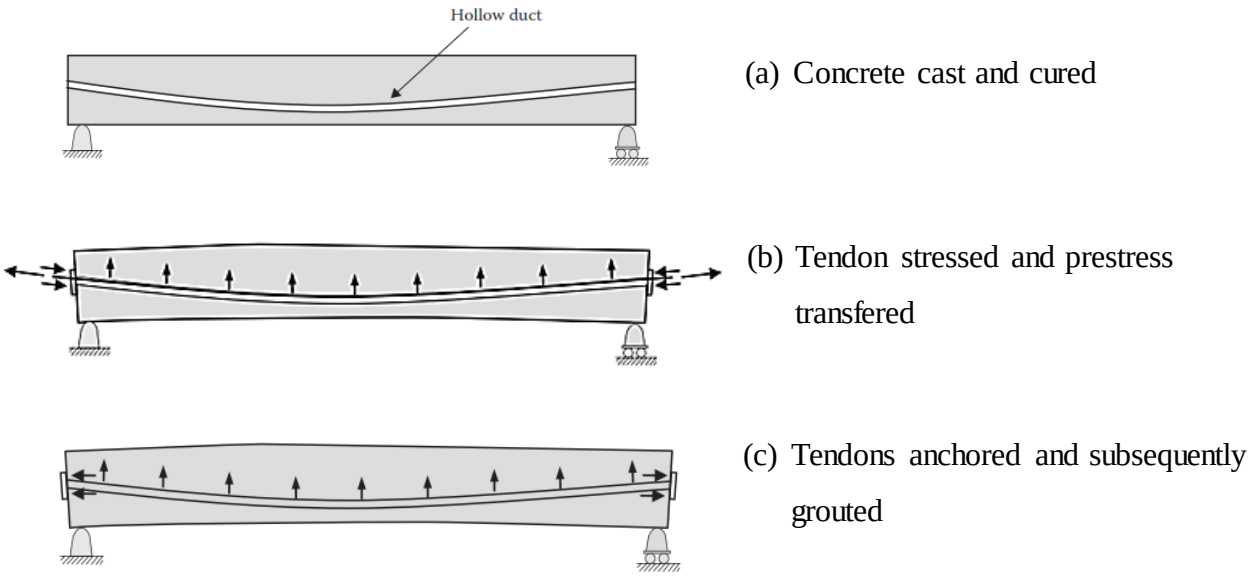

Figure 2.4 Post-tensioning procedure [15]

After the prestressing steels are anchored, the hollow ducts will then be filled with concrete grout under pressure to activate the bond between the steel and the surrounding concrete. Bonded tendons are more efficient in providing ultimate strength and controlling cracks and are less exposed to corrosion problems. However, in some situations, like for reasons of economy, tendons remain un-grouted. Thus to prevent corrosion of these unbonded tendons, they are mostly coated with corrosion-inhibiting grease and encased in a plastic sleeve. Unbonded tendons contribute to the ultimate capacity of a member about 75% of that provided by bonded tendons. Accordingly, in bonded tendons, prestress is transferred to the concrete with the help of the bearing plate and the bond between the tendon and

surrounding concrete. While in unbonded tendons, the tensioning force is transferred to the concrete with the help of end anchorages only. (R. Ian Gilbert [15])

2.2.2.1 *Transmission of prestress in post-tensioned members*

Unlike in pre-tensioned members without anchorage, the stress in the tendon of a post-tensioned member attains the prestress right at the anchorage block because the strands are anchored by the wedge. Thus, the stress at the end is not zero rather it's equal to the applied prestress. Thus, there is no requirement of transmission length or development length in a post-tensioned member.

The bearing plate subjects high stress at the end zone of a post-tensioned member. The complex stress field trajectory at the end zone of a post-tensioned member is shown in Figure 2.5. Initially, the prestress is transferred to the concrete by the bearing plate within the dimensions of the plate (y_{po}) as shown in the figure. These concentrated compressive stresses are not parallel around the bearing region. As the compressive stress trajectories diverge from the end region they expand and become parallel over a certain length of the member as labeled in Figure 2.5. Where y_o is the distance over which the compressive trajectories become parallel and beyond this the stress distribution is uniform. Furthermore, since stress trajectories are not parallel in the bearing region, tensile stress will also be generated within the end zone. The tensile stress trajectories are also shown in Figure 2.5 by which the lines are bent at the end zone and they become parallel as we move away from it. The tensile stress will cause a diagonal cracking at the anchorage zone. Thus additional transverse reinforcement is usually provided at the anchorage zone of a post-tensioned member.

2.2.3 Tendon profiles

The tendon profile used is selected primarily to maximize the beneficial effect of prestress. Some of the more common tendon profiles are straight tendons, trapezoidal tendons, parabolic tendons, and sloping tendons. To sense the possible arrangements of tendons in a beam-column joint frame, Figure 2.6 shows tendon profiles used in precast prestressed beam-column joints. (L. Luoman [16])

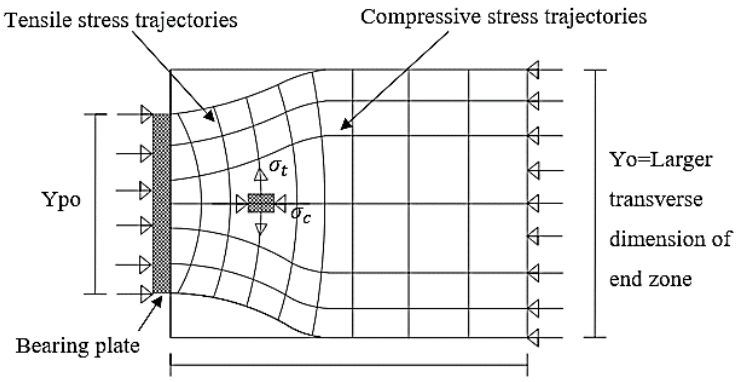

Figure 2.5 Stress trajectories in the end zone of a post-tensioned member

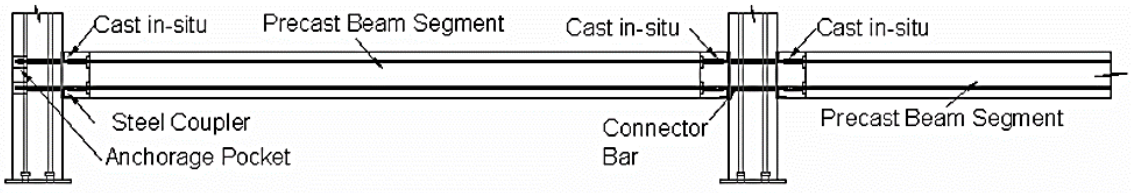

(a) Straight tendons

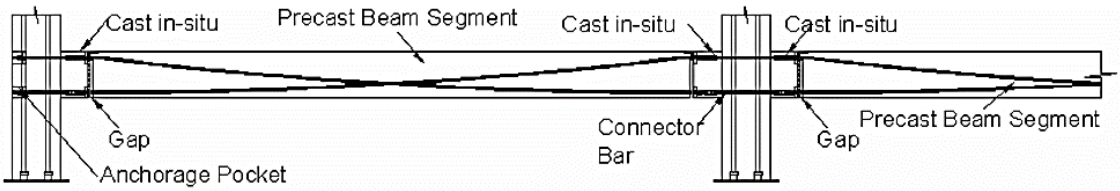

(b) Draped tendons

Figure 2.6 Tendon profiles used in precast prestressed concrete beam-column joints [16]

2.2.4 Prestress loss

At the time of prestress transfer to the concrete, there is a drop of prestressing force from the initially recorded value at the time of jacking. This reduction of prestressing force is called prestress loss. These losses are categorized into immediate and time-dependent losses. Immediate loss is the loss that occurred immediately after the transfer of prestressing force to the concrete. It can be found by taking the difference between the prestressing force applied at the jack and the transferred force. These losses are mostly caused due to slip at the anchorage, elastic deformation of the concrete during prestress transfer, friction along the draped tendon, relaxation of the tendons before transfer, and

deformation in the joints of a precast member assembled in sections. Loss of prestressing that takes place gradually with time is called time-dependent loss. They are mostly caused by gradual shortening of the concrete at the steel level due to relaxation of steel over time, creep, and shrinkage. (R. I. Gilbert and N. C. Mickleborough [17])

According to NZS3101, 1 and 2:1995 (New Zealand Standard) [18] Section 16.3.4, Maximum stress in prestressing tendons shall not exceed the following:

- $0.94f_{py}$: due to jacking force, which represents the prestressing force that is used at the field to stress a tendon including prestress losses
- $0.82f_{py}$: immediately after prestress transfer

2.3 Beam-Column Joint

2.3.1 General

In moment-resisting frame structures that are designed to respond in a ductile manner under severe seismic excitation, beam-column joints need to acquire sufficient strength to maintain and develop the flexural capacity of beams. To satisfy this requirement, it is essential to acquire information on the ultimate behavior and response of the beam-column joints under seismic action. Structural joints are the most critical part of moment-resisting frames due to the high-stress field that develops in their limited volume from the seismic action transferred from the adjacent members. Thus, they must be sufficient to sustain the following stresses in their core. (G. George and G. Gregory [19])

- High shear stresses acting vertically and horizontally due to the internal forces transferred from the adjacent members (beam and column) as shown in Figure 2.7 (a). (T. Paulay and M. J. N. Priestley [2])
- High bond stresses acting at the interface of longitudinal steel bars and concrete at the joint due to beam bending as shown in Figure 2.7 (b). (G. George and G. Gregory [19])

The joint shear forces will cause diagonal tension and compression stresses inside the joint which will result in diagonal cracking of the concrete core. According to J. K. Wight and J. G. MacGregor [20], internal forces due to lateral loads and their respective cracks on

exterior and interior joints are idealized as shown in Figure 2.8 and Figure 2.9. Diagonal cracks develop perpendicular to the tensile force.

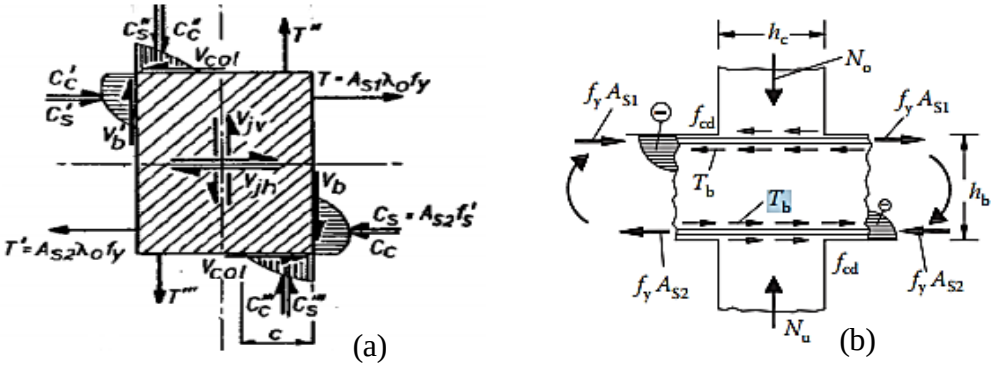

Figure 2.7 Joint shear forces and internal stresses that must be sustained by BCJs [2], [19]

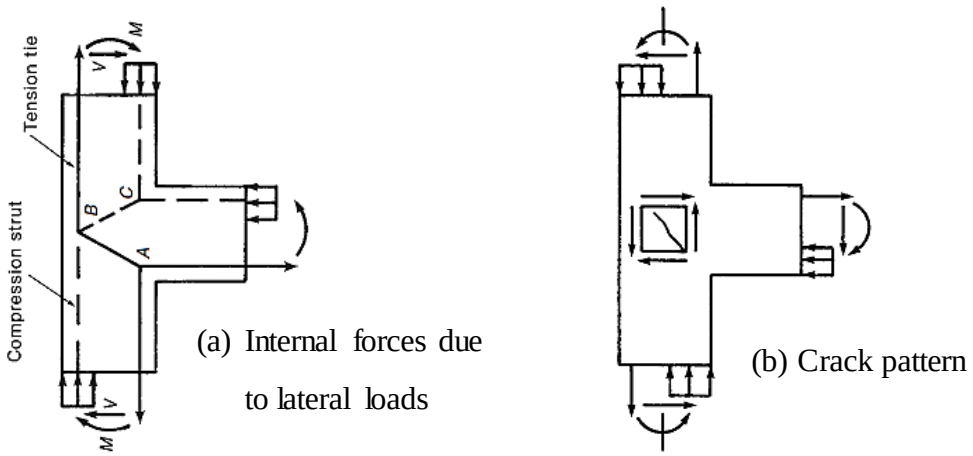

Figure 2.8 Exterior Beam-Column joint internal forces and Crack pattern [20]

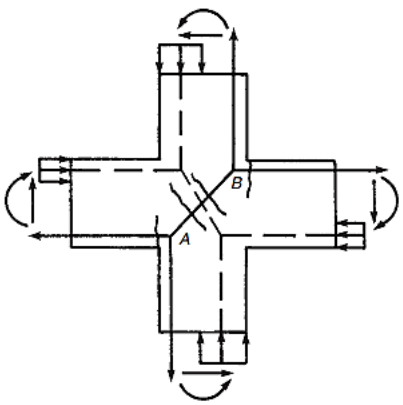

Figure 2.9 Interior Beam-Column joint internal forces and Crack pattern [20]

2.3.2 Beam-Column Joint shear strength

The internal forces transferred from the adjacent member's result in horizontal and vertical shear force, resulting in diagonal tension and compression stresses in the joint core. Figure 2.10 (a) shows the potential failure plane of a joint. The horizontal and vertical shear forces are resisted by two mechanisms. A diagonal compression strut mechanism is generated in the concrete as shown in Figure 2.10 (b) and the truss mechanism is comprised of the horizontal and vertical stirrup in the beam and column as shown in Figure 2.10 (c). At the initial stages of reversal loading, compressive forces are carried by the equilibrium of concrete compressive strength and the bond strength between the reinforcement and concrete. Following the progress of loading, successive degradation in the strength of the compressive strut results. This is due to the immediate change of direction of the diagonal crack at approximately 90^0 following load reversals. Since the complete closing of cracks is not achievable, the bond condition of longitudinal bars is affected. Beam reinforcement is required to be in tension on one side of the joint and in compression on the other side due to the moment reversal. Bond stresses are used to transmit longitudinal reinforcement forces to the concrete. Thus, high bond stress is essential to sustain these forces. High bond stress may cause disintegration of the bond and destruction of the stress transfer mechanism. At this point, the truss mechanism will come to action to resist shear. Web reinforcements apply a passive pressure at the joint, provided that it remains in the elastic range, and diagonal cracks will be closed. As transverse reinforcements start to yield significant shear deformation and reduction of shear strength will result. Consequently, the corresponding hysteretic response of the member will be exposed to a marked reduction of energy dissipation. The pinching effect will also be very significant following this. Thus, prevention of yielding of transverse reinforcements during progressive development of collapse mechanism is very important to have a ductile response. (T. Paulay and M. J. N. Priestley [2])

Both mechanisms rely on the core concrete strength. Thus, the ultimate strength of the joint is controlled by the ultimate concrete strength of the joint core under compression or tension and is diminished by gradual crushing of concrete along with the cross diagonal cracks. (G. George and G. Gregory [19])

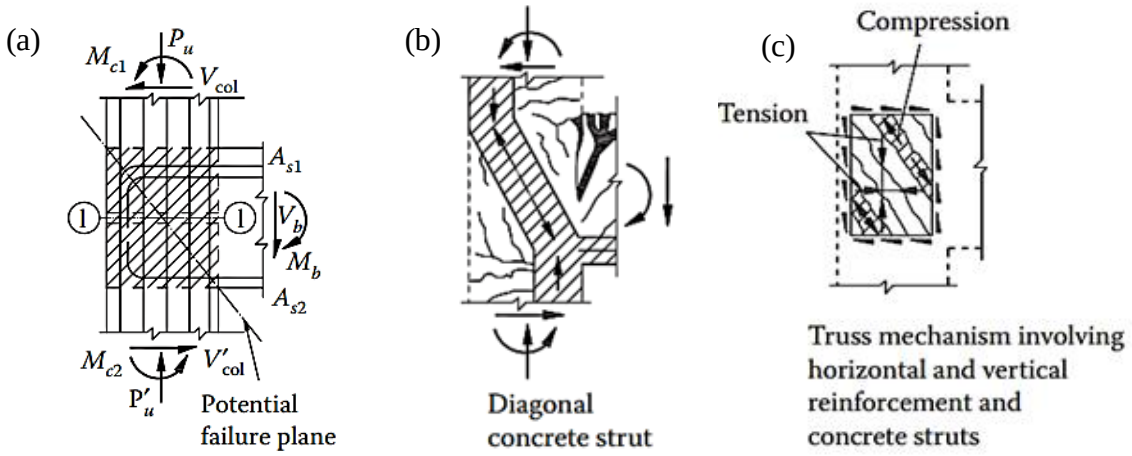

Figure 2.10 Joint shear resistant mechanisms [2]

In partially prestressed concrete members the total resisting moment is comprised of one component from the prestressing steel and another from the deformed longitudinal reinforcement. The fraction of the total resistance supplied by each component might affect the response. For a given total strength, a higher proportion of deformed reinforcement will lead to more damping and lower peak drift but may lead to larger residual drift, and vice versa. (J. F. Stanton and S. D. Nakaki [21])

2.3.3 Joint shear demand of partially prestressed concrete joints

Moment resisting prestressed concrete frames may have beams and columns fully prestressed; beams prestressed, columns normally reinforced and beams partially prestressed, columns normally reinforced. Forces acting on a joint of the unbonded post-tensioned concrete joint with conventional reinforcement corresponding to a design interface rotation of θ_{des} are shown in Figure 2.11. (J. F. Stanton and S. D. Nakaki [21])

Forces in the exterior and interior joints are different, due to the magnitude of loading on the joint and the resistance mechanism within the joint. A typical partially prestressed concrete interior joint is shown in Figure 2.12. Equilibrium of the partially prestressed concrete interior joint requires a joint shear force of:

$$V_{joint} = -F_{c,des} - F'_{s,des} - F_{s,des} + V_{col,des} = -F_{p,des} - 2F_{s,des} + V_{col,des} \quad \textbf{(2.2)}$$

Note that $F_{c,des} = F_{p,des}$ since the prestressing force exert compressive stress in the concrete.

Where $F'_{s,des}$ is the force in compression reinforcing steel at design limit state; $F_{c,des}$ is the force in beam concrete at the beam-column interface at design limit state; $F_{p,des}$ is the force in prestressing tendon at design limit state; $F_{s,des}$ is the force in tension deformed reinforcement at design limit design and $V_{col,des}$ is Column shear force at design limit state.

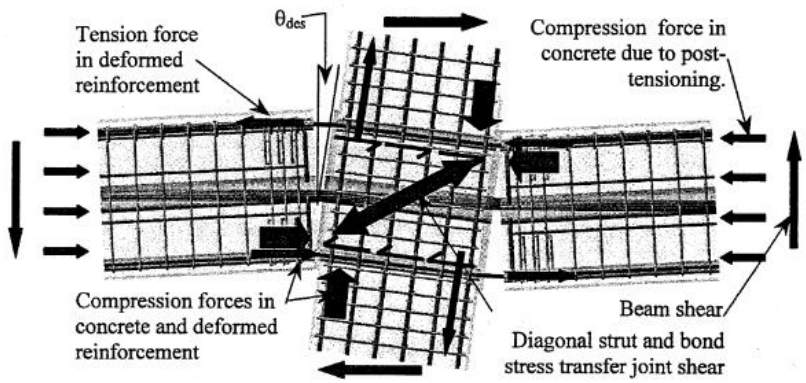

Figure 2.11 Unbonded post-tensioned joint forces at design drift [21]

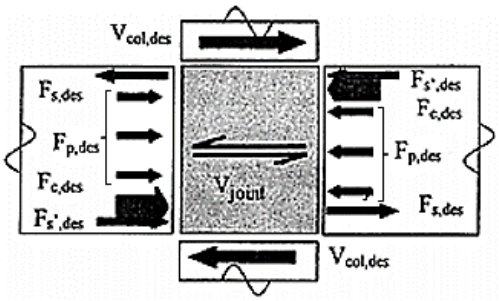

Figure 2.12 Partially prestressed concrete interior joint horizontal shear forces [21]

The joint shear force is the horizontal force anywhere within the joint region between the top and bottom longitudinal reinforcement as shown in Figure 2.12. The critical plane (maximum joint shear stress) occurs at the joint region where the net joint width is the narrowest, which can be calculated by reducing the width of the post-tensioning duct from the gross joint width. If several ducts are used, the summation of each duct area must be minimized. (J. F. Stanton and S. D. Nakaki [21])

A typical partially prestressed concrete exterior joint is also shown in Figure 2.13. Equilibrium of the partially prestressed concrete exterior joint requires a joint shear force of:

$$V_{joint} = -F_{c,des} - F'_{s,des} + V_{col,des} = -F_{p,des} - F_{s,des} + V_{col,des} \quad \textbf{(2.3)}$$

For a partially prestressed concrete exterior joint, the maximum joint shear force occurs between the prestressing anchorage and compression face of the beam, as shown in Figure 2.13. Since the critical plane does not cross the section that contains the prestressing duct, the strand diameter does not need to be deducted from the joint width to obtain the maximum joint shear stress. (J. F. Stanton and S. D. Nakaki [21])

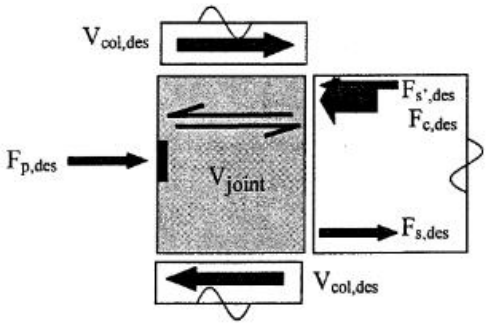

Figure 2.13 Partially prestressed concrete exterior joint horizontal shear forces [21]

2.3.4 Seismic design requirements of prestressed concrete joints

According to AIJ standard, partially prestressed concrete beam-column joints are designed under guidelines for the design of conventional reinforced concrete joints except that additional transverse reinforcements are provided at the joint region to resist the tensile bursting stress induced from the prestressing steel. Among the current design codes, NZS3101, 1 and 2:1995 (New Zealand Standard) [18] specifies the seismic design requirements of prestressed concrete beam-column joint cores. Some of these requirements under section 16.4.5 are as follows:

- The prestressing steels, located at the bottom or top of the beam section, passing through joint cores shall be centered at not more than 150mm from the beam top or bottom.

- For a partially prestressed concrete beam in which the conventional reinforcement sustains at least 80% of the design earthquake moment and gravity load combinations, prestress may be provided by one or more prestressing steels passing through the joint region and located within the middle third of the beam depth. If proper detailing is provided to prevent anchorage failure in the system, ungrouted post-tensioned tendons may be used in such cases.
- Grouted ducts in post-tensioned tendons shall provide good bond characteristics and shall be corrugated sufficiently.
- Joint reinforcement design in partially prestressed concrete shall be compatible with a reinforced concrete beam-column joints.
- Post-tensioning anchors shall only be located inside exterior beam-column joint cores providing that the joint can resist both the diagonal tension from beam and column forces and the anchorage tensile bursting stresses.

To ensure adequate ductility and earthquake performance of prestressed concrete structures, the following provisions need to be considered carefully. (G. H. Powell [22])

- Longitudinal and transverse reinforcement content and longitudinal reinforcement distribution.
- Adequate lapping of prestressing steels or reinforcing bars need to be provided to ensure continuity.
- Anchorages should be positioned carefully to avoid stress raising and congestion in highly stressed zones of post-tensioned systems. They should be positioned as far from possible plastic hinge locations as possible.
- Using unbonded tendons is possible in primary earthquake-resistant members if a sufficient amount of bonded steel is also present in the section. Furthermore, adequate detailing of anchorages for better performance under cyclic loading should be provided and appropriate crack control measures should be taken.

2.4 Seismic Performance evaluation of prestressed concrete members

R. W. G. Blakeley et al [1] reviewed the observation of prestressed concrete structures performance under an actual earthquake in different countries. In Skopje 1963 earthquake, among several prestressed concrete structure buildings, only one faced structural damage.

In Alaska 1964 earthquake, among 28 precast prestressed concrete structures, only 5 of them suffered a partial or total collapse. In Caracas 1968 earthquake, no significant damage was reported among the prestressed concrete structures. These actual seismic performances of prestressed concrete structures led researchers to study more on their response under seismic action and a variety of studies has been made.

In M. Nishiyama's [4] research comparison between ordinary reinforced concrete exterior joint and partially prestressed concrete interior joint with a prestress of $0.5f_{yp}$ was made. The performance of the joints was studied under reversed cyclic loading. The partially prestressed concrete beam-column joints showed better seismic performance than similarly dimensioned reinforced concrete joints. Negligible strength degradation after peak response with wider pinching was observed in the load-deflection Hysteretic loop of the prestressed sections. The applied prestressing force kept the joint from failing in shear and improved the energy absorption capacity. However, these joints were designed to fail in flexure with plastic hinge occurring at the beam-column interface thus the true shear behavior of the joint was not fully understood.

T. Kashiwazaki and H. Noguchi [5] carried out a reverse cyclic loading test on three partially prestressed grouted interior beam-column joints to study the effect of prestressing force level on the joint ultimate shear capacity. These specimens were stressed with a prestress of 0, 0.25fyp, and 0.5fyp. Furthermore, a FE analysis was carried out for an additional three joint specimens with a prestress of 0.6fyp, 0.7fyp, and 0.8fyp. Based on this experimental and analytical program, the authors concluded that the shear capacity of the joint was not significantly affected by the prestressing forces.

Based on A. E. Naaman and J. K. Wight [23] study, an experimental program of partially prestressed concrete beams subjected to monotonic loading was demonstrated to study the effect of level of prestress ($0 - 0.6f_{yp}$) on flexural ductility of the section. It was observed that the increase in the level of prestressing leads to a substantial increase in the yield curvature, which in turn increased the curvature ductility of the section.

M. Nishiyama et al [6] conducted reverse cyclic load tests on seven precast, prestressed concrete exterior beam-column joints and studied the effect of prestressed tendon anchorage location on the ultimate shear capacity of the joint. An average of 0.6fyp

prestress was applied in all specimens. Based on the experimental results, the researchers concluded that joint shear capacity was higher for test units with anchorage outside the face of the joint than in test units with inside anchorage.

In addition to the above experiments on prestressed joints, it is important to consider the effect of high condiment stress coming from prestressing steel and column axial load, which might be a cause for premature failure of prestressed joints. As far as the Authors knowledge is concerned, researches that address this issue have not been executed until now. Rather, premature failure of joints due to high confinement stress from column axial load on a reinforced concrete joint was studied by different researchers. A. A. Mohammed et al [24] studied the effect of column axial load variation on the seismic performance of exterior beam-column joints. He concluded that the column axial load ratio has a significant effect on the joint shear capacity of the joint. The ultimate joint shear capacity increased along with column axial load increment which was taken in a range of 0 to 0.7. However, as the column axial load ratio surpasses 0.6 and approaches 0.7, pure axial failure of the joint was observed. The concrete at the joint was completely crushed by going through some cyclic steps after peak strength. The effect of axial load on the crack pattern of the joint was also covered in this paper. The author reported that high column axial load increased the inclination of the main diagonal shear cracks from 45^0 to 90^0 and delayed the initiation of the first shear crack. The crack pattern observed at the final stage of loading was very significant for the specimen with no axial load. The crack width reduced following the axial load increment. A significant effect of pinching was also observed in his study. Severe pinching was identified for specimens with zero column axial load. Following the increment of column axial load, the pinching effect reduced considerably.

CHAPTER 3 DESCRIPTION OF THE EXAMINED PPC BCJ$_S$

Under this chapter, the sectional and material properties; test setup, and restraint conditions of the examined specimens are discussed. Two experimental programs executed by T. Kashiwazaki et al [5] and M. Nishiyama et al [6] in Chiba and Kyoto University, Japan, were examined. T. Kashiwazaki et al [5] examined a partially prestressed concrete (PPC) interior beam-column joint (BCJ) while M. Nishiyama et al [6] demonstrated a partially prestressed concrete (PPC) exterior beam-column joint (BCJ). Both of the beam-column subassemblies are designed to fail in shear at the joint according to the seismic requirements of Architectural Institute of Japan, AIJ, code provisions. Beams and the columns are strongly reinforced to prevent flexural failure before joint shear failure.

3.1 Partially prestressed concrete interior beam-column joint

3.1.1 Sectional and material properties

All specimens had a beam span of 270 cm and inter-story height of 147 cm as shown in Figure 3.1. The beam's cross-sectional dimension is 200 x 300mm and composed of 6Ø19 deformed longitudinal bars and 2Ø23 post tensioned grouted prestressing steel which are confined by Ø10 shear reinforcement with 50mm spacing. The prestressing steel is a grouted bonded tendon and has good bond performance with the surrounding concrete. The column's cross-sectional dimension is 300x300mm and composed of 12Ø19 deformed longitudinal bars which are confined by Ø10 shear reinforcement with 40mm spacing. Concrete, reinforcement, and prestressing steel material properties are labeled in Table 3.1.

3.1.2 Test setup and restraint conditions

The test setup configuration is designed to simulate the boundary conditions and forces by which the PPC BCJ is subjected to seismic excitation. To simulate the four infection points in real structures, moment release is provided at the bottom and top ends of the column and the right and left ends of the beam. Figure 3.1 shows the testing arrangement of the specimen. The bottom part of the column end is restrained both in a vertical and horizontal direction and since the top part of the column was loaded vertically with a constant axial column force of 320 kN, movement is only restrained along the horizontal direction. In

addition, the positive and negative load at beam ends is applied at a distance of 1350mm from the column centerline along both sides. The test continued up to a storey displacement of 74mm.

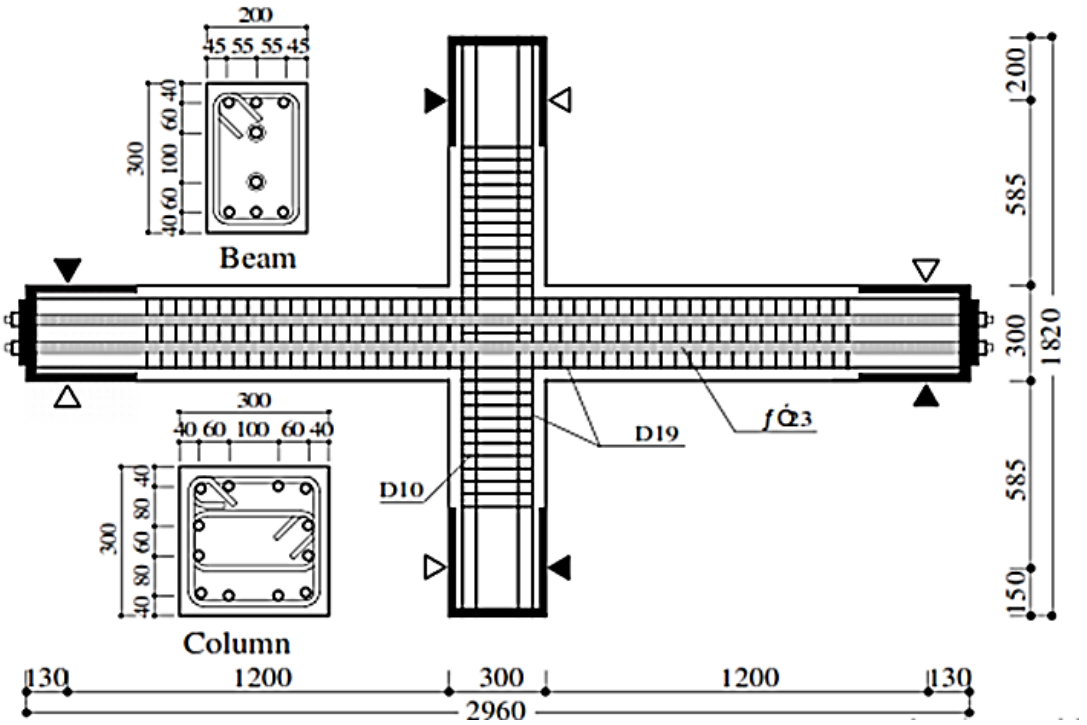

Figure 3.1Sectional detail, reinforcement layout, and test setup of the PPC interior BCJ

Table 3.1 Material properties of PPC interior BCJ specimens

a) Concrete

Specimen	Compressive strength, f_c (MPa)	Elastic modulus of concrete, E_c (GPa)	Split strength, f_t (MPa)
PC-0, PC-1	34.4	28	3.01
PC-2	35.3	28.1	3.01

b) Reinforcement and Prestressing steel

Type of reinforcement	Diameter (mm)	Yield strength, f_y / f_{yp} (MPa)	Yield strain, ε_y (10-6)	Elastic modulus of steel, E_s (GPa)	Ultimate tensile strength, f_u (MPa)
Longitudinal	19	517	2850	181	692
Transverse	10	897	4330	207	1070
Prestressing steel	23	1100	5500	200	1250

3.2 Partially prestressed concrete exterior beam-column joint

3.2.1 Sectional and material properties

Specimen KPC2-1 has a beam span of 145 cm an inter-story height of 150 cm as shown in Figure 3.2. The beam's cross-sectional dimension is 200 x 300mm and is composed of 4Ø16 deformed longitudinal bars and 2Ø25 post tensioned round prestressing steel confined by Ø10 shear reinforcement with 50mm and 80mm spacing. The prestressing steel is a round bar that has poor bond performance with the surrounding concrete. The column's cross-sectional dimension was 250x250mm and is composed of 8Ø19 & 4Ø16 deformed longitudinal bars confined by Ø10 shear reinforcement with 100mm spacing. Concrete, reinforcement, and prestressing steel material properties are labeled in Table 3.2.

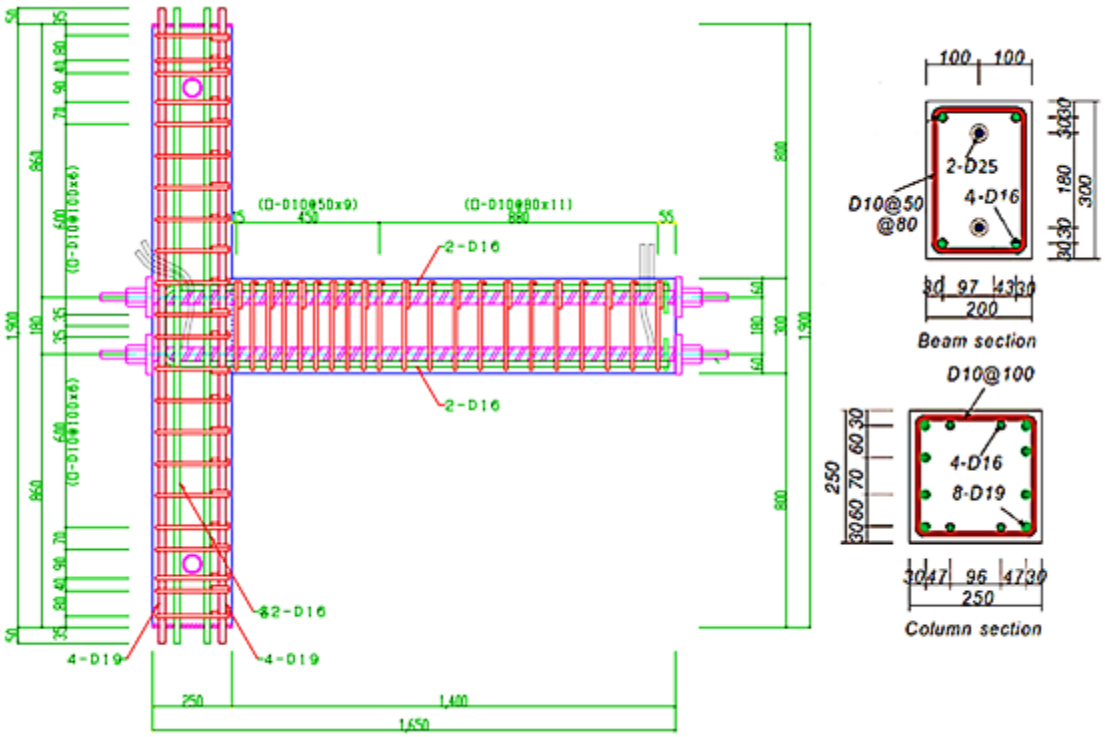

Figure 3.2 Sectional detail, and reinforcement layout for PPC exterior BCJ

3.2.2 Test setup and restraint conditions

The test setup configuration is designed to simulate the boundary conditions and forces by which the PPC BCJ is subjected to seismic excitation. To simulate the three infection points in real structures, moment release is provided at the bottom and top ends of the

column and the right end of the beam. Figure 3.2 shows the testing arrangement of the specimen. The bottom part of the column end is restrained both in the vertical and horizontal direction and the top part is restrained along the horizontal direction only. In addition, the positive and negative load at the beam end is applied at a distance of 1325 mm from the column centerline along both sides. The tests continued up to a storey displacement of 90.32mm.

Table 3.2 Material properties of PPC interior BCJ specimen

a) Concrete

Specimen	Compressive Strength, f_c (MPa)	Stain at f_c, %	Elastic Modulus of concrete, E_c (GPa)	Split Strength, f_t (MPa)
KPC2-1	34.6	0.22	28.2	2.51

b) Reinforcement and Prestressing steel

Type of reinforcement	Diameter (mm)	Yield stress, f_y / f_{yp} (MPa)	Yield strain, ε_y (10-6)	Elastic modulus of steel, E_s (GPa)	Ultimate tensile strength, f_u (MPa)
Transverse	10	307	1744.3	176	436.9
Longitudinal	16	374.7	2025.4	185	533.4
Longitudinal	19	386.8	2113.7	183	569.9
Prestressing steel	25	1026	5104.5	201	1146

Figure 3.3 Experimental test setup for PPC exterior BCJ

CHAPTER 4 FINITE ELEMENT MODELING & VALIDATION

4.1 Introduction to VecTor2

In this study, analyses were undertaken using the VecTor2 finite element program. VecTor2 is a finite element software that is developed to analyze the response of two-dimensional reinforced concrete members subjected to short-term in-plane static monotonic, cyclic, and reverse cyclic loading. The software uses Modified Compression Field Theory (MCFT) and the Disturbed Stress Field Model (DSFM) as a theoretical basis.

MCFT analytically predicts the load-deformation response of a reinforced concrete element subjected to normal and shear stresses. It considers local crack conditions by integrating a rotating smeared crack approach along with average stresses and strains. Member's failure mode could then be determined from this information. Compatibility, equilibrium, and constitutive relationships are used to obtain the load-deformation responses of the elements. (F. J. Vecchio et al [25])

The DSFM is an improved model of MCFT that explicitly calculates crack shear-slip deformations. This excludes the crack shear check required in MCFT. DSFM demonstrates improved performance in estimating strains in the reinforcements for a better redistribution of stresses in an element. It computes higher strains in the transverse reinforcements and lower strains in the longitudinal reinforcements. This model is very significant especially for members with a slight distribution of transverse reinforcements. In such member's crack shear slip is remarkable and the rotation of the principal stress field tends to delay the larger rotation of the principal strain field. Rotations are considered to be constant in MCFT, which then overestimates the strength and stiffness of such elements. (F. J. Vecchio et al [25])

The cyclic displacements are applied at each loading step, which decreases or increases by a common load factor. At the end of each load stage, the finite element program adjusts the structure stiffness matrix of the model before going to the next load stage to realize the non-linear changes in the structure. The convergence of variables highly depends on the nonlinear response of the model, the specified convergence limit, and the maximum number of iteration. For extensive crack formation and loss of stiffness after energy dissipation, the program will diverge and terminate the analysis causing specimen failure.

4.2 Material modeling

In this study, two types of partially prestressed concrete (PPC) beam-column joints (BCJs), exterior and interior, were modeled accordingly. Specimen for the PPC interior BCJ was taken from an experimental study made by T. Kashiwazaki et al [5] and for PPC exterior BCJ from an experimental study made by M. Nishiyama et al [6]. Both of these specimens will be used later on for further investigation. In the following sections material models for concrete, reinforcing steels, prestressing steels, and bond elements used in the fine element program are discussed in detail for both specimens.

4.2.1 Concrete

4.2.1.1 *Elements*

Concrete regions with and without smeared reinforcements are defined in the model. Covers are defined as plain concretes without smeared reinforcements while confined concretes are defined as concretes with smeared reinforcements. Concrete with smeared reinforcements are those confined by transverse reinforcement steels, which are defined according to their reinforcement ratio. Concrete regions were modeled with Plane Stress Rectangular Elements with uniform thickness in the out-of-plane direction. The elements have 8 degrees of freedom which allows translation at every node in x and y directions as shown in Figure 4.1.

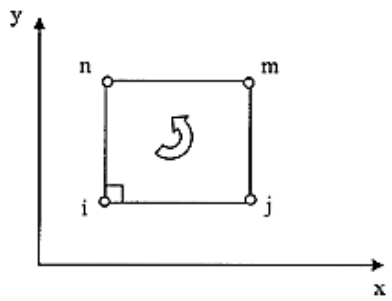

Figure 4.1 Rectangular Concrete Element [25]

4.2.1.2 ***Models***

(a) Constitutive relationship model

Different reinforced concrete compressive stress-strain relationships are available in VecTor2. These relationships can be classified as either pre-peak responses or post-peak responses.

To assign concrete models in the finite element program, a study on the concrete confinement is mandatory. T. Paulay et al [2] and R. Park et al [3] have stated that confinement by stirrups can significantly improve the stress-strain characteristics of concrete at high strain. Confinement can considerably increase the compressive strength of concrete. The compressive strength of confined concrete is related to the effective confining stress that is developed at the yield of transverse reinforcements. Besides, closely spaced stirrups significantly facilitate the bond strength between the longitudinal reinforcement and the boundary concrete by decreasing the unsupported length of the bars. Thus stirrup arrangement also plays a remarkable role in concrete confinement.

In the PPC interior BCJ specimen stirrups were closely spaced (40mm) at the joint and their yield strength (897 MPa) was very large compared to the PPC exterior BCJs with 100mm spacing and 307 MPa transverse yield strength. Besides, grouted prestressing steels with good bond performance were assigned in the interior joint. While in the exterior joint, the prestressing steels were round bars with lower bond capacity than its conventional reinforcements. Accordingly, different concrete constitutive relationships were provided for the interior and exterior specimens. The rest of the concrete models were similar for both joints as discussed in the following.

In the interior joint experiment, Popovics Normal Strength model, S. Popovics [26], was assigned for the ascending part of the curve. This model is suitable for a concrete compressive strength up to 45 MPa. This curve reflects reduced ductility of concrete and greater stiffness as the compressive strength of concrete increases. The descending part was represented by the Modified Park-Kent model, R. Park [27], to account for the enhancement of concrete strength and ductility due to confinement. According to F. J. Vecchio et al [25], both the pre-peak and post-peak models are formulated for confined

concrete members. The responses of both models are shown in Figure 4.2 and Figure 4.3. The corresponding constitutive equations are stated under APPENDIX A.

In the exterior joint experiment, Hognestad (Parabola) model [25] was found to be suitable for the ascending part of the constitutive relation curve. The model is a simple compression response curve, suitable for normal concrete strengths (<40 MPa) as shown in Figure 4.4. Furthermore, the descending part was represented by Attard & Setunge model [28], which provides a good prediction of concrete material behavior for a wide range of concrete strength from normal (20MPa) to a very high concrete strength (130MPa). This model is limited to low confining pressures between 1 and 20MPa. The response of Hognested and Attard & Setunge model is shown in Figure 4.4 and Figure 4.5. The corresponding constitutive equation is stated under APPENDIX A (A.3 and A.4).

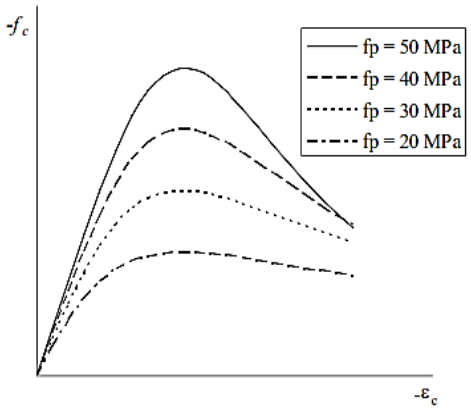

Figure 4.2 Popovics pre-peak and post-peak concrete stress-strain curve [26]

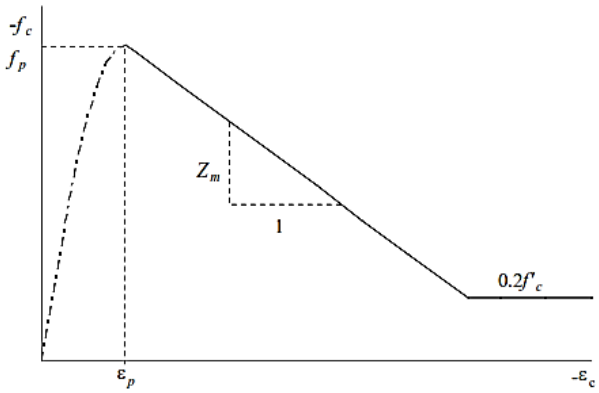

Figure 4.3 Modified Park-Kent pre and post-peak concrete stress-strain curve [27]

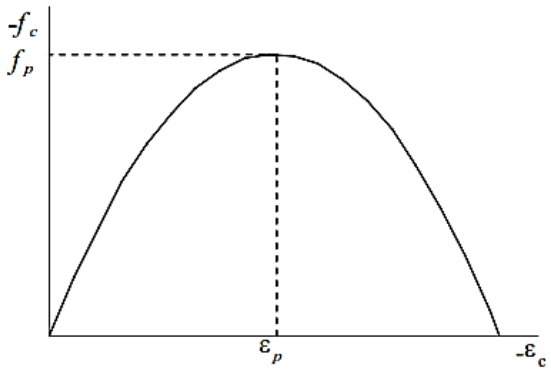

Figure 4.4 Hognestad parabolic pre and post-peak stress-strain curve [25]

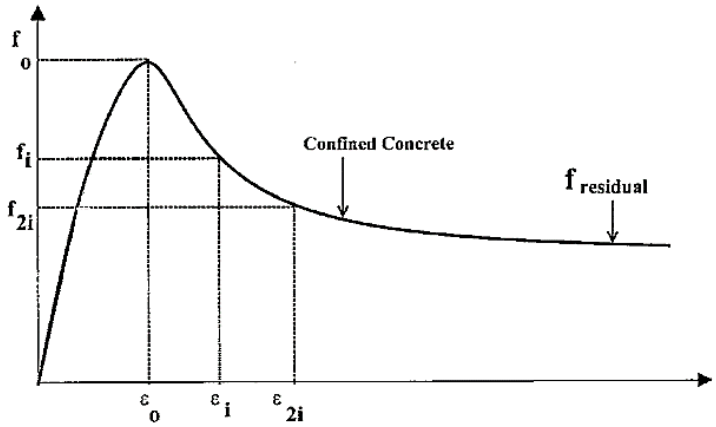

Figure 4.5 Attard & Setunge pre and post-peak stress-strain curve [28]

(b) Hysteretic response model

For the hysteretic analysis, the model proposed by D. Palermo et al [29] with decay was believed to be suitable for both PPC interior and exterior BCJ. The loading and unloading of concrete from the monotonic concrete stress-strain curve is described in this model. Plastic strain offsets and modeling of damage are incorporated in the unloading and reloading curves of the hysteretic response, in both tension and compression domains as shown in Figure 4.6. The unloading part follows the nonlinear Ramsberg-Osgood formulations. Reloading stiffness degradation is incorporated in the linear reloading part based on the amount of strain recovered during the unloading phase. The base curves for compression and tension regions accounts for compression softening and tension stiffening of concrete.

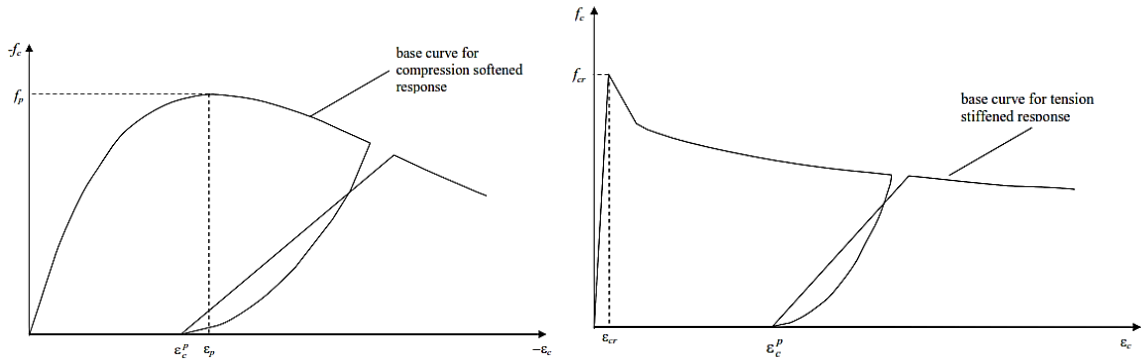

Figure 4.6 Palermo model of concrete hysteretic response in compression (left) and tension (right) [29]

For the rest, the program default models were believed to be appropriate to capture important features as described below.

(c) Compression softening

Compression softening was modeled by F. J. Vecchio model [30]. This model accounts for the reduction of both strain and strength due to cracking. This reduction may be significant and have considerable effects on the load-deformation response of reinforced concrete members, in terms of, ultimate strength capacity, stiffness, and ductility.

(d) Tension stiffening

Tension stiffening was considered by using the Modified Bentz model [25]. This model accounts for bond characteristics between the concrete and bonded reinforcement, to consider the stiffness of reinforced concrete after cracking. This phenomenon increases the stiffness of a concrete section in tension between two adjacent cracks, by transferring the stress from the reinforcement to the surrounding concrete.

(e) Tension softening

Tension softening was represented by the Bilinear model [25], which represents the linear reduction of tensile stress in plain concrete after cracking under increased tensile strain. It addresses circumstances in members with no or small reinforcements and still contributes to the ductility and strength of the structure.

(f) Dilation

The dilation or lateral expansion of concrete was accounted for by the Kupfer-variable isotropic model, H. Kupfer et al [31]. This model considers the lateral expansion of concrete following internal micro cracking and increases with compressive stresses.

(g) Confinement strength

Confinement strength was also considered by Kupfer/Richart model, H. Kupfer et al [31]. Concrete cracking strength was characterized by the Mohr-Coulomb stress model [25]. Concrete cracking strength according to this model is determined based on the stress or strain state of an assumed failure condition. Analysis conducted by the MCFT model require a crack shear check to make sure that shear stress, on a cracked surface, does not surpass the maximum allowable stress related to sliding shear failure. The F. J. Vecchio model [32] was used to calculate the maximum shear stress permitted at a crack. Crack width is also checked to reduce the average compressive stresses when the crack width exceeds the limit.

The constitutive and behavioral models that are used for the concrete modeling of both interior and exterior joint are summarized in Table 4.1.

Table 4.1 Material Models for Concrete

Concrete Property	VecTor2 Concrete Model
Compression Pre-Peak Response	Popovics (NSC)[1] , Hognestad (Parabola)[2]
Compression Post-Peak Response	Modified Park-Kent[1] , Attard & Setunge[2]
Hysteretic Response	Palermo (w/ Decay) *
Compression Softening	Vecchio *
Tension Stiffening	Modified Bentz*
Tension Softening	Bilinear*
Dilation	Kuper Variable - Isotropic*
Confined Strength	Kupfer/Richard*
Cracking Criterion	Mohr-Coulomb (Stress) *
Crack Stress Calculation	Basic (DSFM/MCFT) *
Crack Slip Calculation	Walraven*
Crack Width Check	Agg/2.5 Max Crack Width*

N.B: [1] is for interior joint; [2] is for exterior joint and * is for both

4.2.2 Reinforcement and prestressing steel

4.2.2.1 *Elements*

All reinforcement and prestressing steels in both PPC interior and exterior BCJ specimens were modeled using discrete bar elements. Based on F. J. Vecchio et al [25], this option of modeling is useful when the area of interest is the bond-slip response or the local stress-strain in the reinforcement. Discrete reinforcement is modeled using truss elements as shown in Figure 4.7. The truss element is a structural element with two nodes having four degrees of freedom, allowing translation in the x and y direction at each node. Its axial stiffness is related to its length, area, and modulus of elasticity. The truss element can be modeled with or without bond stress-slip elements. If bond stress-slip elements are not defined, the truss and concrete elements share common nodes and a perfect bond is assumed. In this paper, reinforcement bars in the interior joint specimens are modeled as being perfectly bonded with the surrounding concrete while in the exterior joint a link element is defined to represent the bond behavior. This phenomenon is discussed in detail later on in the 'bond' section of this paper.

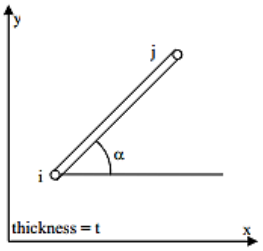

Figure 4.7 Truss bar element [25]

4.2.2.2 *Models*

(a) Ductile steel reinforcement constitutive model

In this paper, a trilinear response model is used to define the stress-strain behavior of the ductile reinforcements. This model is composed of an initial linear elastic response, yield plateau, and linear or nonlinear strain hardening until failure. The stress-strain response of the reinforcement is shown in Figure 4.8. The stress-strain relationship of this response can be determined based on APPENDIX B.

(b) Prestressing steel constitutive model

In VecTor2, the stress-strain response for the prestressing steel is defined as an initial elastic branch followed by a second hardening linear branch through a transition curve as shown in Figure 4.9. The response does not exhibit a distinct yield plateau.

VecTor2 also allows the user to account for the relaxation loss of prestressing tendons with time by assigning a 'P/S Relaxation Coefficient'. Young's modulus of the prestressing tendons will be divided, throughout the analysis, by a value of one plus the value entered for this coefficient. A. E. Naaman et al [33] discussed that, as the initial prestressing force increases, the drop of prestressing due to relaxation will increase. Codes limit 80% initial prestress so that the relaxation loss is relatively limited. Thus, the maximum prestress used in this paper is limited to 80% prestressing yield strength. Relaxation loss at 1000 hours is 5% of the initial prestress. In this study, the specimens are cast and tested in less than 1000 hours so the effect of prestress relaxation loss is neglected.

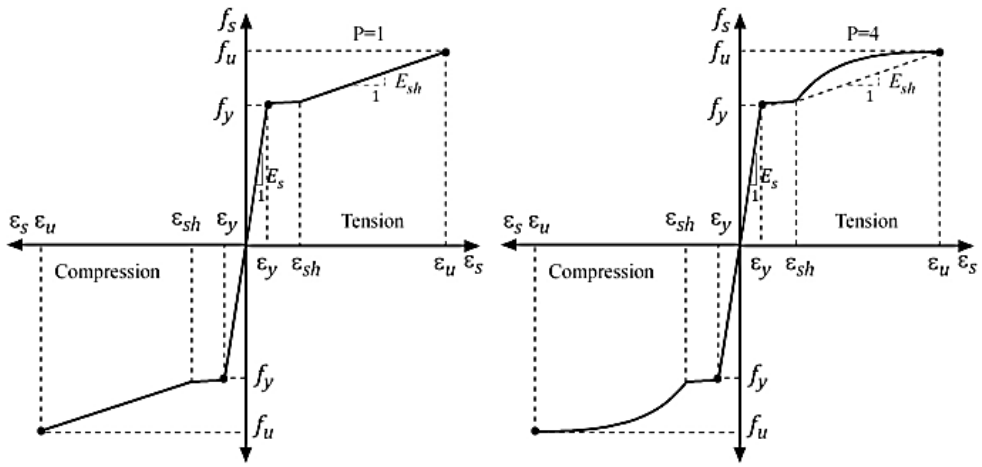

Figure 4.8 Trilinear stress-strain response of ductile steel reinforcement with linear and non-linear strain-hardening [25]

(c) Hysteretic response model

Different reinforcement hysteretic response models are defined in VecTor2 using the monotonic stress-strain behavior as a base. These hysteretic models discuss the loading and unloading behavior of reinforcement under a reverse cyclic loading. In this study, the response model proposed by M. Seckin [34] was used as shown in Figure 4.10. This model

includes the Bauschinger effect by which the reinforcement exhibits premature yielding upon load reversal after plastic pre-straining, due to stress changes at the microscopic level.

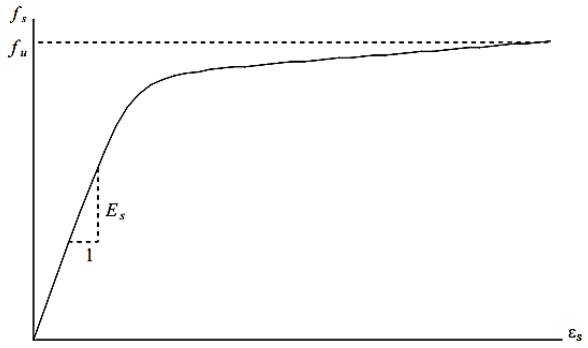

Figure 4.9 Prestressing steel reinforcement stress-strain response [25]

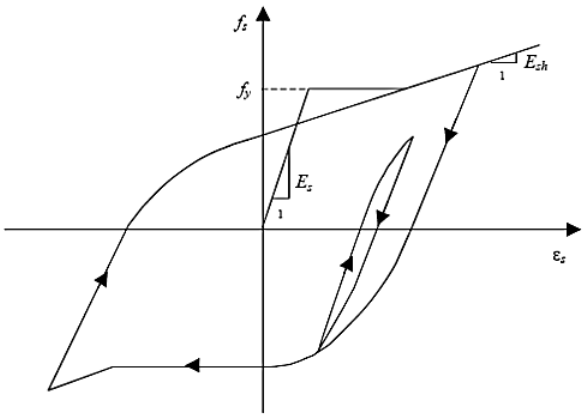

Figure 4.10 Seckin model for reinforcement hysteretic response [34]

(d) Dowel action

Dowel action refers to shear resistance by reinforcing bars crossing a crack as the crack slips perpendicular to the axis of the rebar. Dowel action has a great contribution to shear strength and post-peak ductility especially if a small amount of transverse reinforcements exists in a member. The Tassios (Crack Slip) and Tassios (Crack Strength) options are available in VecTor2 for calculating rebar dowel action [25]. In the Tassios (Crack Slip) option, the dowel force is subtracted from the stress of the concrete at a crack. For Tassios (Crack Strength) option, the dowel force acts as a resisting force. In this study, Tassios (Crack Strength) option was used for both PPC interior and exterior specimens.

(e) Reinforcement Buckling

The reinforcement Buckling model is effective in an analysis where discrete reinforcements are attached to concrete with bond link elements. Buckling failure results due to high compressive stress subjected to the reinforcement. The contribution of shear and flexure resistance of a structure by reinforcement will be neglected if a buckling failure mechanism occurs.

Three models are available for considering reinforcing bar buckling. Among these models Modified Dhakal-Maekawa Model (MDM), R. P. Dhakal et al [35], was used for the PPC interior BCJ specimens. This model defines a stress equation, which is less than the yield stress, to obtain the reinforcement buckling stress. While for the PPC exterior BCJ specimens, Asatsu model was found to be suitable. According to F. J. Vecchio et al [25], Asatsu model is appropriate for truss bar elements that are attached to concrete with bond link elements. Reinforcement bucking in this model occurs when compressive stress exceeds 80% of reinforcement yield strength and bond deterioration is severe. As will be discussed in the 'bond' section of this chapter, the reinforcements and prestressing steels in the PPC exterior BCJs are connected to concrete with bond link elements.

The constitutive and behavioral models that are used for the reinforcement in both interior and exterior joints are summarized in Table 4.2.

Table 4.2 Material Models for reinforcement

Reinforcement property	VecTor2 Reinforcement Model
Hysteretic Response	Bauschinger Effect (Seckin)*
Dowel Action	Tassios Model (Crack Strength)*
Buckling	Akkaya (Modified Dhakal-Maekawa)[1] , Asatsu Model[2]

N.B: [1] is for interior joint; [2] is for exterior joint and * is for both

4.2.3 Bond

4.2.3.1 *Bond properties*

The bond model for embedded bars first determines the stress-slip relationship for unconfined bars and confined bars. Unconfined bars correspond to splitting failure while

confined bars correspond to pull-out type bond failure. Splitting failures are defined in terms of split bond stress (τ_s) and split bond-slip (Δ_s) while pull-out type bond failure is defined in terms of pull-out bond stress (τ_p) and pull out a bond-slip (Δ_p). (F. J. Vecchio et al [25])

Bond material properties for the embedded rebar were specified in the finite element software by defining a confinement pressure index (β). The pressure index represents the lateral confining pressure obtained from the transverse reinforcements and can be defined according to Equation (4.1). The confinement pressure index (β) value is in a range of 0 to 1. A confined pressure value of 1 represents the confined case (pull out type failure) and a value of 0 represents the unconfined case (split type failure). (F. J. Vecchio et al [25])

$$\beta = \frac{\rho_v * f_y}{7.5\ Mpa} \qquad 0 \leq \beta \leq 1 \tag{4.1}$$

Where ρ_v is the transverse reinforcement ratio within the bond region, f_y (MPa) is the yield stress of the reinforcement, 7.5 MPa is the high confinement pressure value accepted by Committee Euro-International Du Beton, CEB-FIP Model Code 90 [36].

Bar clear cover, the spacing of transverse reinforcement, and the number of reinforcement layers through depth are also the most important parameters in defining the bond properties for embedded bars.

In the PPC interior BCJ specimens, the yield strength of shear reinforcements was 897 MPa. The corresponding joint and the beam members had a shear reinforcement ratio of 1.57% and 1.5%. Accordingly, a confinement pressure factor (β) of 1.87 and 1.79 was calculated. These values are greater than 1, which means that the confinement pressure that can be provided by the transverse reinforcements is almost twice greater than that of the high confinement pressure value accepted by Committee Euro-International Du Beton, CEB-FIP Model Code 90 [32]. Also, the provided prestressing steel was grouted with a good bond performance with the surrounding concrete. Thus, the bond property was not defined in the interior joint specimens and both the deformed reinforcement and prestressing steel were assumed to have a perfect bond with the surrounding concrete.

While in the PPC exterior BCJ specimens, the transverse reinforcements had significantly smaller yield strength (307MPa) as compared to those in the interior BCJ. Thus, a confinement pressure index was calculated to be 0.64 and introduced in the model to represent the bond material property for the conventional reinforcements. Furthermore, round steel with low bond performance was provided for the prestressing steel. Thus, a bond property was defined in the software as round bars (smooth bars) for the prestressing steels.

4.2.3.2 *Bond stress-slip elements*

In this study bond stress-slip element between the reinforcement/prestressing steel and surrounding concrete as defined in the PPC exterior BCJ according to their assigned bond property. There are two bond-slip elements available in VecTor2: Contact element and Link element. In this study, link-element is chosen.

Link Element is an element used to measure the bond-slip property between reinforcement and the surrounding concrete. The link element contains two nodes, one associated with a concrete element and one associated with a truss element as shown in Figure 4.11. These two nodes will be at the same location until slippage occurs between the concrete and reinforcement. This element measures bond-slip at a particular node through a combination of stresses and displacements measured tangential and radial to the reinforcement, for a total of four degrees of freedom as shown in Figure 4.11.

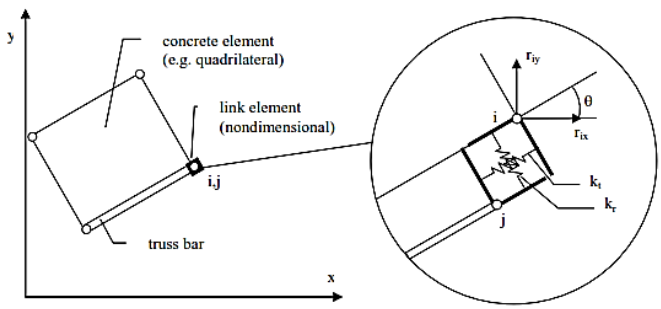

Figure 4.11 VecTor2 Link Element [25]

The link element can be conceptualized as two springs connected orthogonally, linking the discrete reinforcement element and reinforced concrete element as shown in Figure 4.11. One spring deforms radially to the discrete reinforcement element and the other deforms

tangentially to the discrete reinforcement element, representing radial and tangential displacements (Δ_r, Δ_t) and stresses (τ_r, τ_t). (F. J. Vecchio et al [25])

4.2.3.3 *Bond stress-slip models*

VecTor2 has different bond stress-slip models for embedded bars: Perfect Bond Model, Eligehausen Model, Gan Model, Harajli Model, Fujii Model, Eligehausen, and Gan Models with No Cyclic Damage. In this paper, Eligehausen bond model, R. Eligehausen [37], with cyclic damage was assigned for the PPC exterior BCJ and a perfect bond model was used for the interior joint as specified under Table 4.3. In a perfect bond model, deformation of the bond element is prevented by assigning large stiffness and strength properties.

In Eligehausen et al. model [37], the unconfined and confined bond stress-slip relationships are described by an ascending non-linear curve, a constant bond stress plateau, a non-linearly declining branch, and a continuous residual stress branch, as shown in Figure 4.12.

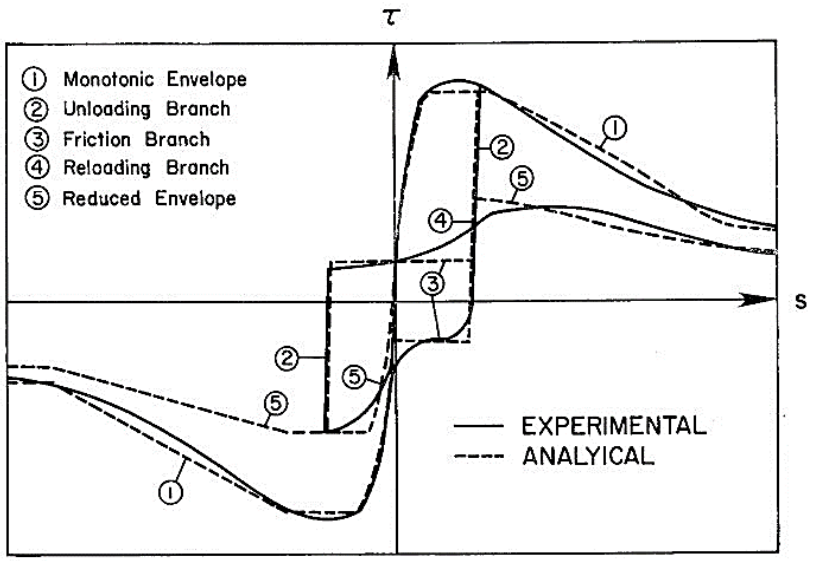

Figure 4.12 Eligehausen bonds stress-slip response [25]

Table 4.3 Bond Model for Specimen KPC2-1

Bond Property	VecTor2 Model
Concrete bond	Eligehausen et al.[2], Perfect bond[1]

N.B: [1] is for interior joint; [2] is for exterior joint and [*] is for both

4.3 Finite element software validation

A finite element model was developed and analyzed in the finite element software to validate its responses with previously investigated experiments. Two experimental programs executed in Chiba and Kyoto University, Japan, were examined. The first experiment to be validated is a partially prestressed concrete (PPC) interior beam-column joint (BCJ) from T. Kashiwazaki et al [5] study and the second was a partially prestressed concrete (PPC) exterior beam-column joint (BCJ) from M. Nishiyama et al [6] study. These experiments were chosen to see if the finite element software captures the effect of prestressing level on the seismic performance. The first experiment contains interior joint specimens with a prestress of 0, 0.25 $f_{yp,}$ and 0.5 f_{yp}, where f_{yp} is the yield strength of the prestressing steel. The second experiment incorporates an exterior joint specimen with prestress of 0.59 f_{yp}.

A reverse cyclic lateral displacement loading was applied at the beam ends in both programs to simulate the seismic action. The analytically obtained hysteretic responses of the tests were presented and compared with the experimental results in the following section. The comparison was made regarding, Ultimate storey shear and story displacement, maximum storey displacement, pinching, strength degradation, displacement at yield, and crack pattern at final loading stages. Comparison of these parameters is considered to be sufficient for further investigation made on these specimens in the next chapter.

4.3.1 Partially prestressed concrete interior beam-column joint

4.3.1.1 *Experimental data*

In this experimental study, three post-tensioned partially prestressed concrete interior beam-column joints (PPC interior BCJ) with different prestressing forces were chosen for the validation. All the specimens were under a constant column axial load of 320 kN. The summary of the specimens is labeled under Table 4.4.

4.3.1.2 *Regional, mesh, and material definitions*

The PPC interior BCJ specimens were modeled with 7 regions which are composed of 1215 rectangular elements and 480 truss elements to represent the concrete and

reinforcement properties as shown in Figure 4.13. Two regions were assigned in each column and beam sections for concrete cover and confined reinforced concrete. One confined reinforced concrete region was assigned to the joint. The last two regions were a stiffened load bearing and support regions, by which the reverse cyclic load and restraint conditions are applied. These stiffened elements are modeled as structural steel elements to facilitate a proper loading transfer to the beam without unrealistic local failures. A rectangular mesh type was used with an element size of 40mm by 40mm in all regions except the load-bearing region at the beam ends and top and bottom of the column, which is 23x40mm and 25x40mm.

Table 4.4 Prestresss assignment for the PPC interior BCJ specimens

Specimen	Joint type	Experimental Program	Prestress (MPa)
PC-0	PPC interior BCJ	Reverse cyclic loading	0
PC-1			$0.25f_{yp}$
PC-2			$0.5f_{yp}$

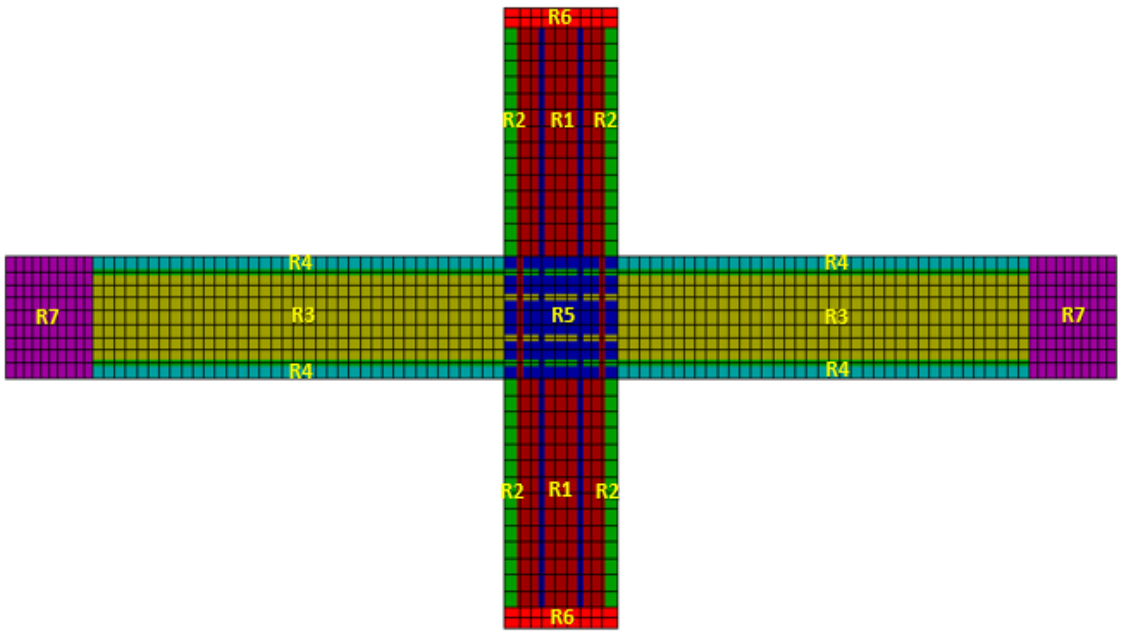

Figure 4.13 Material region definition for PPC interior BCJ specimen defined in VecTor2

The confined concretes (R1, R3, and R5) were modeled with in-plane and out-plane smeared reinforcements by assigning transverse reinforcement ratio ($\rho_x, \rho_y \; and \; \rho_z$) calculated as per EN 1992-1-1 [38] section 9.2.2 (5). A transverse reinforcement ratio of 2.62%, 1.50%, and 1.57% were obtained for column (R1), beam (R3), and joint (R5), respectively. Truss elements were assigned to both the longitudinal reinforcements and bonded prestressing steel.

4.3.1.3 *Initial stress definition*

Two methods are available to define the initial stresses in tendons; Predefined field strain and initial temperature load method. In this study, the predefined strain method is used by which we define the intensity of the strains at the beginning of the analysis. Thus, a prestrain value of 0, 1.37, and 2.75 were defined for specimen PC-0, PC-1, and PC-2, respectively.

4.3.1.4 *Loading*

In this study, four load cases were defined. Load case 1 was a monotonic loading which was assigned for the constant column axial load and the own weight of the specimen. Load case 2, 3 and 4 was a reverse cyclic loading which was applied progressively at the beam ends as shown in Figure 4.14. The first four loading cycles were assigned in load case 2; the 5^{th} loading cycle was assigned in load case 3, and the last cycle of loading was assigned in load case 6. The applied lateral displacement pattern is shown in Figure 4.15.

4.3.1.5 *Analytical result*

The hysteretic response in terms of storey shear force and storey displacement was obtained as shown in Figure 4.16. The storey displacement is the displacement equal to the lateral displacement history applied at the tip of the beam as shown in Figure 4.15. The storey shear force is the lateral reaction at the tip of the beam under the applied lateral displacement.

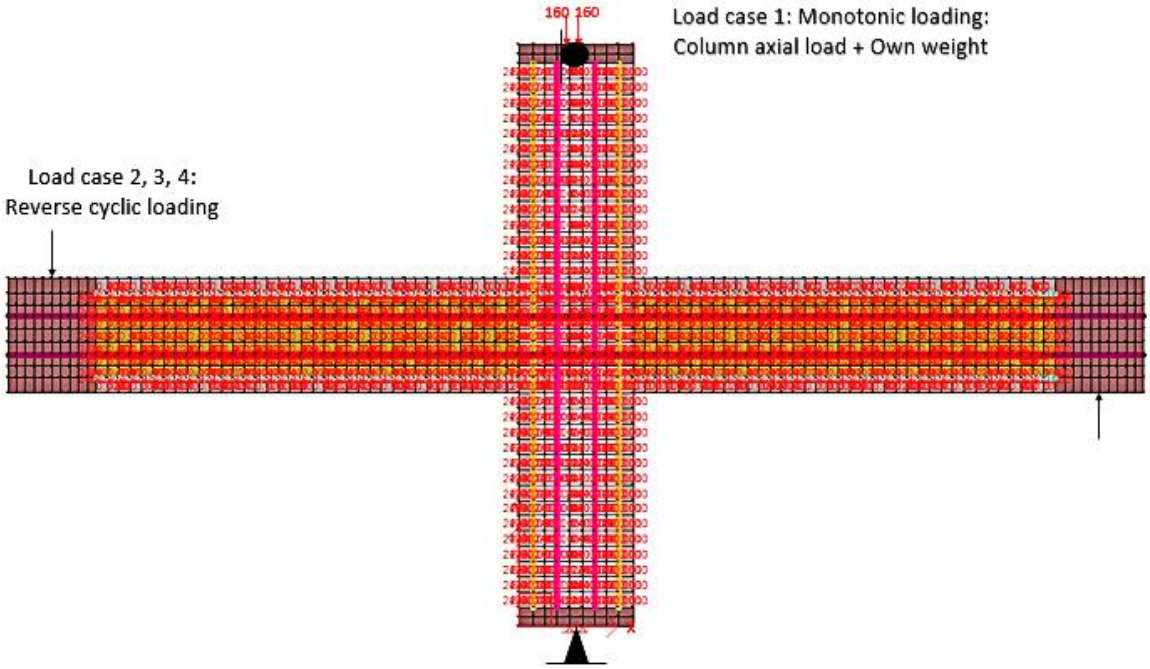

Figure 4.14 Loading and boundary condition definition for PPC interior BCJ

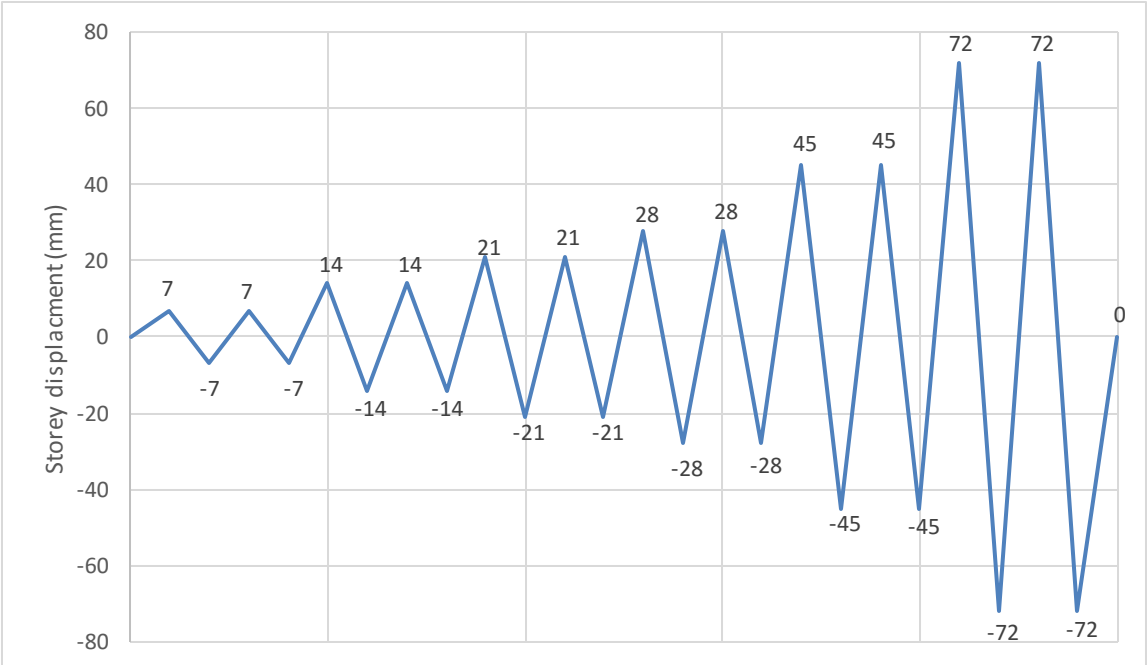

Figure 4.15 Lateral displacement history in PPC interior BCJ

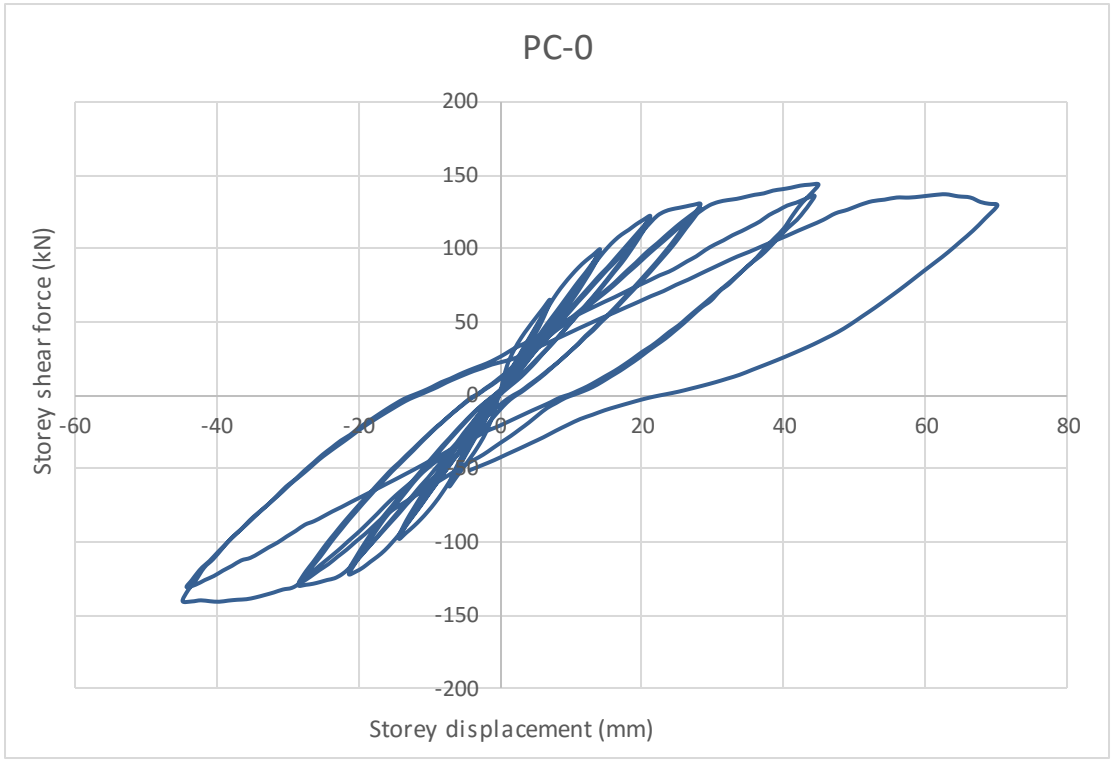
PC-0
Storey shear force (kN)
200
150
100
50
0
-100
-150
-200
-60
-40
-20
0
20
40
60
80
Storey displacement (mm)

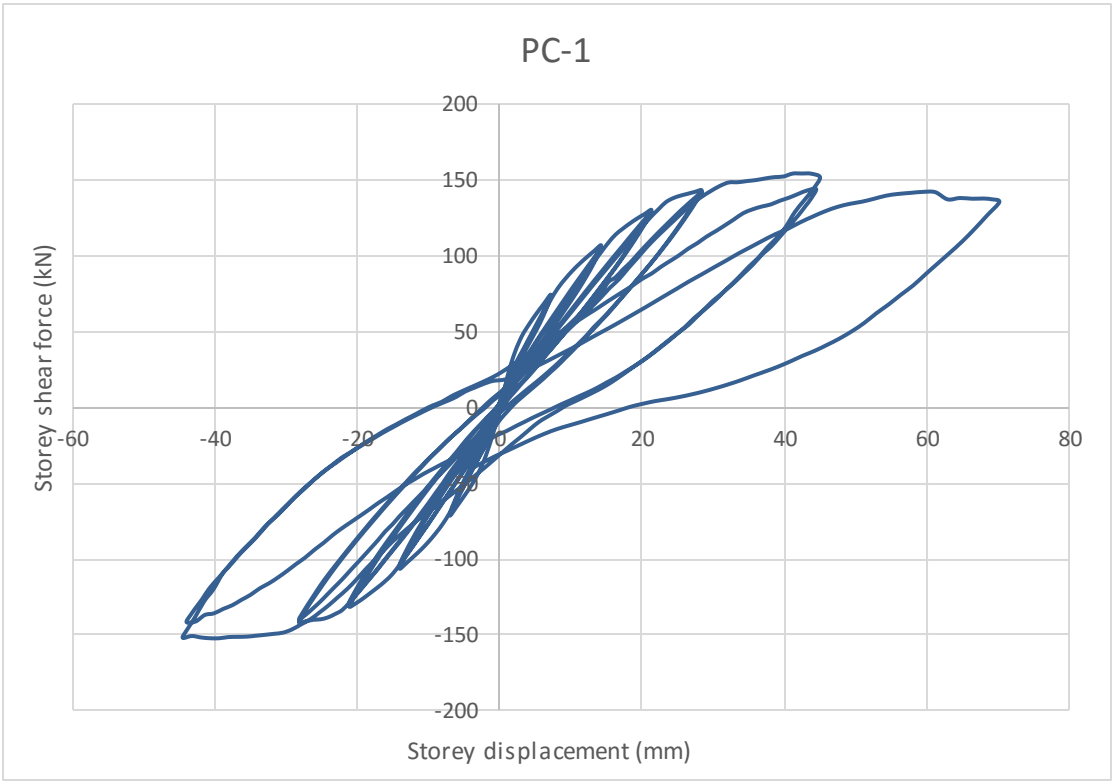
PC-1
Storey shear force (kN)
200
150
100
50
0
-100
-150
-200
-60
-40
-20
0
20
40
60
80
Storey displacement (mm)

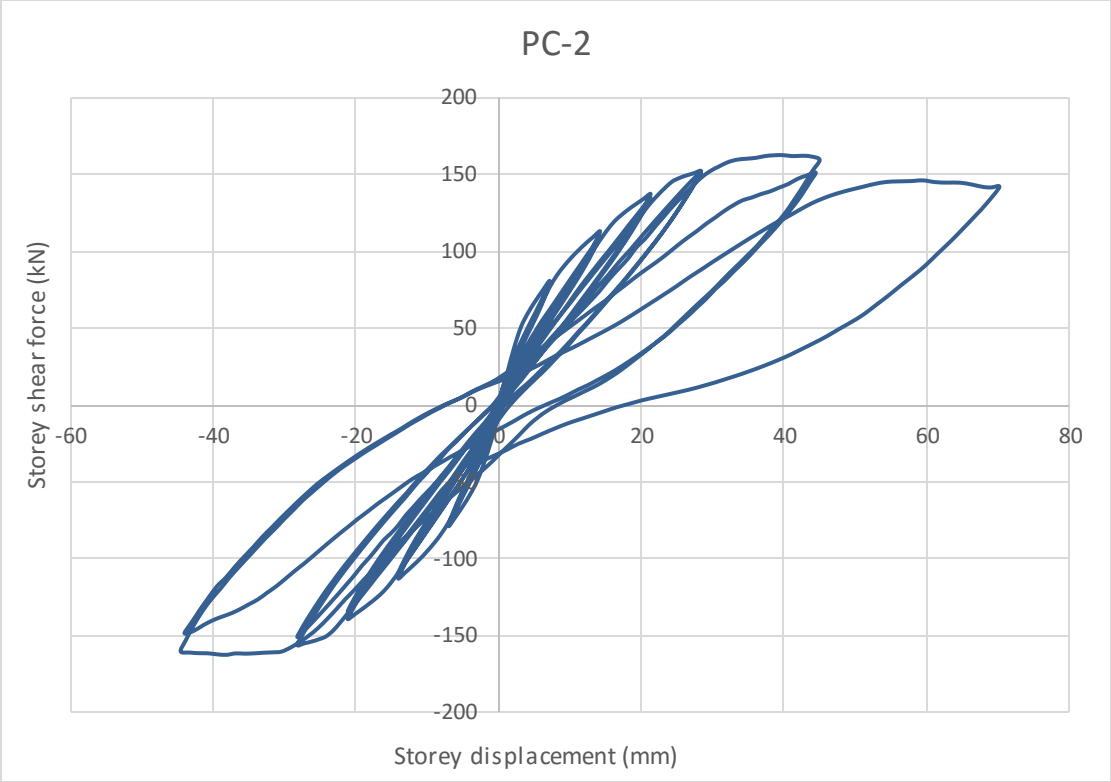

Figure 4.16 Hysteretic response of specimen PC-0, PC-1, and PC-2 according to VecTor2

4.3.1.6 *Analytical and Experimental result comparison*

The analytical and experimental hysteretic response comparison is given under Figure 4.17. The crack pattern observed at a storey displacement of 74mm for specimen PC-1 and PC-2 is compared in

Figure 4.18. The ultimate storey shear capacity with its respective storey displacement obtained analytically is also compared in detail and the percentage error is summarized in Table 4.5 and Table 4.6. Furthermore, additional seismic response parameters were investigated under Table 4.7.

As can be seen from the Hysteretic curves of Specimen PC-0, PC-1, and PC-2, the analytical model slightly underestimated the loads at the pre-peak response (before the 5th cycle) compared to the experimental result. The analytical and experimental results correlate fairly around the peak response (at the 5th cycle) and at the post-peak response (after the 5th cycle). According to this observation, the analytical response was softer and dissipated with lesser energy than the experimental one in the early stages of loading. At the last loading cycle, the stiffness of the analytical response and the experimental test was

comparable but the analytical model dissipated lesser energy. The Variation of analytical and experimental results was not that significant but the difference could be due to the material models assigned, mesh size used, rate of cyclic loading, and idealized boundary conditions in the FEM.

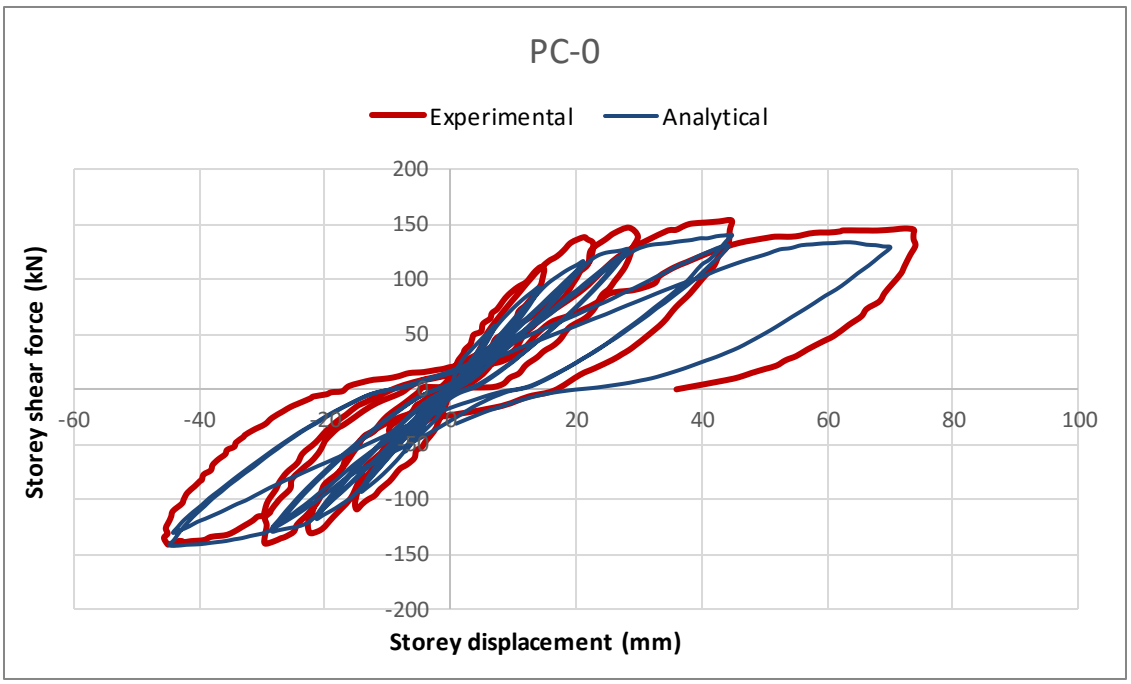

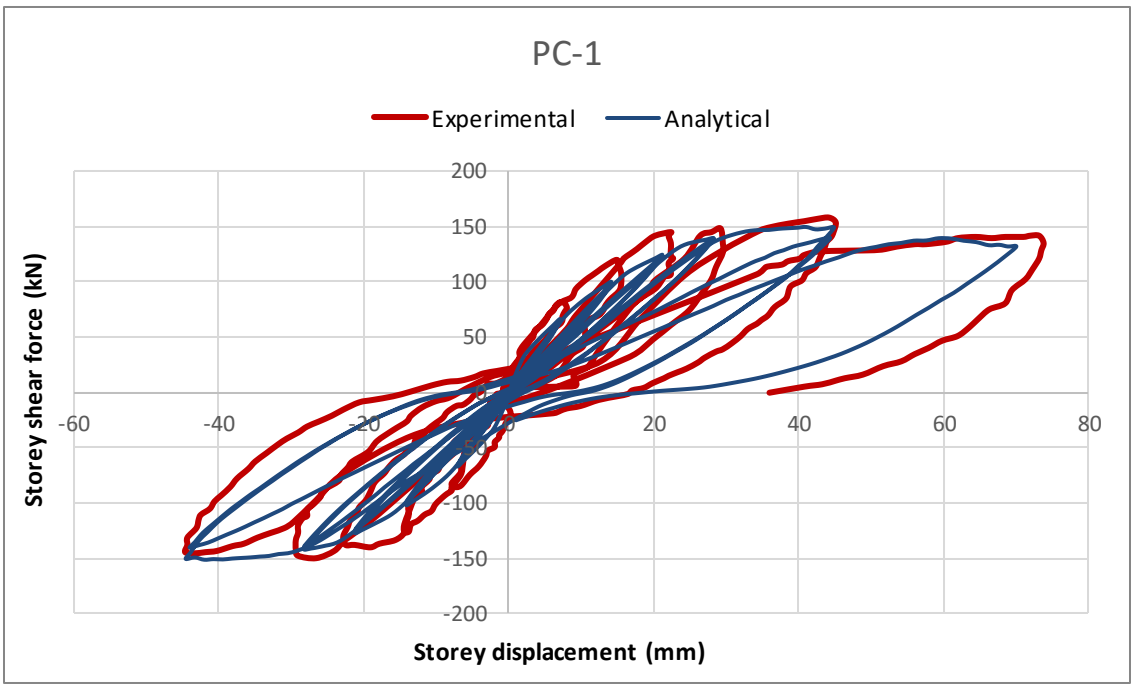

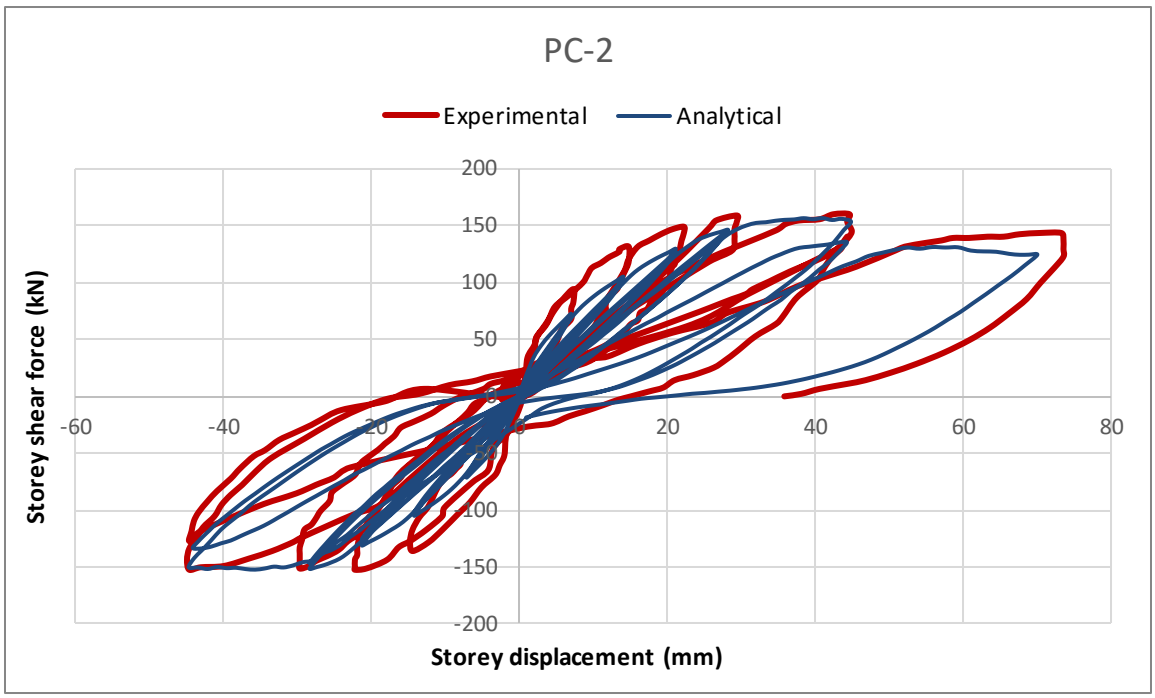

Figure 4.17 Analytical & experimental hysteretic response comparison for Specimen PC-0, PC-1, and PC-2

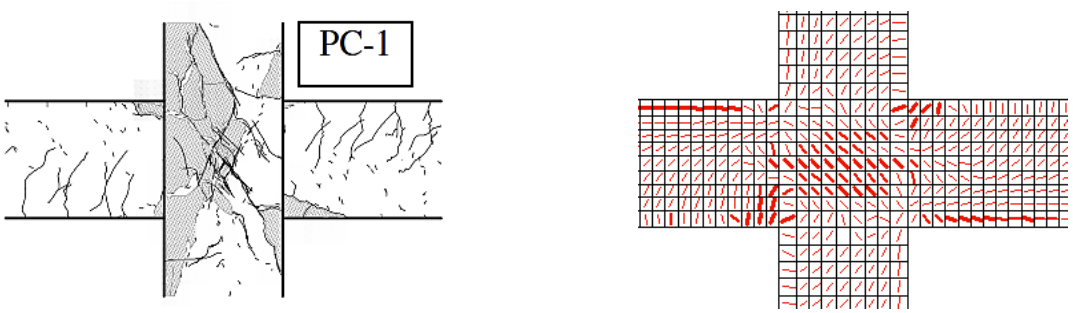

(a) Specimen PC-1 (Left: Experimental and Right: Analytical model)

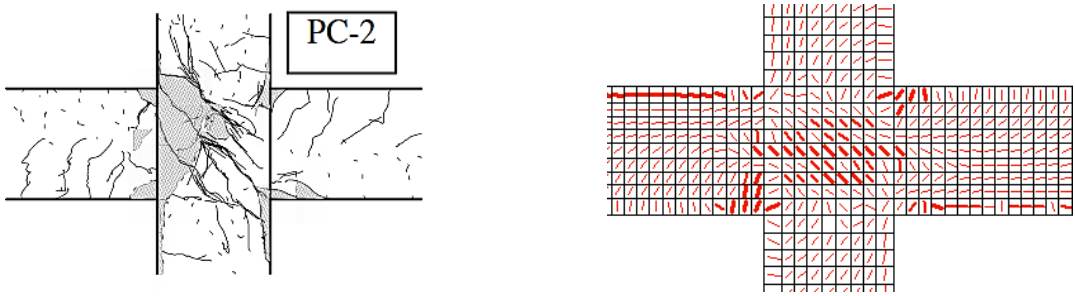

(b) Specimen PC-2 (Left: Experimental and Right: Analytical model)

Figure 4.18 Experimental and Analytical comparison of crack patterns observed at a storey displacement of 74mm for specimen PC-1 and PC-2

Table 4.5 Ultimate Storey shear capacity comparison between the experimental and analytical model

Specimen	Maximum storey shear (kN)					
	Positive loading			Negative loading		
	Experimental	Analytical	Error (%)	Experimental	Analytical	Error (%)
PC-0	157	143.18	+8.80	141.4	140.59	+0.57
PC-1	157	154.5	+1.59	149.7	146.2	+2.34
PC-2	159	159.12	-0.08	151.9	162.2	-6.35

N.B: The negative values imply that the analytical model overestimates the result while the positive values indicate the analytical model underestimates the result

Table 4.6 Storey displacement comparison between the experimental and analytical model

Specimen	Storey displacement (mm)					
	Positive loading			Negative loading		
	Experimental	Analytical	Error (%)	Experimental	Analytical	Error (%)
PC-0	43.8	44.91	-2.47	44	44.63	-1.41
PC-1	44.7	42.3	+5.37	28	30.7	-8.79
PC-2	44.7	44.9	-0.45	39.5	39.7	-0.50

N.B: The negative values imply that the analytical model overestimates the result while the positive values indicate the analytical model underestimates the result

Generally, results show that the hysteretic response from the experimental program correlated fairly well with the analytical result. The analytical model captures the failure mechanism and the hysteretic behavior of the specimens with prestressing levels of 0%, 25%, and 50% of tendon yield strength. However, since no experimental program was executed for the interior joint specimens with a prestress level of more than 0.5fyp, further validation was made on exterior joint specimens with prestress level of 0.59 fyp in the next section.

Table 4.7 Experimental and analytical comparison of seismic response parameters for specimen PC-0, PC-1 & PC-2

Parameters	Experimental	Analytical	Comparison remark
Shear strength degradation after peak response	Small	Small	Deterioration of shear capacity after the maximum storey shear force in the experiment is similar to the Vector2 model.
Pinching effect	Moderate	Moderate	VecTor2 model fairly simulated the pinching behavior as shown in Figure 4.17.
Failure mechanism	Joint shear failure	Joint shear failure	A similar failure mechanism is observed in both the experiment and VecTor2 model
Joint Cracks	Remarkable	Remarkable	Remarkable joint cracks are observed in both the experiment and Vector2 model as shown in Figure 4.18.
Maximum displacement (mm)	74	70	VecTor2 model slightly underestimated the maximum storey displacement experienced by the specimen with a 5.41% error.

4.3.2 Partially prestressed concrete exterior beam-column joint

In this study, further validation on the effect of the prestressing level was made on partially prestressed concrete exterior beam-column joint (PPC exterior BCJ) specimen which was taken from an experiment conducted at Kyoto University [6]. Explanation about the experiment and validation is given in the preceding sections.

4.3.2.1 *Experimental data*

From this experimental study, one post-tensioned PPC exterior BCJ with a prestress of $0.59f_{yp}$ with no column axial load was selected for further validation, as shown in Table 4.8. This specimen has an anchorage location outside the joint. At the final stages of loading, the joint failed in shear after longitudinal reinforcement yielding.

Table 4.8 Prestresss assignment for the PPC exterior BCJ specimen

Specimen	Joint type	Experimental Program	Prestress (MPa)
KPC2-1	PPC exterior BCJ	Reverse cyclic loading	$0.59\ f_{yp}$

4.3.2.2 *Regional and material definition*

The PPC exterior BCJ specimens were modeled with 9 regions, composed of 1040 rectangular elements and 424 truss elements to represent the concrete and reinforcement properties as shown in Figure 4.19. Two regions were assigned in each column and beam section to represent concrete cover and confined reinforced concrete. One confined concrete region was assigned to the joint. While the beam section was composed of three regions. The two regions being confined reinforced concrete sections with different lateral reinforcement ratios and one region being the concrete cover. A stiffened region was also assigned at the outer part of the joint to represent the anchorage plate. The last two regions were a stiffened load bearing and support regions, by which the reverse cyclic load and restraint conditions are applied. These stiffened elements are modeled as structural steel elements to facilitate a proper loading transfer to the beam without unrealistic local failures. A rectangular mesh was used with an element size of 25x30mm at the beam region and 30x30mm for the rest of the regions.

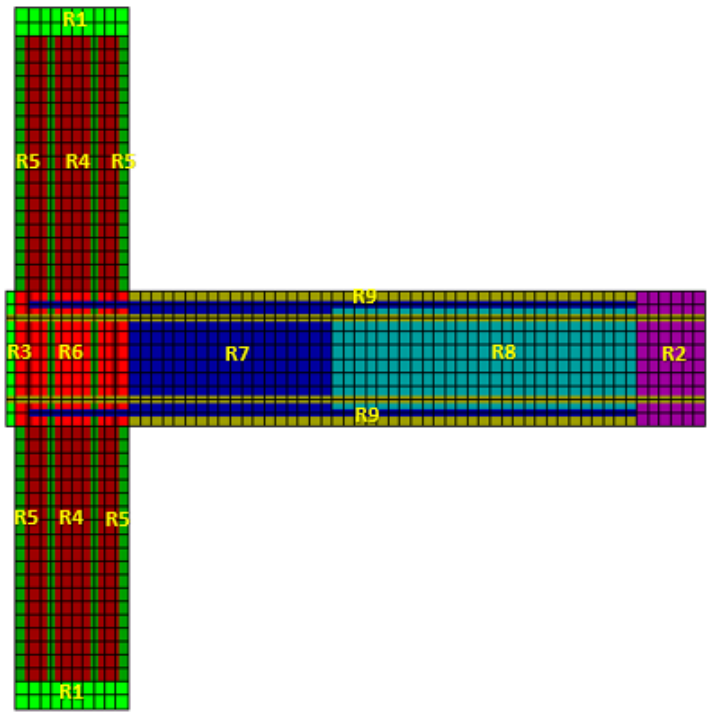

Figure 4.19 Material region definition for the PPC exterior BCJ specimens in VecTor2

The confined concretes (R4, R6, R7, and R8) were modeled with in-plane and out-plane smeared reinforcements by assigning transverse reinforcement ratio (ρ_x, ρ_y *and* ρ_z) which

were calculated as per EN 1992-1-1 [38] section 9.2.2 (5). A transverse reinforcement ratio of 0.63% for column (R4) & joint (R6); 1.57% and 0.98% for 2 regions in the beam (R7 and R8) was obtained, respectively. Truss elements were assigned to both longitudinal reinforcements and prestressing steels. Material properties for concrete, lateral and longitudinal reinforcement definitions were used according to the experiment.

4.3.2.3 *Link element*

In this analytical model, a bond-link element was created to allow a slip of reinforcement over the concrete. The link element is modeled at the joint and some portion of the beam since these regions face high bond stress during cyclic loading. The rest of the concrete regions were kept to be perfectly bonded with the local reinforcement. Two bond properties were assigned in the link elements. The top and bottom end reinforcement of the joint was hooked at an angle of 90^0. Slip of reinforcement at hooked ends is approximately zero. Thus, a perfect bond was assumed at this specific node. Similarly, the prestressing steel was welded to a 20cm thick anchorage steel plate. Thus a perfect bond was also assumed inside the anchorage plate. The bond-slip behavior for the rest of the nodes was modeled by introducing a confinement pressure (β) factor. The detailed arrangement of the bond-link elements is given in Figure 4.20.

4.3.2.4 *Initial stress definition*

As explained in detail under the prestressed concrete interior beam-column joint validation section, here also a predefined field strain method was used to define the amount of prestrain applied on the prestressing steel. A prestrain of $3.01x10^{-3}$, which is 59% of the tendon yield strain, as defined in the finite element software.

4.3.2.5 *Loading*

In this study, three load cases were defined. Load case 1 was a monotonic loading which was assigned the own weight of the specimen. Load case 2 and 3 is a reverse cyclic loading which was applied progressively at the beam ends as shown in Figure 4.20. The first five loading cycles were assigned in load case 2 and the last cycle was assigned in load case 3. The applied lateral displacement pattern is shown in Figure 4.21.

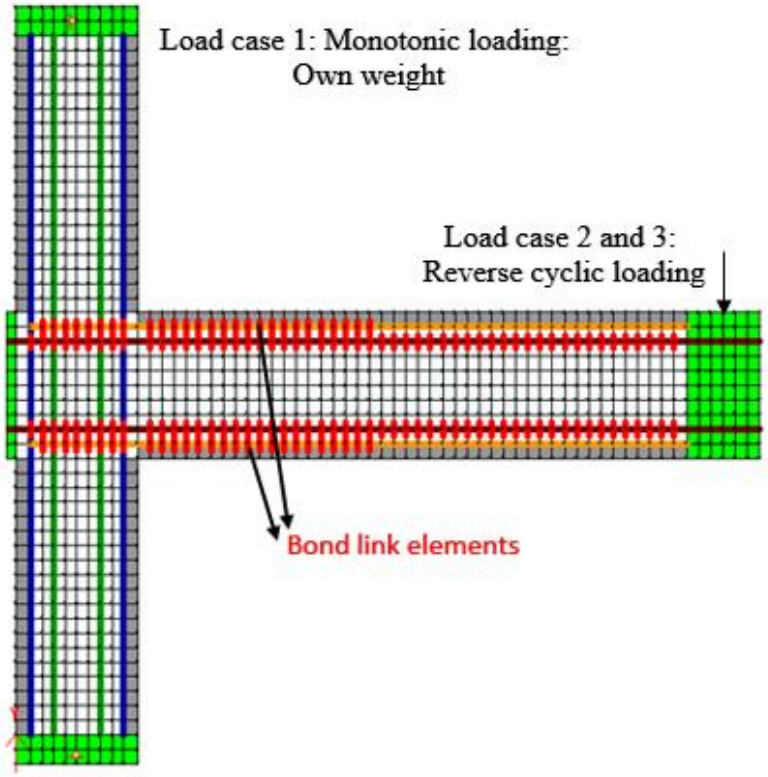

Figure 4.20 Bond link element and loading definition for PPC exterior BCJ in VecTor2

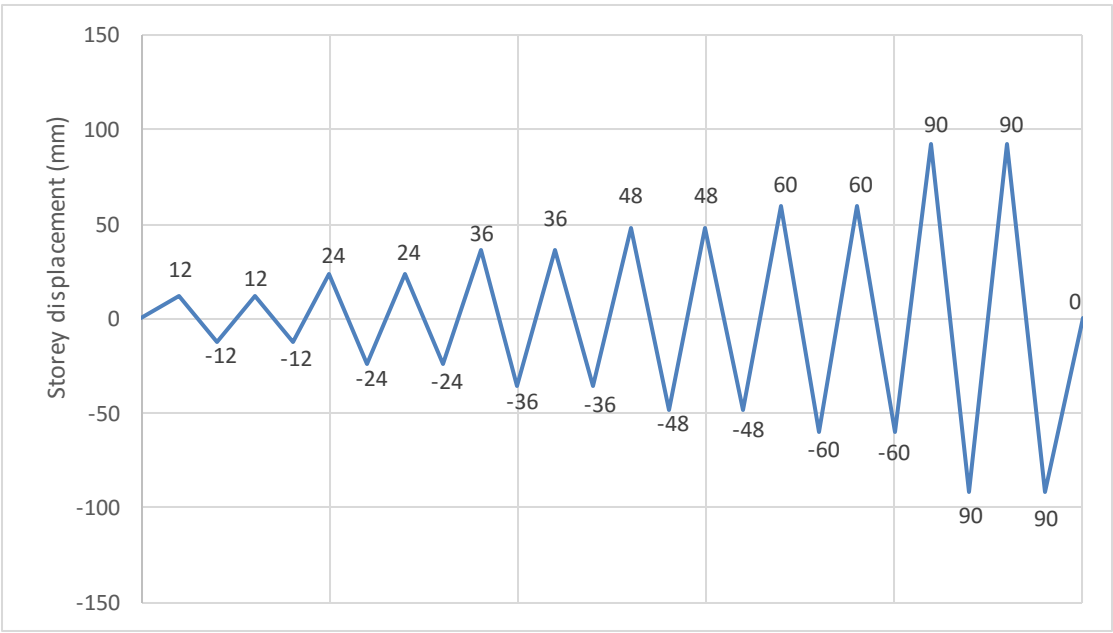

Figure 4.21 Lateral displacement history in PPC exterior BCJ

4.3.2.6 *Analytical result*

The hysteretic response in terms of storey shear force and storey displacement was obtained as shown in Figure 4.22. The storey displacement is the displacement equal to the lateral displacement history applied at the beam end as shown in Figure 4.21. The storey shear force is the lateral reaction at the beam end under the applied lateral displacement.

4.3.2.7 *Analytical and Experimental result comparison*

Analytical and experimental hysteretic response comparison for specimen KPC2-1 is shown in Figure 4.23. Comparison based on the crack pattern observed at a storey displacement of 36mm was also made as shown in Figure 4.24. The ultimate storey shear Vs story displacement obtained analytically was also compared in detail and the percentage error is summarized as shown in Table 4.9. Furthermore, additional seismic response parameters were investigated for further validation under Table 4.11.

As can be seen from the Hysteretic curve of Specimen KPC2-1, the analytical model slightly overestimated the loads at the pre-peak response (before the 3rd cycle) compared to the experimental result. The analytical and experimental results correlate fairly at the peak response (3rd cycle). According to this observation, the analytical model was stiffer and dissipated more energy than the experimental one in the early stages of loading.

At post-peak response (5th and 6th cycle) the analytical model underestimated the results relative to the experimental one, especially at the 6th cycle. The error occurred at this loading cycle was significant compared to previous cycles. Strength degradation after peak response was remarkable as the number of loading cycles increases. Accordingly, the analytical model becomes softer and dissipated less energy compared to the experimental model. Since the specimen undergoes 3 repeated loading cycles after peak capacity is attained, material nonlinearities are more pronounced with remarkable crack formation at the later cycles. Therefore, the software's capability in capturing the response at the last cycles was questionable. These responses might be improved by using 3D finite element software's since 3D models have the ability to capture crack propagation in the out of plane direction which results in smaller crack width close to the concrete surface near reinforcements.

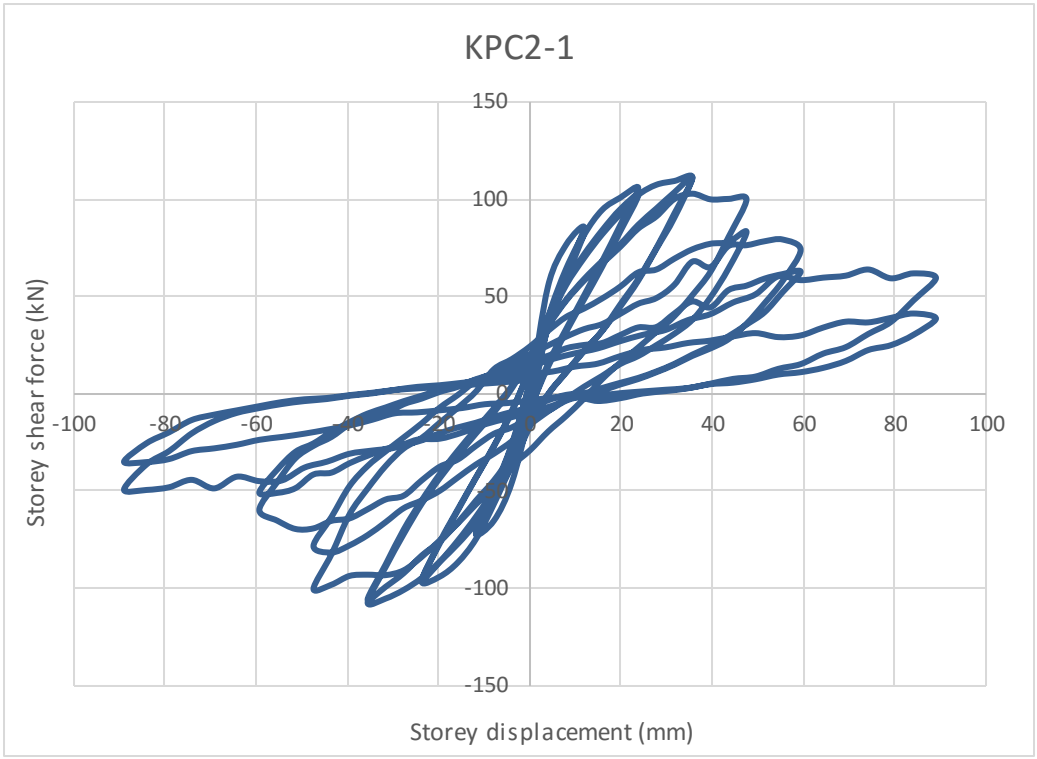

Figure 4.22 Hysteretic response of specimen KPC2-1 according to VecTor2

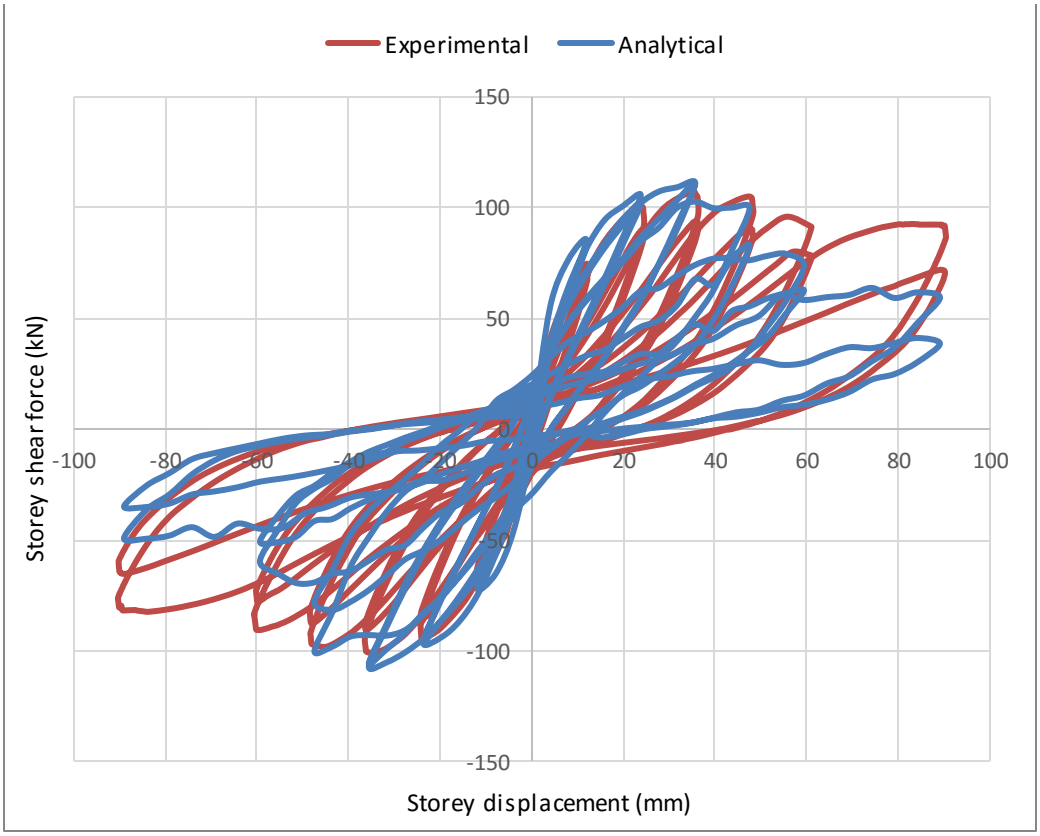

Figure 4.23 Analytical & experimental hysteretic response comparison of specimen KPC2-1

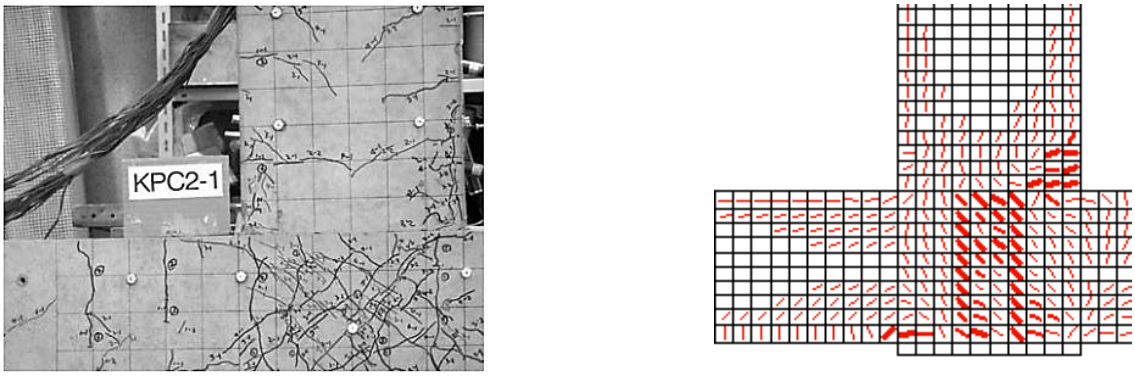

Figure 4.24 Experimental and Analytical comparison of crack patterns observed at a storey displacement of 36mm for specimen KPC2-1

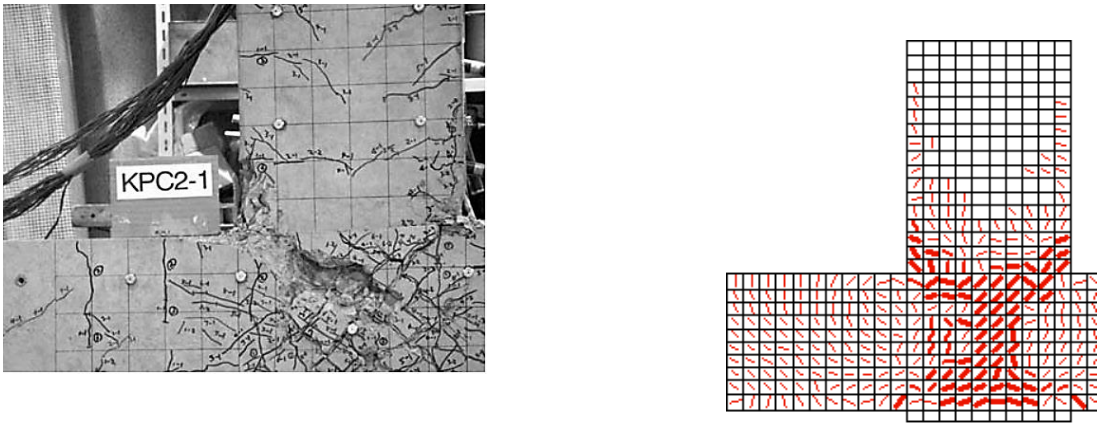

Figure 4.25 Experimental and Analytical comparison of crack patterns observed at a storey displacement of 90mm for specimen KPC2-1

Table 4.9 Ultimate Storey shear comparison between the experimental and analytical model

Specimen	Ultimate storey shear (kN)					
	Positive loading			Negative loading		
	Experimental	Analytical	Error(%)	Experimental	Analytical	Error(%)
KPC2-1	107.3	111.5	3.77	100.7	107.2	6.06

Table 4.10 Storey displacement comparison between the experimental and analytical model

Specimen	Storey displacement (mm)					
	Positive loading			Negative loading		
	Experimental	Analytical	Error(%)	Experimental	Analytical	Error(%)
KPC2-1	35.02	35.6	1.63	35.4	35.6	0.56

Table 4.11 Experimental and analytical comparison of seismic response parameters for specimen KPC2-1

Parameters	Experimental	Analytical	Comparison remark
Shear strength degradation after peak response	Small	Moderate	Shear strength degradation after the ultimate storey shear capacity in the experiment is smaller compared to the analytical result.
Pinching effect	Moderate	Moderate	VecTor2 model fairly simulated the pinching behavior as shown in Figure 4.23.
Failure mechanism	Joint shear failure	Joint shear failure	A similar failure type is observed in both the experiment and VecTor2 model
Joint Cracks	Remarkable	Remarkable	Remarkable joint cracks are observed in both the experiment and Vector2 model as shown in Figure 4.24.
Displacement at yield (mm)	18	16	Fair validation of yield displacement was achieved.
Maximum displacement (mm)	90	89	VecTor2 model perfectly simulated the maximum storey displacement experienced by the specimen.

CHAPTER 5 PARAMETRIC ANALYSIS, ANALYTICAL RESULT AND DISCUSSION

5.1 Parametric analysis

In this study, the previously validated partially prestressed concrete (PPC) beam-column joints (BCJs), exterior and interior, specimens were analyzed using VecTor2. A reverse cyclic lateral displacement loading was applied at the tip of the beams in both types of BCJs to simulate the seismic excitation. The applied storey displacement history was similar to that of the experiments. The effect of two variables was studied: prestressing force level effect and column axial load effect on a highly prestressed BCJ.

The effect of prestressing force level was first assessed by analyzing six PPC exterior BCJs by varying the applied prestress in the prestressing steel (PS), holding other parameters to be constant. The specimen details were defined according to their prestressing force level and tabulated in Table 5.1. The applied prestress level ratio vary from 0 to 0.8 of PS yield strength ($0.8f_{py}$) to capture the seismic behavior over the entire range. According to NZS3101, 1 and 2:1995 (New Zealand Standard) [18], the maximum prestress to be applied in a PS is limited to $0.82f_{py}$, to account for immediate prestress losses that might occur during the prestressing process. Specimen A0P0, A0P25, A0P40, A0P59, A0P70, and A0P80 were subjected to a prestress of 0, $0.25f_{py}$, $0.40f_{py}$, $0.59f_{py}$, $0.70f_{py}$, and $0.80f_{py}$, respectively, as shown in Table 5.1. Column axial load was not applied to these specimens. Specimen A0P0, with 0 prestress, is believed to have an approximately similar response with conventional reinforced concrete (RC) BCJ.

Table 5.1 Summary of prestress loading on PPC exterior BCJ specimens

Specimen	Prestress ratio (%)	Prestress σ_{pp}, (MPa) ($\%f_{py}$)	Prestrain ε_{pp}, (10^{-3}) (σ_{pp}/E_p)
A0P0	0	0.00	0.00
A0P25	25	256.50	1.28
A0P40	40	410.40	2.04
A0P59	59	615.60	3.01
A0P70	70	718.20	3.57
A0P80	80	820.80	4.08

N.B: f_{py} is PS yield strength (1026MPa) and E_p is the modulus of elasticity of PS.

On the other hand, the effect of column axial load on a highly prestressed BCJ was evaluated by analyzing four PPC interior BCJs. The specimens were subjected to an axial load ratio of 0, 0.1, 0.4, and 0.65, respectively. The maximum restriction of the column axial load was made according to EN 1998-1 [39]. Euro code restricts the column axial compressive force ($N_{ED}/A_c f_{cd}$) to 0.65 to limit the adverse effect of cover spalling and avoid the situation where only limited ductility is available due to premature failure. The PSs in all the specimens were prestressed with $0.8f_{py}$ stress. The axial load protocol is tabulated in Table 5.2.

Table 5.2 Summary of column axial loading on PPC interior BCJ specimens

Specimen	N_{ED} (kN)	Axial load ratio, $N_{ED}/(A_c*f_{cd})$
IA0P80	0	0
IA10P80	320	0.1
IA40P80	1238	0.4
IA65P80	2012	0.65

N.B: N_{ED} is the magnitude of column axial load; A_c is the gross sectional area of the column and f_{cd} is the design compressive strength of concrete

5.2 Analytical result and failure mechanism

5.2.1 PPC Exterior BCJs

Six specimens of PPC exterior BCJs (as shown in the parametric analysis) were subjected to a reverse cyclic loading at the tip of their beam and analyzed in the FE software. The seismic performance of the BCJs was evaluated based on the storey shear force vs storey displacement hysteretic response. The storey displacement is the displacement equal to the lateral displacement history applied at the tip of the beam as shown in the validation section of Figure 4.21. The storey shear force is the lateral reaction at the tip of the beam under the applied lateral displacement. Figure 5.1 shows the storey shear vs storey displacement hysteresis response of each specimen. The seismic performance of specimens was evaluated based on storey shear capacity, stiffness, shear strength degradation after peak response, ductility, absorption, and energy dissipation capacity.

At the initial stages of loading, minor diagonal shear cracks at the joints and flexural cracks at the BCJ interface were observed. The crack propagated along the outer edge of the top and bottom column part and the left beam part following the line of tensile stress. These

cracks were similar for all the specimens and shown in Figure 5.2, as the frame sways to the right. As the storey displacement increases, beam longitudinal reinforcement yielded at the beam-column interface. Following the yielding of the rebar, high bond stress was applied at the perimeter of the joint region. This highly minimized the contribution of the diagonal compression strut shear resistance mechanism and the truss mechanism was accelerated. At this point, diagonal shear cracks started to get severe and extended to more than half of the joint dimension. Joint shear reinforcements, which are modeled as smeared reinforcements, yielded progressively throughout the joint area as the cycle goes by. Transverse reinforcements are capable of transmitting tensile force only which results in irreversible inelastic steel strains during subsequent reversal of loading. Based on T. Paulay and M. J. N. Priestley [2] Shear reinforcements can only contribute to shear resistance if the incoming tensile strains are greater than the previously developed ones. Accordingly, drastic loss of stiffness and energy dissipation capacity resulted immediately after progressive yielding of shear reinforcement. Consequently, joint shear failure took place. The stress distribution of longitudinal reinforcements and the yielding percentage of shear reinforcement along with the loading cycles is shown under APPENDIX C. The concrete shear strain distribution and crack pattern at final storey displacement for all specimens are shown in APPENDIX D.

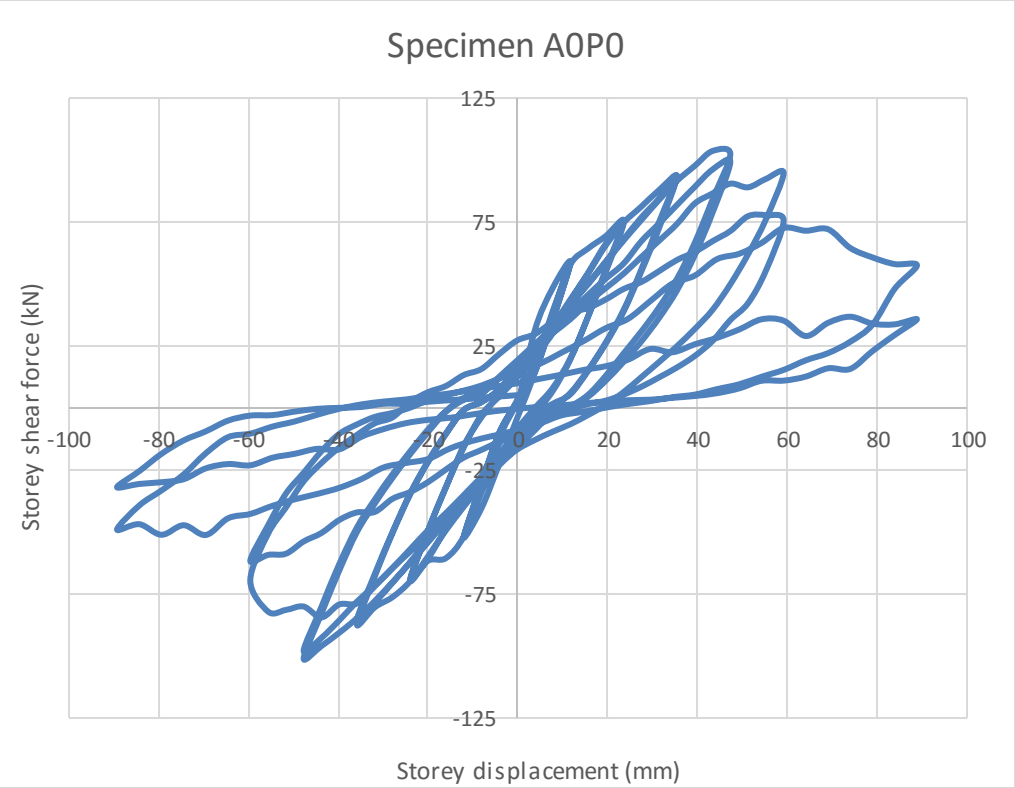


Specimen A0P25
125
75
25
-25
-75
-125
-100
-80
-60
-40
-20
0
20
40
60
80
100
Storey shear force (kN)
Storey displacement (mm)

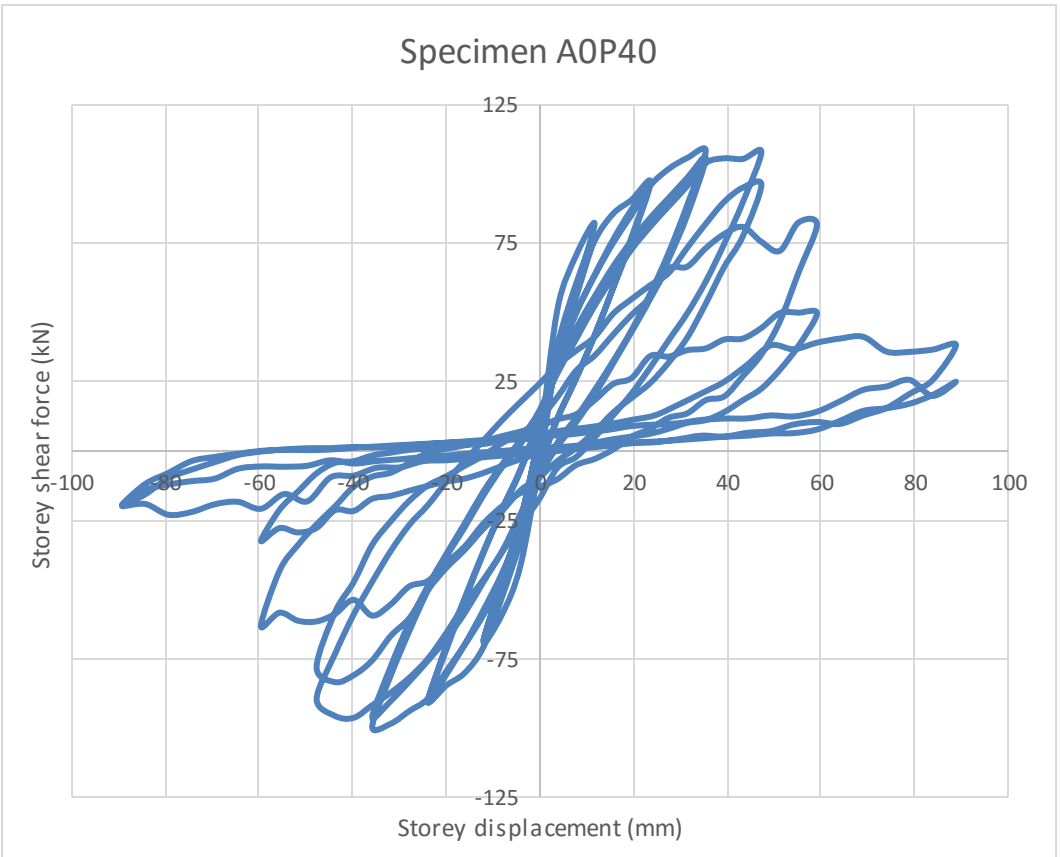
Specimen A0P40
125
75
25
-25
-75
-125
-100
-80
-60
-40
-20
0
20
40
60
80
100
Storey shear force (kN)
Storey displacement (mm)

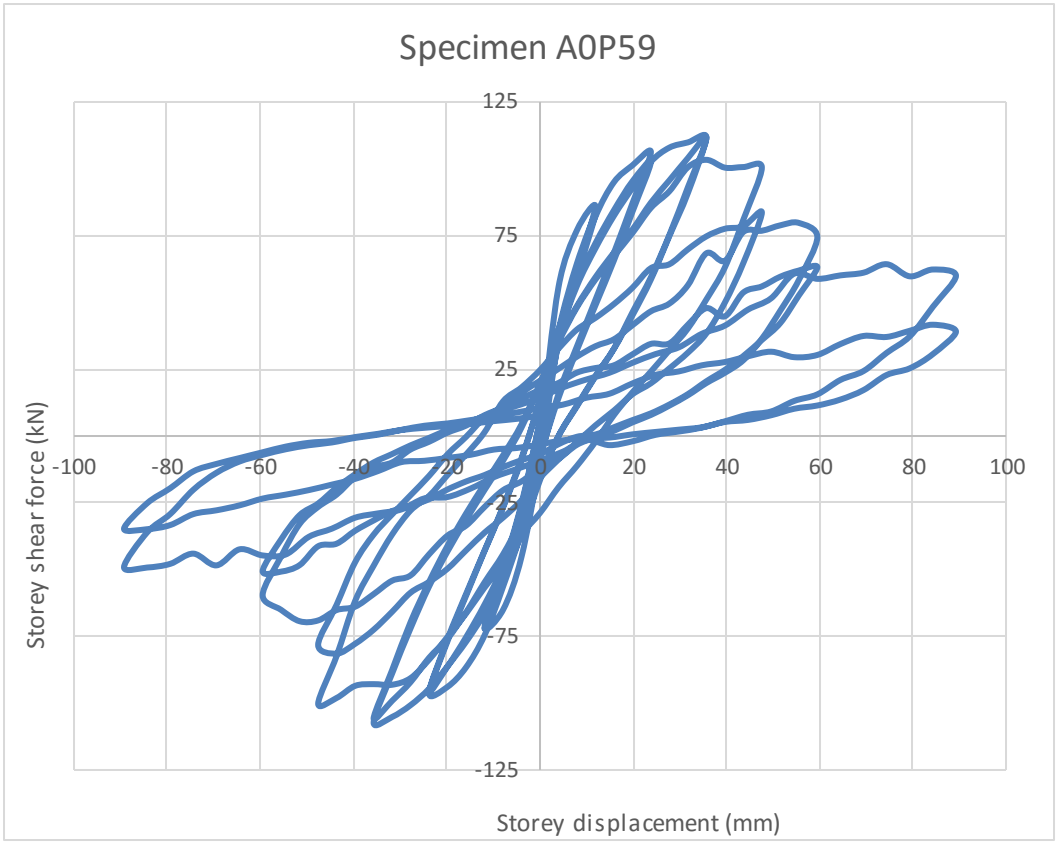
Specimen A0P59
125
75
25
-25
-75
-125
-100
-80
-60
-40
-20
0
20
40
60
80
100
Storey shear force (kN)
Storey displacement (mm)

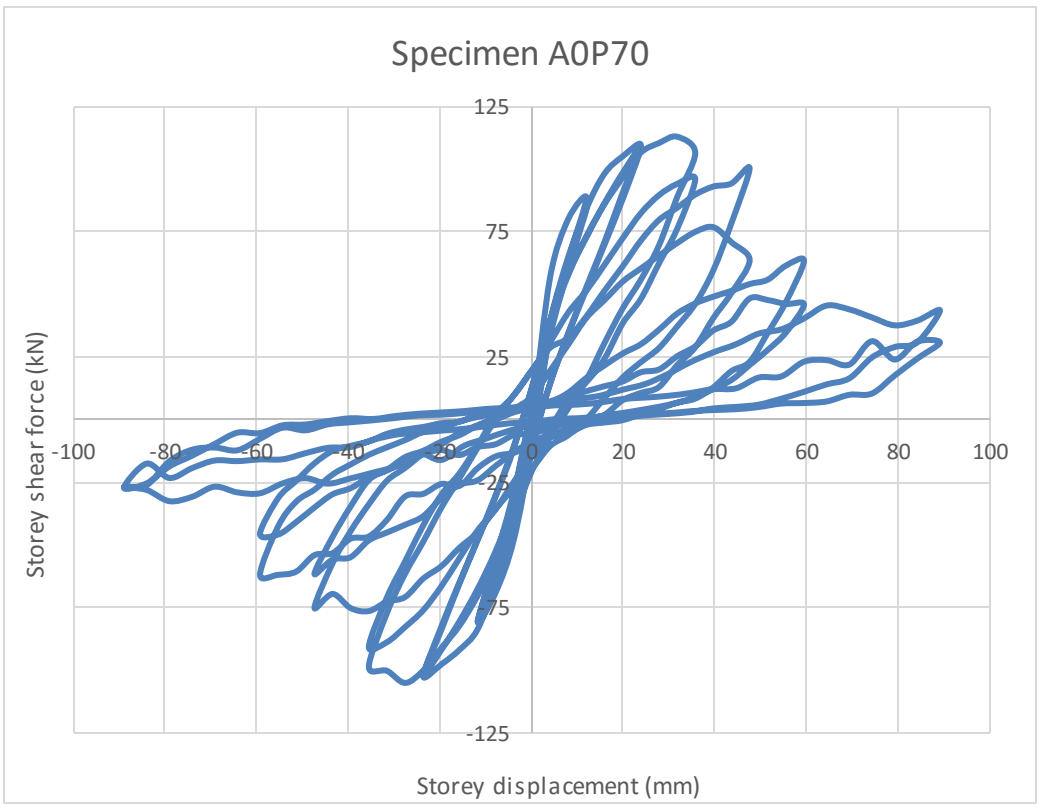
Specimen A0P70
125
75
25
-25
-75
-125
-100
-80
-60
-40
-20
0
20
40
60
80
100
Storey shear force (kN)
Storey displacement (mm)

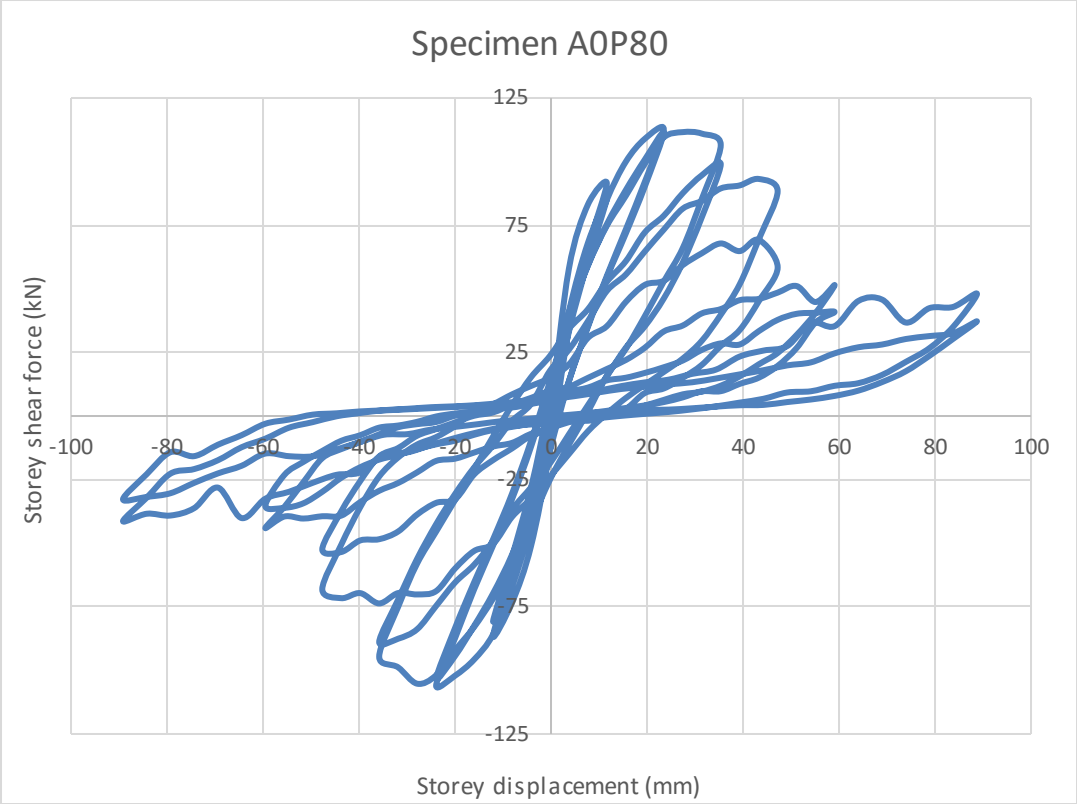

Figure 5.1 Hysteresis response of PPC Exterior BCJs

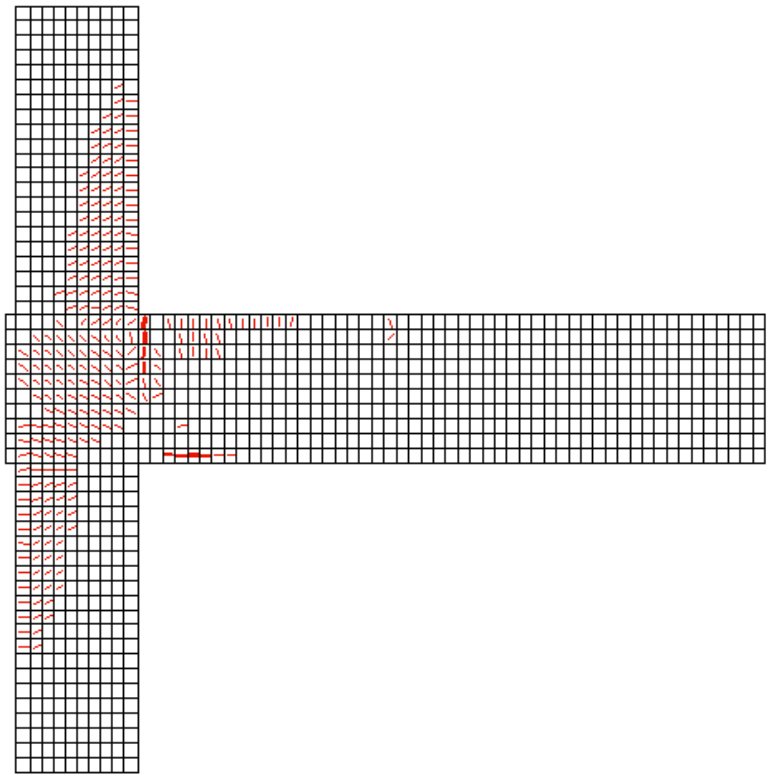

Figure 5.2 First crack observed in the PPC exterior BCJ as the joint sway to the right

5.2.2 PPC Interior BCJs

Four specimens of PPC interior BCJs (as shown in the parametric analysis) were analyzed by applying a reverse cyclic loading at the tip of their beams in the FE software. The specimens were subjected to column axial load ratio, $\frac{N_{ED}}{A_c f_{cd}}$, of 0, 0.1, 0.4, and 0.65 at the top of the column. All the specimens were highly prestressed with $0.8f_{yp}$ stress. The seismic performance of the BCJs was evaluated based on the storey shear force and storey displacement hysteretic response as is done in the PPC exterior BCJs. Figure 5.3 shows the storey shear - storey displacement hysteresis response for each specimen.

In this investigation, two parameters were studied. Primarily, the effect of column axial load on the premature failure of the joint core due to concrete crushing is evaluated. Then the seismic response of specimens was compared in terms of pinching.

Just like the exterior specimens, all the PPC interior BCJ specimens also failed in shear at the joint due to the development of diagonal tensile strain as the loading cycle progresses. At the initial stage of loading, a minor diagonal shear crack at the BCJ and flexural crack at the beam were observed. The crack propagated along the outer edge of the top and bottom column part and the left and right of the beam part following the line of tensile stress. The first observed cracks were similar for all the specimens and shown in Figure 5.4, as the system sways to the left. Following storey displacement increment, the diagonal shear cracks behaved differently for each specimen. In specimen IA0P80, with no column axial load applied, extensive cracks resulted and extended to more than half of the joint dimension as shown in Figure 5.5 (a). Following the application of column axial load, relatively smaller cracks were concentrated around the center of the joint as shown in Figure 5.5 (b) for specimen IA10P80. For a higher axial load ratio of 0.4 and 0.65, specimen IA40P80 and IA65P80, cracks were very minimal and concentrated horizontally at the center of the joint as can be seen in Figure 5.5 (c) and (d). The performance of cracks in the joint was improved due to the effect of confinement resulted from the column axial load. The contribution of the diagonal compression strut mechanism for shear resistance was significantly enhanced following the column axial load application. This mechanism accelerated the bond performance between the beam reinforcement and the surrounding concrete. Due to good bond performance, stress transfer from the reinforcement to the

compression strut region was highly facilitated. Accordingly, the joint core became more and more confined against shear crack and joint performance was improved in general.

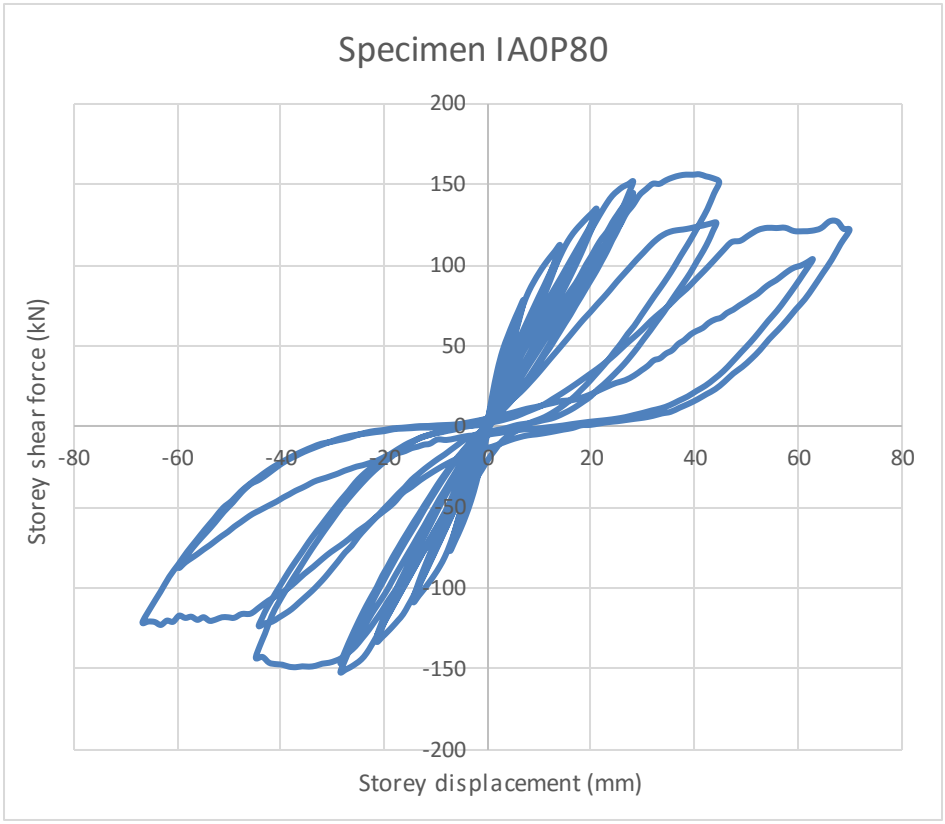

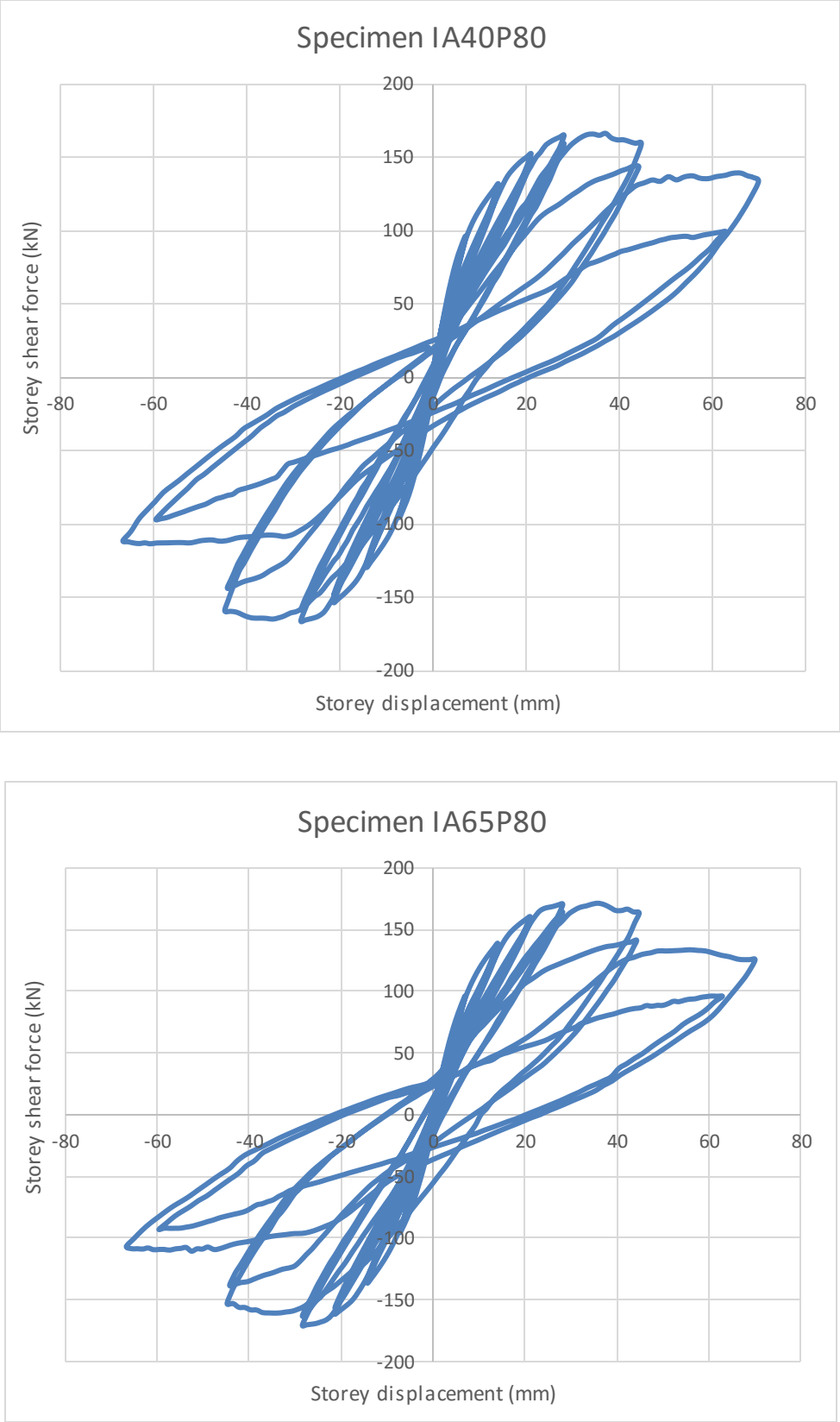

Figure 5.3 Hysteresis response of PPC Interior BCJs

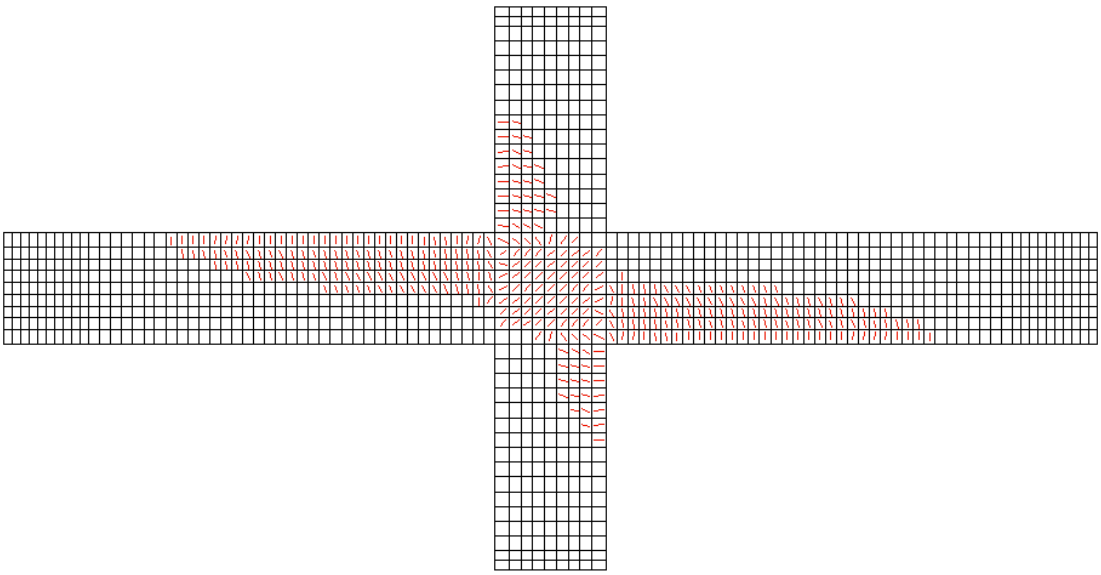

Figure 5.4 First crack observed in the PPC interior BCJs as the joint sway to the left

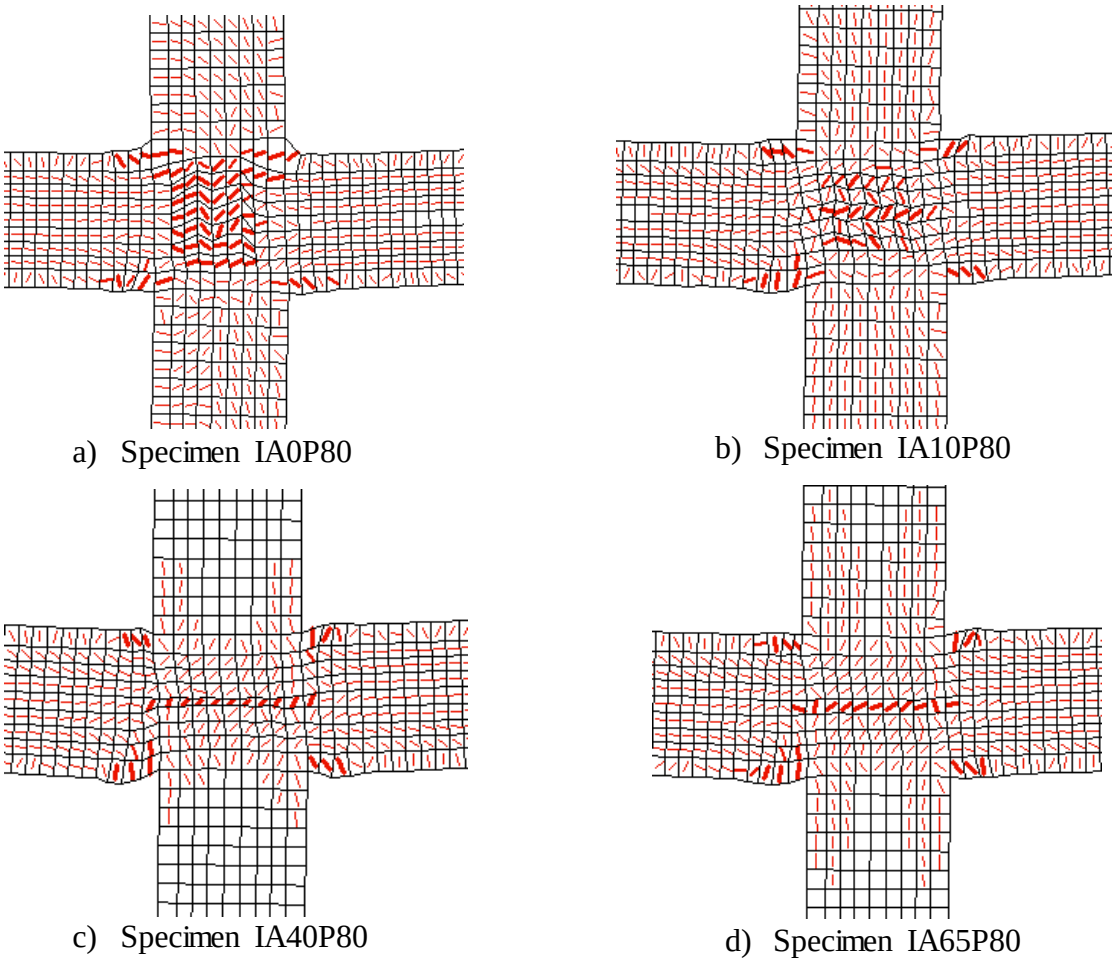

a) Specimen IA0P80

b) Specimen IA10P80

c) Specimen IA40P80

d) Specimen IA65P80

Figure 5.5 Crack pattern at final loading stage of PPC interior BCJ

5.3 Response evaluation parameters and methods

5.3.1 Storey shear strength

Strength can be defined as the capacity of a member or assembly of members to resist incoming loads. Shear, bending and axial resistances are used to measure the performance of members in earthquake engineering. In concrete moment resisting ductile frame structures, it is required that BCJs have sufficient strength to develop and maintain the flexural capacity of the beams. Thus to meet this requirement, knowing the ultimate capacity of BCJs is very essential. In this study, the storey shear force is the lateral reaction at the tip of the beam under the applied lateral displacement and is obtained directly from the FE software post processer program, Augustus. The ultimate storey shear capacity is the maximum shear force that can be laterally resisted by the joint specimen, which is obtained from the hysteretic response.

5.3.2 Stiffness

The relationship between action and deformation of a structure is often expressed by stiffness. Member stiffness is a function of three parameters; length, section properties, and boundary conditions while system stiffness is a function of lateral resisting mechanisms utilized such as moment-resisting frames. The stiffness of a system is highly related to the satisfaction of serviceability (or functionality) of a structure under dynamic loads. Consequently, high deformability results in low stiffness which intern reduces the structural functionality drastically. A reduction in stiffness indicates the softening of a structure under load.

Lateral stiffness is a very essential parameter for structures subjected to earthquake excitation, as the horizontal components of inertial forces generated due to vibration are often dominant. Adequate lateral stiffness is important to control deformations, prevent instability, ensure human comfort during vibration and prevent damage to non-structural components. When subjected to cyclic loading, reinforced concrete structures exhibit stiffness degradation depending on the loading history and characteristics of the structure. Concrete cracking; yielding of reinforcement bars and loss of bond between the reinforcement and concrete, and other sources of inelasticity are the main causes for reinforced concrete structures to degrade in stiffness.

In this study, the calculated stiffness was expressed in terms of secant stiffness which is mostly the method used in evaluating the response of inelastic structures as discussed under A. S. Elnashai et al [8]. According to S. Eshghi et al [7], if the ultimate loading capacities differ significantly for the positive and negative loading direction, it is recommended to take the average of the stiffness for both directions. Since this is not the case in this study, stiffness was computed from the positive loading portion of the hysteretic curve. A line was drawn from the origin up to the point of maximum storey shear for each loading cycle and the slop is computed according to Equation (5.1).

$$K_i = \frac{P_{max,i}}{\Delta_{max,i}} \tag{5.1}$$

Where $P_{max,i}$ is maximum storey shear capacity per cycle, i, and $\Delta_{max,i}$ is maximum storey displacement per cycle, i.

5.3.3 Ductility

Ductility is the ability of a structure to undergo inelastic deformation prior to collapse without substantial loss in strength. High ductility is essential in seismic design to delay the local failure of members by allowing plastic redistribution of actions from one critical section to another and to allow absorption and dissipation capacity of the input energy. Various factors may lead to a reduction of ductility like over-strength leading to structures not yield; strain rate effects causing an increase in yield strength and the tendency of some materials to exhibit brittle fracture. There are four types of ductility: Material, section (curvature), member (rotation), and system (displacement) ductility. System ductility, μ_Δ, depends on the sectional behavior and member configuration or structural system. It is calculated when stability failure occurs or when lateral displacement reaches its ultimate displacement capacity from the load-displacement curve. Therefore, in this study since the ductility of beam-column assemblages is examined displacement ductility is inspected to evaluate their ductility performance.

According to A. S. Elnashai et al [8], Equation (5.2) can be used to evaluate the ductility imposed on a structure under reversed cyclic loading. This equation reflects the actual maximum deformations experienced by the member due to reverse cyclic response under earthquake loads, strength degradation, cyclic stiffness, and residual plastic deformations.

$$\mu_{\Delta} = \frac{|\Delta^{+}_{max}| + |\Delta^{-}_{max}|}{|\Delta^{+}_{y}| + |\Delta^{-}_{y}|} = \frac{\Delta_{max,avg}}{\Delta_{y,avg}} \quad \textbf{(5.2)}$$

Where "Δ^{+}_{max}" and "Δ^{-}_{max}" are the positive and negative deformations at 75% of ultimate shear strength that can be imposed on the structure under several cycles of loading without significant loss in strength and "Δ^{+}_{y}" and "Δ^{-}_{y}" are the corresponding deformations at the yield point.

Ultimate displacement (Δ_{max}) is the displacement corresponding to the maximum load-carrying capacity. But since this definition is too conservative different codes suggest an acceptable limit of load-carrying capacity reduction after peak response. The ultimate deflection greatly depends on the degree of damage to the structural member that can be tolerated by practicing engineers. According to EN 1998-1 [39] and R. Park et al [3], the ultimate displacement is taken to be the displacement that corresponds to a load that drops 15 percent from the peak (displacement at 85% of the ultimate shear strength). While in A. Tsiavos et al's study [40], they allowed using a displacement corresponding to a reduction of 20 to 25 percent load carrying. Thus, in this study the deformation that corresponds to more than a 25 percent load drop was not considered, to avoid using unrealistically high member deflection.

The definition of yield displacement (Δ_{y}) often cause difficulty since the load-deformation response doesn't have a well-defined yield point. In reinforced concrete structures, taking the yield displacement which corresponds to the yielding of reinforcing steel might be unsafe when a small amount of reinforcement ratio is present in a section. While in prestressed concrete members, taking the yield displacement that corresponds to the yielding of prestressing steels might be very conservative. Thus, considering these problems, A. S. Elnashai et. al. [8] proposed a different way of determining the yield displacement. It is computed as the secant stiffness at 75% of the ultimate lateral load of the real system.

5.3.4 Energy dissipation capacity

For strong seismic excitation, a large portion of the input energy is dissipated through hysteretic action which is mostly associated with the damage potential of the structure. Ductility factors are written in terms of deformations only thus they do not give a measure

of the energy dissipation of the structural systems. Energy dissipation during loading is the area enclosed by the hysteresis loops of the load-displacement curve. In this study, the accumulated dissipated energy (ADE) was computed by taking the summation of the product of storey shear force and storey displacement for each loading cycle as shown in Equation (5.3). This equation is based on A. Sayed and A. Tawfik's [9] study.

$$ADE = \sum_{LS_i}^{LS_f} |V_{ED} * d| \tag{5.3}$$

Where "ADE" is the accumulated dissipated energy; "LS_i" is the initial loading stage; "LS_f" is the final loading stage; "V_{ED}" is the storey shear force and "d" is storey displacement.

5.4 Discussion

5.4.1 Effect of prestressing force

Prestress subjects compressive stress in a concrete member prior to external load application. This phenomenon is captured in the FE software as shown in Figure 5.6. In the figure, negative stress indicates compressive stress and positive stress indicates tensile stress at zero loading stage. It can be seen that for the specimen with no initial stress applied (A0P0) no compressive stress is observed at the joint. On contrary, the rest of the specimens were under compression according to the prestress level applied. More confinement was observed for joints with higher prestress levels.

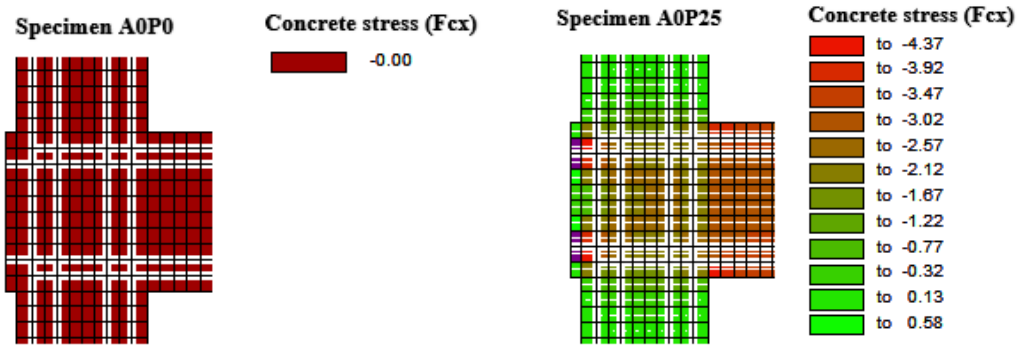

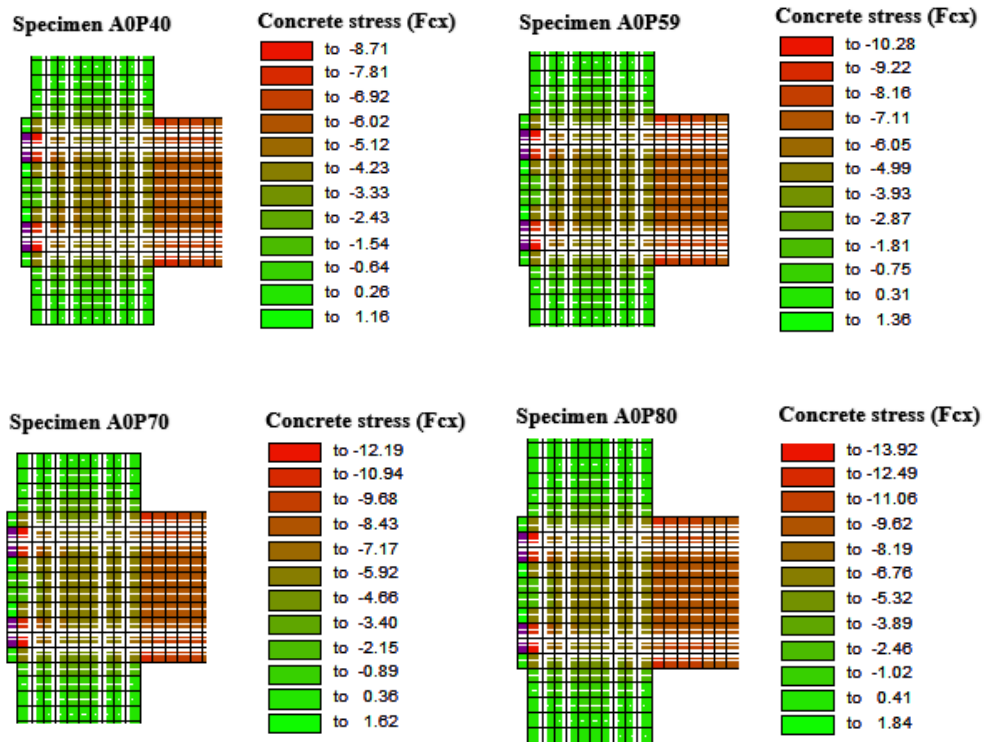

Figure 5.6 Concrete stress (MPa) in PPC exterior BCJs at zero loading stage

5.4.1.1 *On shear strength of PPC exterior BCJs*

As explained in the previous section, the ultimate storey shear capacity was one of the parameters that are utilized to evaluate the seismic performance of the PPC BCJ under reversed cyclic loading. Figure 5.7 displays the effect of prestressing force on the ultimate storey shear capacity of the specimens. As it can be observed, the prestressing force resulted in an insignificant effect on the ultimate storey shear capacity, under both positive and negative loading protocol. In reference to specimen A0P0, a percentage ultimate shear capacity increment of 5.3%, 3.9%, 7.2%, 8.9%, and 8.6% was obtained for specimen A0P25, A0P40, A0P59, A0P70, and A0P80, respectively, in the positive loading direction. Additionally, a percentage ultimate shear capacity increment of 3.7%, 6.1%, 3.7%, and 4.7% was obtained for specimens A0P25, A0P59, A0P70, and A0P80, respectively, in the negative loading direction. Prestress level did not show a significant effect on the ultimate storey shear strength maybe because, under higher cyclic displacement prestressed concrete sections resemble the behavior of reinforced concretes. D. Mitchell and M. P. Collins [41] stated that, prestressed concretes have no significance in providing resistance after crack is developed within a section. The extensive crack formation in the joint shifted the shear resistance mechanism from strut to truss mechanism due to high bond stress

around the perimeters of the joint. This mechanism employs high stress against the transverse reinforcements. Accordingly, the shift of the shear resistance mechanism weakened the confinement of the joint supplied by the prestressing steels, which degrades its contribution in resisting shear. As shown under APPENDIX C (C.2), the shear reinforcements started to yield after the 2nd loading cycle, thus before the ultimate capacity is achieved in any of the specimens. This information implies that the strut region of the joint is being destroyed and most of the shear resistance is provided by the transverse reinforcements, truss mechanism. Therefore, after the 2nd cycle, the role of the prestressing steels in assisting the strut resistance mechanism by providing confinement to the joint started to decrease. Thus, prestressing force did not play a prominent role in enhancing the storey shear capacity. This conclusion is also supported by T. Kashiwazaki and H. Noguchi [5], as discussed in the literature review.

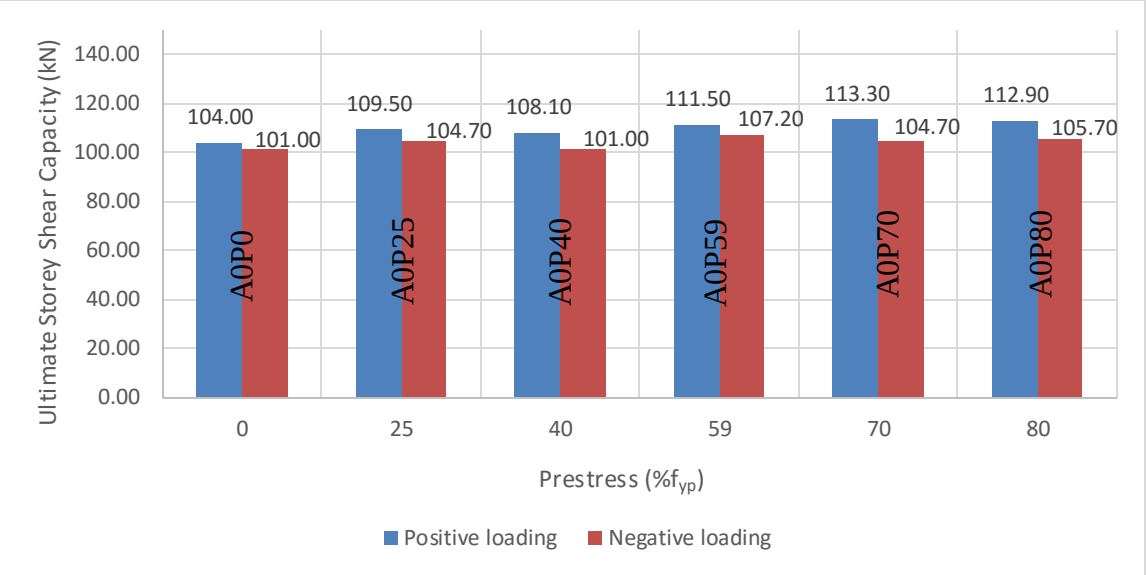

Figure 5.7 Effect of prestressing force on the ultimate shear capacity of PPC exterior BCJs

5.4.1.2 *On ductility*

High ductility is essential in seismic design to delay the local failure of members by allowing plastic redistribution of actions from one critical section to another and to allow absorption and dissipation capacity of the input energy. Figure 5.8 shows the effect of prestressing force on the displacement ductility factor. It can be seen that the increase in prestressing force in the BCJ resulted in a substantial increment in the ductility of the specimen. From the analysis result, it can be seen that the yield displacement created a

significant difference in the displacement ductility factor rather than the maximum displacement. The highly prestressed joints were able to delay the onset of yielding according to their prestress level as shown in detail under Table 5.3.

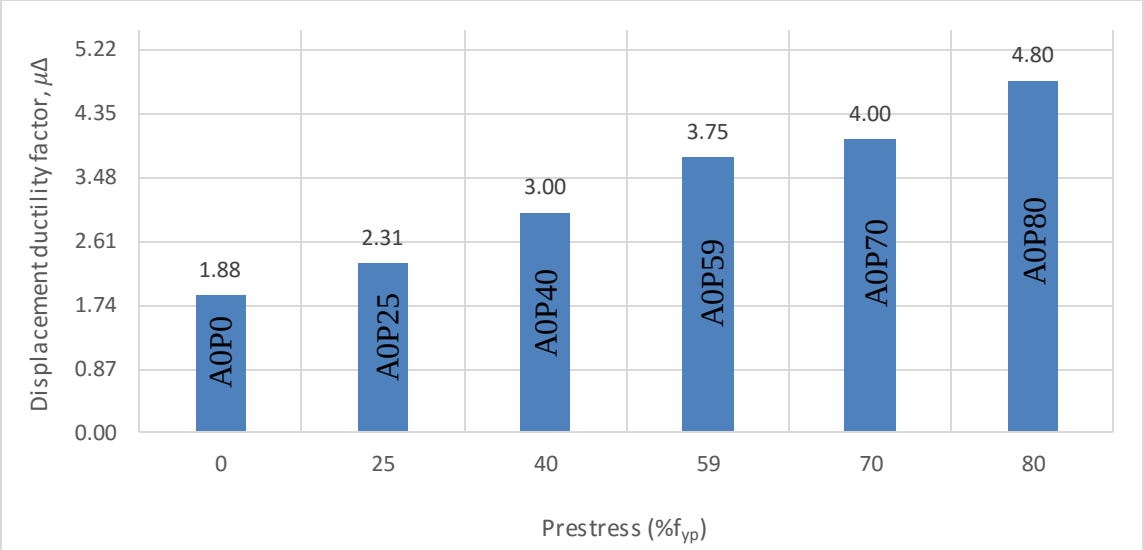

Figure 5.8 Effect of prestressing force on displacement ductility factor

Table 5.3 Displacement ductility factor for PPC exterior BCJs

Specimen	Maximum displacement $\Delta_{max,avg}$, (mm)	Yield displacement $\Delta_{y,avg}$, (mm)	Displacement ductility μ_Δ	Ductility remark (D. Dowrick [43])
A0P0	60	32	1.88	Limited ductility
A0P25	60	26	2.31	Limited ductility
A0P40	60	20	3.00	Limited ductility
A0P59	60	16	3.75	Fully ductile
A0P70	48	12	4.00	Fully ductile
A0P80	48	10	4.80	Fully ductile

Beams under flexure are usually designed as tensioned controlled members by which reinforcing steels yield before concrete crushes. Concrete is considered as a brittle material that gives no time and warning before collapse. This results in a significant reduction of ductility if concrete fails prior to reinforcing steel. Thus, an increase in yield strength can have a negative impact on the ductility of a member. Accordingly, the major advantage of introducing prestressing steel in concrete is to make up for the weakness of concrete under tensile stress. Due to the primarily applied compressive stress, prestressed concrete members initially go through a negative deformation according to the prestress level.

Following the application of external load, the member starts to deform contrary to the negative deformation and the deformation becomes zero at a specified point of external loading. At this point of zero deformation, they are active in providing resistance, unlike reinforced concrete members which resist no force at zero displacements. After the development of tensile cracks, their behavior becomes more or less similar to reinforced concrete members. Thus, since prestressed members compensate for the incoming positive deformation at the initial stages of loading, the structural yield and ultimate shear capacities were achieved at lower deformation. The higher the prestress the smaller the yield and ultimate displacement.

The conclusion made in this section is reasonable based on A. E. Naaman and J. K. Wight [23]. They demonstrated an experimental program of a partially prestressed concrete beam to study the effect of the level of prestress ($0 - 0.6f_{yp}$) on the curvature ductility of the section. It was observed that the increase in the level of prestress lead to a substantial decrease in the yield curvature, which in turn increased the curvature ductility of the section.

5.4.1.3 *On stiffness of PPC BCJs*

The secant stiffness of each joint specimen was calculated according to Equation (5.1) and is presented under Table 5.4 for each loading cycle. Figure 5.9 shows the prestessing force effect on the stiffness of PPC exterior BCJs under each loading cycle. The analysis results show that prestressing force significantly increases the stiffness of the joint before the loading protocol reaches the 4^{th} cycle. Percentage variation of stiffness up to this cycle, about specimen A0P0, is clearly stated under Table 5.5.

The displacement encountered by each specimen, at each loading cycle, to reach their shear capacity varies significantly. To clearly show this effect, storey shear - storey displacement pre-peak response is plotted in Figure 5.10 by connecting maximum shear values of each cycle from the hysteresis response. As shown in the figure, the highly prestressed joint, labeled as specimen A0P80, encountered its ultimate shear capacity at a storey displacement of 24mm. While less prestressed joints, labeled as specimen A0P70, A0P59, and A0P40, reached their ultimate shear capacity at a storey displacement of 36mm. The specimen with a prestress ratio of 0.25 and 0, labeled as A0P25 and A0P0, attained their

ultimate shear capacity at a storey displacement of 48mm. According to this, a substantial reduction of storey displacement was encountered at the ultimate capacity, as the applied prestress increases. In conformity with A. S. Elnashai et al [8], stiffer components and structural systems reach their capacity at earlier deformations than flexible elements. Prestressed members can carry nearly equal amounts of shear force with that of the similar reinforced concrete element, without extensive displacement of the member. Corresponding to this, the PPC exterior BCJs with greater prestress levels are subjected to larger compressive stress, which provides good confinement in the joint at the initial stages of loading. This improves the strut mechanism, which delays the development of crack and led highly prestressed joints to reach their capacity at smaller deformations. This conclusion is rational according to M. Nishiyama's research [4] as discussed in the literature review.

Table 5.4 Secant stiffness of PPC exterior BCJs computed for each loading cycle

	Specimen					
Loading Cycle	A0P0	A0P25	A0P40	A0P59	A0P70	A0P80
	Stiffness (kN/mm)					
1	4.99	6.35	6.90	7.23	7.49	7.73
2	3.19	3.81	4.09	4.47	4.63	4.76
3	2.64	2.99	3.03	3.13	3.18	3.14
4	2.19	2.31	2.27	2.17	2.12	1.97
5	1.60	1.59	1.39	1.34	1.07	0.87
6	0.82	0.61	0.46	0.72	0.52	0.54

On the contrary, the effect was completely reversed at the later stages of loading. At greater storey deformations, bond stresses developed around the perimeter of the joint after yielding resulted in the beam longitudinal reinforcements. Due to these stresses, progressive internal cracks are formed causing the concrete to expand laterally against the shear reinforcements. Afterward, the transverse reinforcements yielded progressively. In this study, the yielding of localized transverse reinforcements started at the 2nd loading cycle and started to expand following the increment of the loading cycle, as shown in APPENDIX C (C.2). After the formation of internal cracks, the incoming compressive stress from the prestressing steel is resisted by smaller diagonal compression strut mechanisms which are developed between cracks. As the crack becomes prominent, the contribution of these small diagonal strut mechanisms is diminished and finally they reach

at a point where they can't provide any resistance. This phenomenon significantly led the PS to lose its prestress as shown in Figure 5.11 and also considerable degradation of strength occurs, as discussed in detail in the next section. This is reasonable according to A. S. Elnashai et al [8], FEMA [11], R. M. Oinam et al [42], which point out the fact that loss of strength and extensive crack formation causes a remarkable drop of prestress in the PS. But as explained in the validation part, the software's capability in capturing the response at the last cycles of the loading is questionable. Thus, the conclusions made at this stages of loading might need further investigation to obtain a more accurate result.

Table 5.5 Percentage variation of stiffness at every loading cycle about A0P0

Loading Cycle	Specimen					
	A0P0	A0P25	A0P40	A0P59	A0P70	A0P80
	Stiffness variation w.r.t A0P0 (%)					
1	0.00	+27.22	+38.26	+44.80	+50.07	+54.92
2	0.00	+19.23	+27.95	+39.82	+44.81	+48.95
3	0.00	+13.35	+15.12	+18.74	+20.68	+19.10
4	0.00	+5.27	+3.51	-0.88	-3.25	-10.20

N.B: Positive value indicates increment percentage and a negative value indicates decrement percentage about specimen A0P0

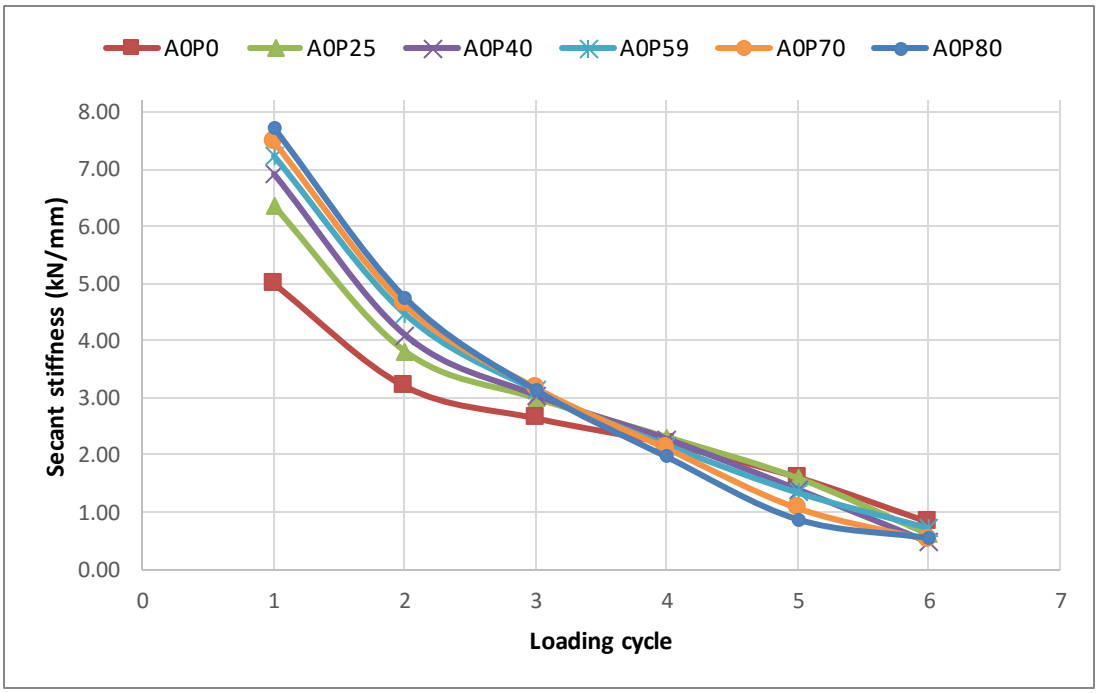

Figure 5.9 Secant stiffness of PPC exterior BCJs computed for each loading cycle

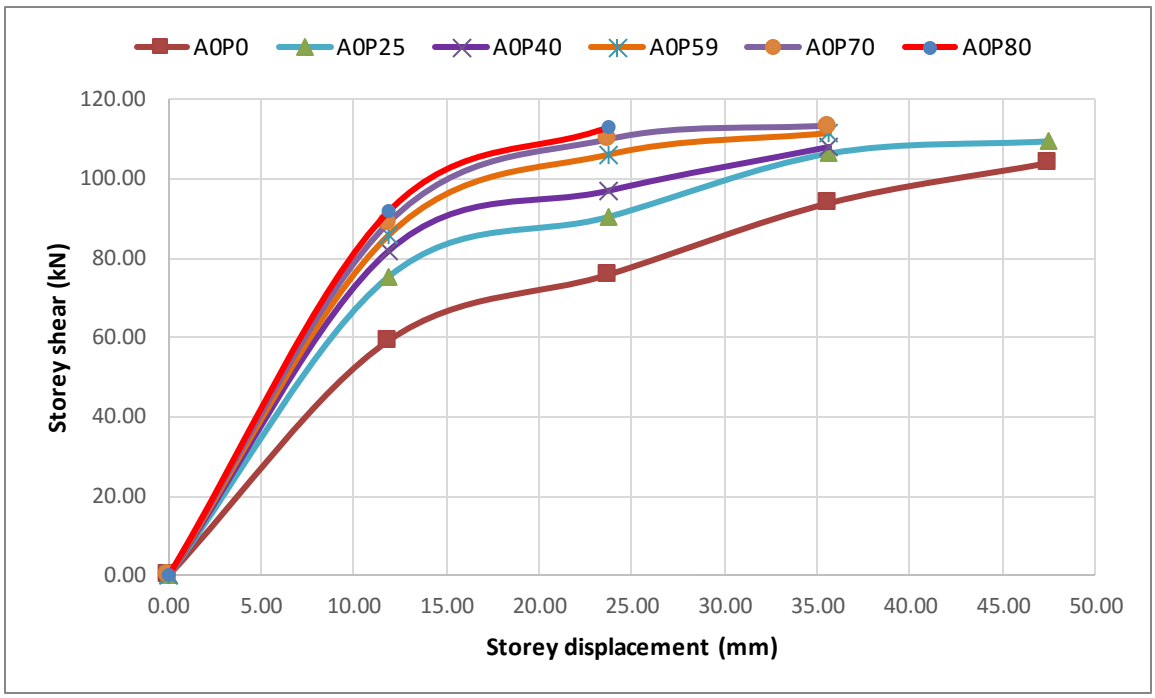

Figure 5.10 Peak storey shear values at each cycle corresponding to storey displacement up to ultimate capacity

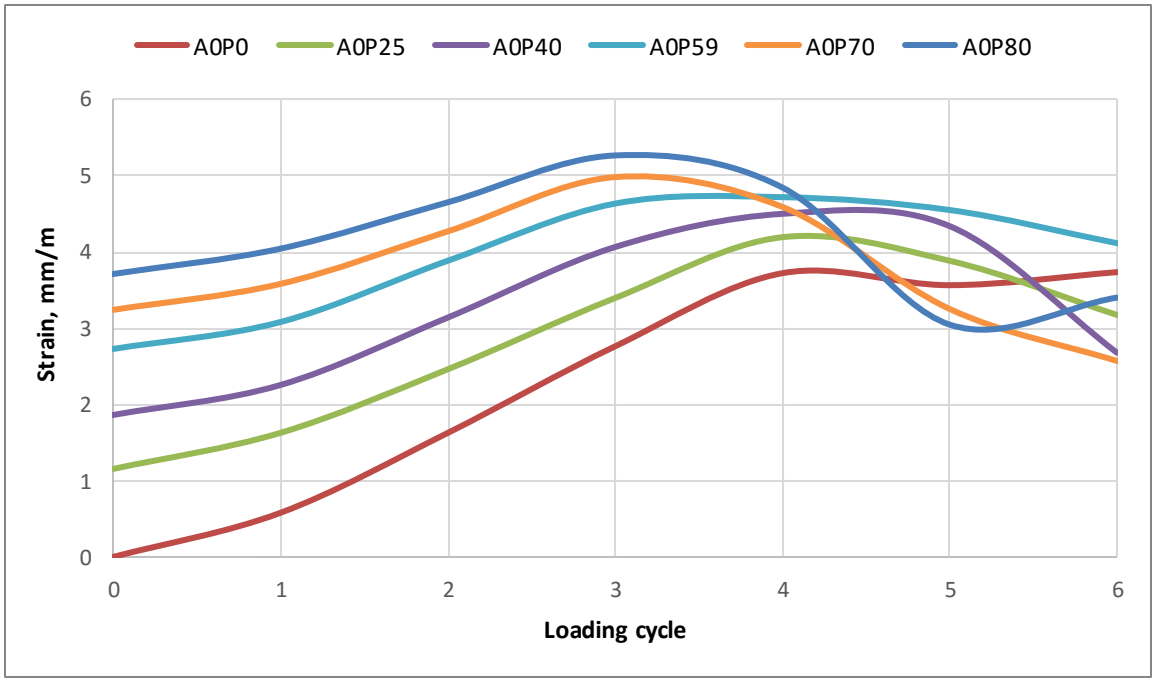

Figure 5.11 Strain distribution in the prestressing steel at the BCJ for each loading cycle

5.4.1.4 *On strength degradation after peak response*

RC structures exhibit strength degradation when subjected to lateral reversed cyclic loading. Strength degradation or deterioration is a reduction in lateral strength due to an increase in inelastic displacement, repeated cyclic displacement, concrete cracking, reinforcement yielding, and bond-slip progression between the reinforcement and the concrete.

Figure 5.12 demonstrates the effect of prestressing force on shear strength degradation of PPC exterior BCJ specimens. The figure shows the response after ultimate shear capacity since the post-peak response is the focus area for strength degradation. Strength degradation was severe in all specimens. This might be due to extensive crack development following yielding of reinforcement at the joint at higher loading cycles. At the initial cycles of loading, the longitudinal reinforcements transfer the applied lateral load on the beam to the joint core in terms of a diagonal compressive stress mechanism. The transferred load is resisted by the equilibrium of the compressive strength of concrete in the joint. At later loading stages, the contribution of the longitudinal reinforcement reduces due to permanent elongation of reinforcement in the beam by tensile yielding. In this study, the longitudinal reinforcements yielded at the beam-column joint interface at the 2nd loading cycle, as shown in APPENDIX C (C.1). Consequently, after this loading cycle, the compressive stress transfer by longitudinal reinforcements to the joint strut becomes negligible. These stresses are then transferred to the longitudinal bars and bond stress develops around the joint core. As the cycle progresses, the joints become very much exposed to high shear and bond stresses. Under high inelastic displacement, a bond has a very poor performance in terms of dissipation energy, strength, and stiffness degradation. This phenomenon led to the strength degradation of the PPC exterior BCJs.

From the analysis result, it was also observed that joints with higher prestressing forces were prone to a much higher shear strength degradation as compared to less prestressed joints. This could be the joint's weak performance in providing resistance to the compressive stress coming from the PS. At higher inelastic storey displacement, the strut mechanism of joints is destroyed and most of the resistance is provided by shear reinforcements. Thus, the incoming compressive stress from the PS couldn’t be resisted by the joint. Since the compressive stress is high for higher prestressed PSs, they employ

greater compressive force towards the cracked joint. This results in significant damage to the core concrete. Shear strength degradation is severe following a high level of damage. Thus, highly prestressed members are prone to remarkable loss of strength after significant crack development. This conclusion is reasonable according to A. E. Naaman et al [33] which states that, after extensive crack development, members with higher prestress levels are capable of losing more of their prestress than members with lower prestress levels. Therefore, more loss in prestress leads to more loss in strength.

As shown in the validation part, the software underestimated the specimen's capacity at the last 2 cycles of the loading after peak response is achieved. Thus, it is crucial to consider the software's questionable performance at larger cycles of loading, when material non-linearity is more pronounced. Thus, the conclusions made at this stage of loading might need further investigation to obtain a more accurate result.

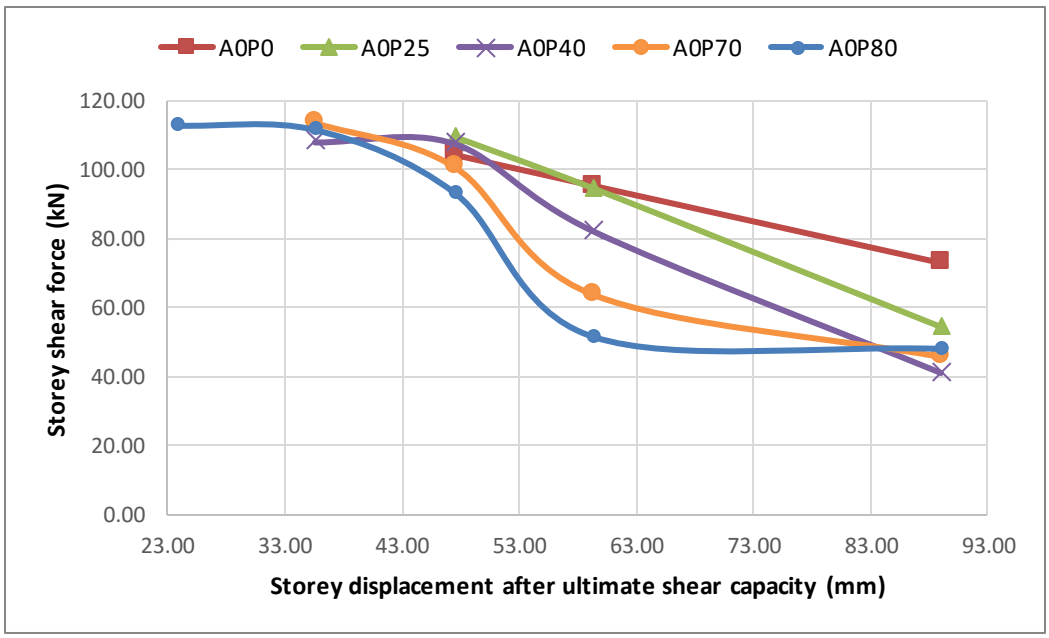

Figure 5.12 Effect of prestressing force on the shear strength degradation of PPC exterior BCJs with respect to the storey displacement

5.4.1.5 *On absorption and energy dissipation capacity*

During energy transformation to the structure, following the lateral action, some of the energy can be absorbed whilst the rest is dissipated through a different mechanism. The absorbed energy is related to the stiffness and mass of the structure, while the dissipated energy is associated with the strength and ductility of the structure. For a structure to store

a high amount of energy elastically it needs to have larger stiffness and mass. This is why reinforced concrete structures designed for an elastic response usually have large cross-sectional dimensions. As explained in detail earlier, BCJs subjected to higher prestressing force possess greater stiffness in the earlier stages of loading due to their capacity to sustain load with small deformation. This indicates their capacity to store high elastic strain energy initially before inelastic deformation of the structure takes place. Hence, PPC exterior BCJs with higher prestressing force had a good energy absorption capacity. Unlike reinforced concrete members, this response was achieved by the application of prestressing force in the member without any increment in the size of the members.

Figure 5.13 shows the effect of prestressing force on accumulated dissipated energy calculated at each loading cycle. The accumulated energy dissipation results for each specimen can also be found in Table 5.6. In earlier loading cycles, before ultimate shear capacity was achieved, energy dissipation was slightly enhanced following prestressing force increment. On the contrary, the effect was completely reversed at the later loading cycles. The reversal occurred due to sudden loss of strength and stiffness following extensive joint shear crack development at a higher prestress, as explained in detail in earlier parts. The specimen's potential to resist the lateral action by going through further damage was lost. This effect was remarkable for highly prestressed concrete joints. This also shows that; diagonal strut shear resistance mechanism stage is more advantageous for prestressed joints to sustain shear capacity without excessive degradation. But, their effectiveness in the truss shear resistance mechanism might be achieved if good bond performance exists in the specimen throughout the loading stage.

On contrary to this, M. Nishiyama [4] demonstrated and showed that prestressed joints have good performance in keeping their strength after ultimate shear capacity, which in turn led them to have good inelastic energy dissipation capacity. However, the joints in M. Nishiyama's [4] research were designed to fail in flexure before joint shear failure with plastic hinge occurring at the beam-column interface, as discussed in the literature review. Thus, the effect of prestressing force level on the remarkably cracked joints on this research was not well understood. This implies how unsafe it is for a prestressed joint to fail in shear at the joint before flexural failure at the beam.

Yet, it is essential to consider the software's questionable performance at the last stages of the loading, when material nonlinearity is more pronounced. Thus, further investigation need to be performed to have a more accurate result on the specimen's performance at the last loading stages.

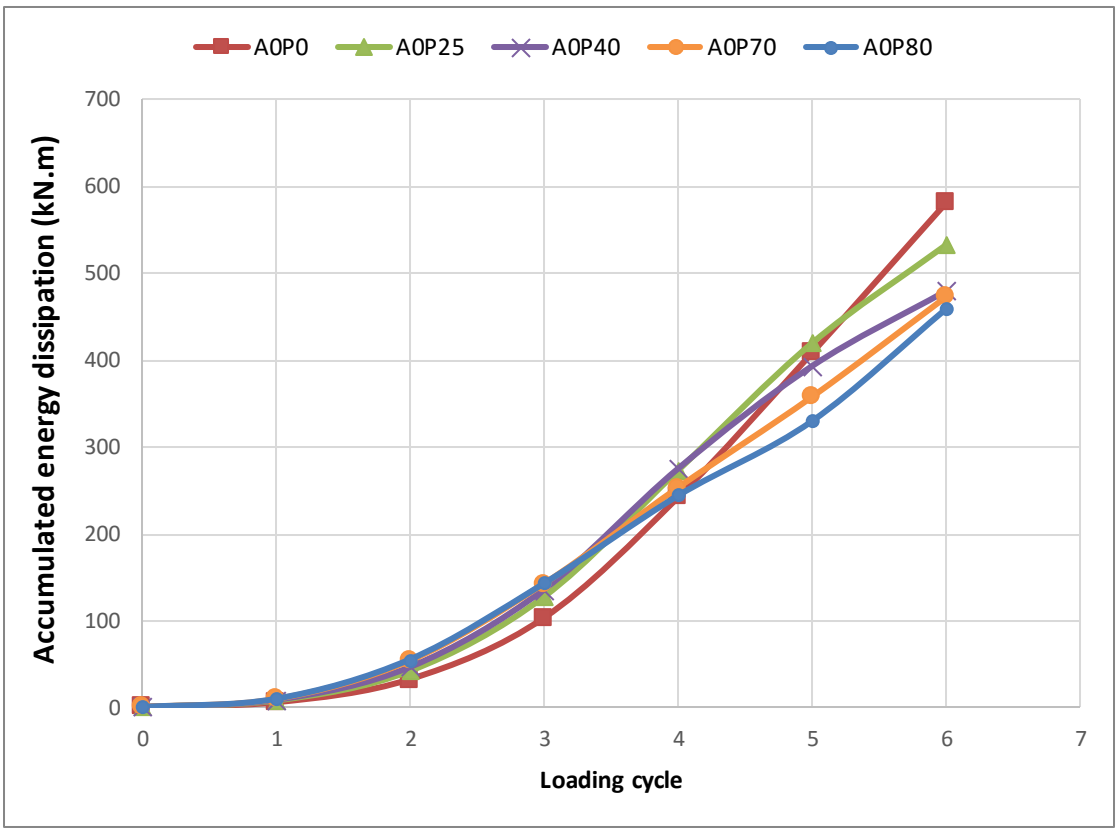

Figure 5.13 Effect of prestressing force on accumulated energy dissipation at each loading cycle

Table 5.6 Accumulated energy dissipation for PPC exterior BCJ specimens

Loading cycle	Accumulated energy dissipation (kN.m)				
	A0P0	A0P25	A0P40	A0P70	A0P80
0	0.00	0.00	0.00	0.00	0.00
1	5.45	7.42	8.14	9.18	9.51
2	32.03	41.68	46.14	53.51	55.07
3	102.86	127.41	135.54	142.13	142.89
4	241.63	273.19	274.90	252.74	244.25
5	408.22	420.27	393.14	357.30	330.34
6	581.17	533.71	479.78	472.32	459.96

5.4.2 Effect of column axial load

5.4.2.1 *On ultimate shear capacity and premature failure*

When column axial load is applied in a highly prestressed joint, the crushing of concrete in the joint core due to high compressive stress, from the axial load and prestressing force, must be considered as a potential cause of failure. It must be ensured that the combined effect of stress due to both loads is within permissible concrete stress limit to prevent premature failure. Thus, to check this effect a PPC interior BCJ specimen was analyzed at an axial load ratio of 0, 0.1, 0.4, and 0.65, as described in the parametric analysis. Four specimens with similar detailing and prestressing force ($80\%F_{yp}$) were subjected to different magnitudes of column axial load as shown in Table 5.2. According to the tabulated axial load protocol, these specimens were analyzed and the hysteresis response is shown in Figure 5.3.

Figure 5.14 clearly shows the effect of column axial load on the shear capacity of the specimens. Based on the analysis result, column axial load increment slightly enhanced the shear capacity of the BCJs. This might be due to the fact that the higher axial load is capable of confining the joint region against shear failure. Adequate confinement of joints considerably improves bond performance by preventing slippage of reinforcement bars. Provision of column axial load also widens the diagonal strut region in the joint as a result of an enlarged compression block across the column region. Due to the formation of a wider diagonal compression strut, horizontal bond forces along the longitudinal beam bars can now be disposed of more easily. The demand for transverse reinforcements is then be reduced and their contribution is required only to enable bond forces to be introduced into the joint region outside the diagonal compressive strut region.

About specimen IA0P80, an ultimate shear capacity increment of 4.15%, 6.76%, and 10.05% was obtained for specimen IA10P80, IA40P80, and IA65P80, respectively, in the positive loading direction. Furthermore, a percentage ultimate shear capacity increment of 5.10%, 8.83%, and 12.15% was obtained, respectively, in the negative loading direction. The ultimate storey shear capacity increment might be resulted due to greater joint confinement with higher column axial load application. This conclusion is also reasonable based on A. A. Mohammed et al [24], as discussed in the literature review.

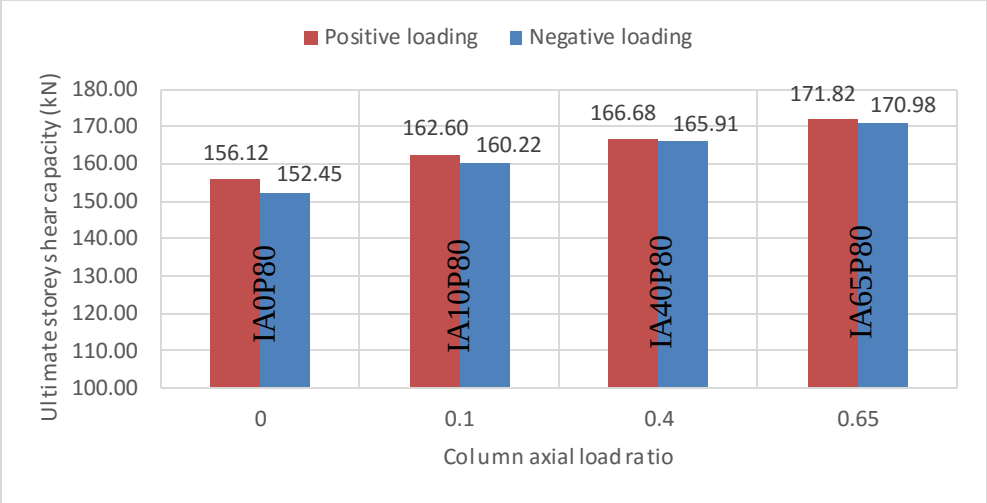

Figure 5.14 Effect of column axial loading on the ultimate shear capacity of PPC interior BCJ

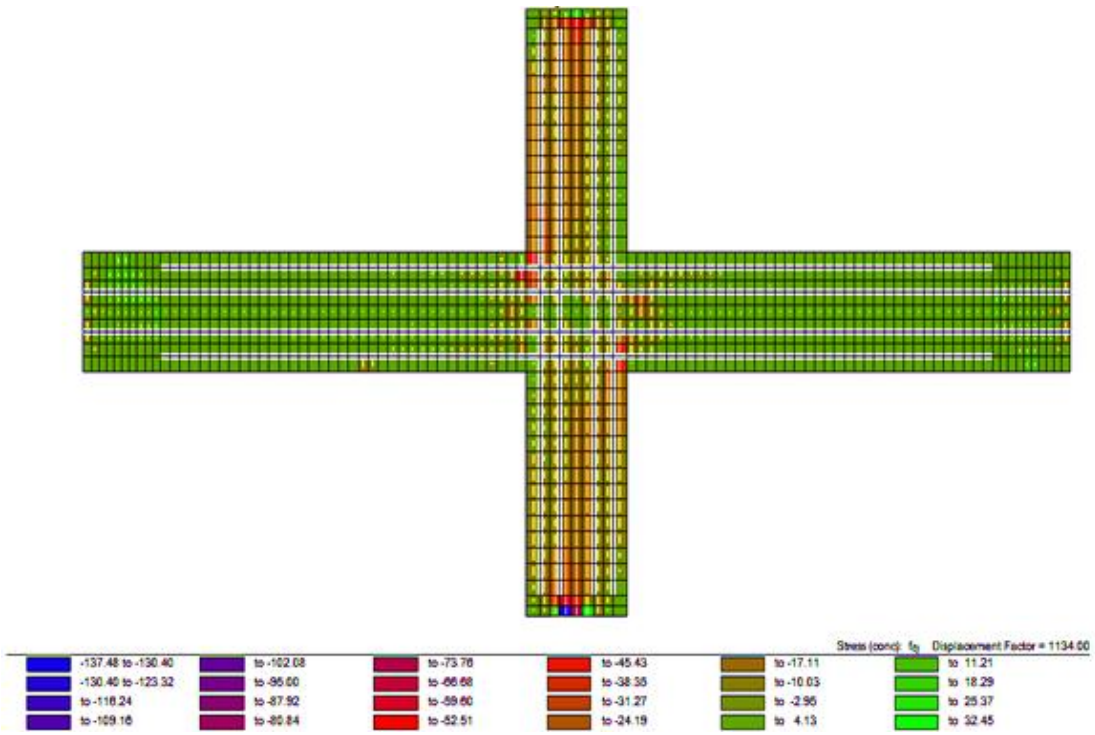

Figure 5.15 Vertical concrete stress of specimen IA65P80

Crushing of concrete in the joint core was also examined by observing concrete stresses at the joint region, as shown in Figure 5.15. In the figure, the negative and positive sign indicates the compressive and tensile stress of concrete. The average compressive stress observed in the BCJ at the final loading stage of specimen IA65P80 was 15MPa which is 56.3% of the compressive strength of the concrete (34.4MPa). Since the incoming stress

is still much less than the compressive strength, crushing of concrete is not expected to occur. Thus, the combined effect of the stated axial stresses and tendon prestress didn't cause any premature failure at the joint core. A. A. Mohammed et al [24] resembles the conclusion made in this study as discussed in the literature review.

5.4.2.2 *On pinching behavior*

In reinforced concrete structures subjected to reverse cyclic loading, a large reduction in loading stiffness after unloading might occur. In the reloading branch of a hysteresis curve, after repeated cycles, cracks that occur previously in the tension side might still be opened in addition to the one that's going to be created at the new face under tension. As a consequence, the concrete at the section will be fully cracked and the concrete will be ineffective in resisting the shear. This phenomenon cause pinching in the hysteresis curve. As the reloading increases, the cracks formed from the previous loading start to close, and partial stiffness recovery will be achieved. Pronounced pinching indicates the poor performance of energy dissipation capacity.

In the PPC interior BCJs, the column axial load largely affects the pinching behavior of the joint. As shown in Figure 5.3, specimen IA0P80, with no column axial load, experienced severe pinching. But as the column axial load increased, a moderate pinching was observed in the specimens. The column axial load confined the BCJ by applying a compressive force, which further enhanced the compressive strength of the concrete. This prevented the formation of tension cracks by improving the concrete strut mechanism in the joint as shown in Figure 5.5. The more the axial load was applied, the formation of joint crack was prevented. In specimen IA0P80 and IA10P80, as the loading cycle proceeds wider cracks started to form. During reloading, the stiffness of the specimens was lost until previously formed cracks were closed. These phenomena resulted in severe pinching. As soon as previously opened cracks start to close, the joint began recovering its stiffness. For the rest of the specimens, IA40P80 and IA65P80, since the cracks were not substantial immediate recovery of stiffness was achieved. Thus axial load largely decreases the effect of pinching by providing confinement which significantly delays the development of cracks at the joint. The less pronounced the pinching is the better the hysteresis energy dissipation capacity. These results are reasonable according to A. A. Mohammed et al [24], as discussed in the literature review.

CHAPTER 6 CONCLUSIONS AND RECOMMENDATIONS

6.1 Conclusion

In this study, PPC exterior and interior BCJ specimens were analytically investigated to study their performance under repeated reverse cyclic loading. The effect of prestressing force and column axial load were examined in the exterior and interior joints. The seismic behaviors of the exterior joint specimens were evaluated in terms of ultimate storey shear capacity; stiffness; ductility; strength degradation after peak response; energy absorption and dissipation capacity. On the other hand, the combined compressive stress effects, obtained from the column axial load and prestressing force, were examined to study premature failure of the joint core concrete in the interior joint specimen. Additionally, the pinching effect was evaluated with column axial load variation.

According to the analysis result of the exterior joint, variation of prestressing force didn't show a significant effect on the ultimate shear capacity. This was because, as cracks become extensive, following inelastic displacement, joint shear resistance was mainly provided by the truss mechanism rather than the strut mechanism. This resistance mechanism degraded the contribution of prestress in resisting shear. On the other hand, stiffness and displacement ductility of the joints increased remarkably with prestressing force level. This was due to the initially provided confinement subjected by the prestressing steels. This phenomenon favored the energy absorption and dissipation capacity of these joints at initial stages of loading. On contrary, at later stages of loading, bond stress was significant and progressive yielding of shear reinforcement resulted with remarkable crack development occurred at the joint. At this point, the cracked concrete couldn't be able to resist the incoming compressive stress from the prestressing steel. This phenomenon significantly led the PS to lose its prestress. Consequently, stiffness and strength degradation after peak response became remarkable and energy absorption and dissipation capacity degraded with prestressing force level. This implied how unsafe it is for a prestressed joint to fail in shear at the joint before flexural failure at the beam. Yet, it is important to consider the software's questionable performance at the last cycles of the loading and conclusions made at this stages need further evaluation to have a more accurate result.

In the interior joint specimens, column axial load ratio variation in a highly prestressed joint didn't result in concrete crushing at any level of the loading. Thus, all the specimens were safe against premature failure. Furthermore, a less pronounced pinching was observed with column axial load increment. This was due to the incoming compressive stress from the column axial load, which confined the joint against the shear crack. Following the smaller effect of pinching, a better hysteresis energy dissipation capacity was believed to be obtained for axially loaded joints.

6.2 Recommendation

This study is not adequate to fully understand the performance of prestressed members under repeated reverse cyclic loading. The author recommends further research on the following points:

I. Effect of transverse and longitudinal reinforcement ratio and yield strength; joint size; and other parameters that might affect the performance of PPC BCJs need to be studied along with the prestressing level.
II. Analysis needs to be performed on PPC BCJs that have good bond performance under inelastic displacement to prevent loss of prestress and evaluate the effect of prestress level on the energy absorption and dissipation capacity at the later cycles.
III. Specimens need to be modeled and analyzed with other finite element software's which are specialized in the analysis of prestressed concrete members.
IV. A 3D non-linear analysis is also preferable to 2D analysis since 2D models predicts a larger crack width therefore, their ability to capture crack propagation in the out of plane direction is undermined.
V. Dynamic analysis of partially prestressed concrete beam-column joint specimens, either experimentally or analytically, should be performed since it is more precise in simulating seismic responses of structures.
VI. An experimental investigation is important due to its accuracy in obtaining hysteretic shear response than finite element models.

REFERENCES

[1] R. W. G. Blakeley, R. Park, and R. Shepherd, "A review of the seismic resistance of prestressed concrete," in Annual conference of the New Zealand prestressed concrete institute at Wairakei, 1968, pp. 3–23.

[2] T. Paulay and M. J. N. Priestley, "Seismic Design of Reinforced Concrete and Masonry Buildings," Second edi. JOHN WILEY AND SONS, INC., 1992.

[3] R. Park and T. Paulay, "Reinforced concrete structures," First edit. JHON WILEY & SONS, INC., 1975.

[4] M. Nishiyama, "Seismic design of prestressed concrete buildings," Bull. New Zeal. Natl. Soc. Earthq. Eng., vol. 23, no. 4, pp. 288–304, 1990.

[5] T. Kashiwazaki and H. Noguchi, "Structural performances of prestressed concrete interior beam-column joints," Proc. 12th World Conf. Earthq. Eng. (12WCEE), Auckland, New Zealand, January 30-February 4, 2000, pp. 1–8, 2000.

[6] M. Nishiyama and Y. Wei, "Effect of post-tensioning steel anchorage location on seismic performance of exterior beam-to-column joints for precast, prestressed concrete members," PCI J., vol. 52, pp. 18–30, 2007.

[7] S. Eshghi and V. Zanjanizadeh, "Retrofit of slender square reinforced concrete columns with glass fiber-reinforced polymer for seismic resistance," Iran. J. Sci. Technol., vol. 32, no. B5, pp. 437–450, 2008.

[8] A. S. Elnashai and L. Di Sarno,"Fundamentals of earthquake," First Edit. JHON WILEY & SONS, INC., 2008.

[9] A. Sayed and A. Tawfik, "Effect of infill wall on the ductility and behavior of high strength reinforced concrete frames," HBRC J., vol. 10, no. 3, pp. 258–264, 2015.

[10] D. P. Clough, "Design of connections for precast prestressed concrete buildings for the effects of earthquake," Technical Report, ABAM Consulting Engineers, 1985.

[11] A. T. Council, "Effects of strength and stiffness degradation on seismic response," FEMA P440A, 2009.

[12] J. M. Robberts and V. Marshall,"Prestressed concrete design and practice," Concrete Society of Southern Africa.

[13] K. E. Williamson, "Prestressed concrete seismic design," Partn. Lewis Williamson, Consult. Eng. Auckl., pp. 251–266, 1968.

[14] Ersin Arioglu, "Earthquake response and design criteria of prestressed concrete structures," in Fourth Regional Seminar of European Association for Earthquake Engineering, " 1976, no. September 13-25.

[15] R. Ian Gilbert, N. Colin Mickleborough, and G. Ranzi,"Design of prestressed concrete to Eurocode 2," Second Edi. CRC Press Taylor & Francis Group, 2017.

[16] L. Luoman, "Further experiments on the seismic beam-column joints designed in accordance with the principles of damage avoidance," A thesis submitted in partial fulfilment of the requirements for the Degree of Master of Engineering in Civil Engineering in University of Canterbury, 2006.

[17] R. I. Gilbert and N. C. Mickleborough, "Design of prestressed concrete," Second Edi. Spon Press Taylor & Francis Group, 2005.

[18] N. Z. Standard Committee, "New Zealand Standard: Concrete Structures Standard, Commentary on the design of concrete structures," 1995.

[19] G. George and G. Gregory, "Concrete buildings in seismic regions," First Edit. CRC Press Taylor & Francis Group, 2014.

[20] J. K. Wight and J. G. MacGregor, "Reinforced concrete mechanics and design," Sixth Edit. PEARSON, 2012.

[21] J. F. Stanton and S. D. Nakaki, "PREcast seismic structural systems: Design guidelines for Precast concrete seismic structural systems," Press. Rep., vol. 3–09, no. 1, 2002.

[22] G. H. Powell, "Displacement-Based Seismic Design of Structures," First Edit., vol. 24, no. 2. IUSS Press, 2007.

[23] A. E. Naaman and J. K. Wight, "Analysis of Ductility in Partially Prestressed Concrete Flexural Members," PCI J., pp. 64–87, 1986.

[24] M. Ali, A. Osta, U. Khan, M. H. Baluch, and M. K. Rahman, "Effects of Variation of Axial Load on Seismic Performance of Shear Deficient RC Exterior BCJs," Int. J. Concr. Struct. Mater., pp. 1–20, 2018.

[25] P. S. Wong, F. J. Vecchio, and H. Trommels, "VecTor2 and formworks user's manual," Second Edi. 2013.

[26] S. Popovics, "A Numerical Approach to the Complete Stress-Strain Curve of Concrete," Cem. Concr. Res., vol. 3, no. 5, pp. 583–599, 1973.

[27] B. D. Scott, R. Park, and M. J. N. Priestley, "Stress-Strain Behavior of Concrete Confined by Overlapping Hoops at Low and High Strain Rates," ACI J., vol. 79, no. 1, pp. 13–27, 1982.

[28] M. M. Attard and S. Setunge, "Stress-Strain Relationship of Confined and Unconfined Concrete," ACI Mater. J., vol. 93, no. 5, pp. 432–441, 1996.

[29] D. Palermo and F. J. Vecchio, "Compression field modeling of reinforced concrete subjected to reversed loading," ACI Struct. J., vol. 100, no. 5, pp. 616–625, 2003.

[30] F. J. Vecchio, "Finite element modeling of concrete expansion and confinement," ASCE J., vol. 118, no. 9, pp. 2390–2406, 1993.

[31] H. Kupfer, H. K. Hilsdorf, and H. Rusch, "Behavior of concrete under biaxial

stresses," ACI J., vol. 87, no. 2, pp. 656–666, 1969.

[32] F. J. Vecchio and M. P. Collins, "The modified compression-field theory for reinforced concrete elements subjected to shear," ACI J., vol. 83, no. 2, pp. 219–231, 1986.

[33] A. E. Naaman and A. M. Hamza, "Prestress losses in partially prestressed high strength concrete beams," PCI J., pp. 98–114.

[34] M. Seckin, "Hysteretic Behaviour of Cast-in-Place Exterior Beam-Column-Slab Subassemblies," Ph.D. Thesis, Dep. Civ. Eng. Univ. Toronto, p. 266, 1981.

[35] R. P. Dhakal and K. Maekawa, "Modeling for post-yield buckling of reinforcement," ASCE J., vol. 128, no. 9, pp. 1139–1147, 2002.

[36] "CEB-FIP Model Code 90," ICE Publ., pp. 82–116.

[37] R. Eligehausen, E. P. Popov, and V. V Bertero, "Local bond stress-slip relationship of deformed bars under generalized excitations," Rep. No. UCB/EERC-83/23, Earthq. Eng. Center, Univ. California, Berkeley, 1983.

[38] E. Standard Committee, "Design of concrete structures - En 1992-1-1," 2004.

[39] E. Standard Committee, "Design of structures for earthquake resistance - EN 1998-1," 2003.

[40] A. Tsiavos and B. Stojadinović, "Constant yield displacement procedure for seismic evaluation of existing structures," Bull. Earthq. Eng., vol. 17, pp. 2137–2164, 2019.

[41] D. Mitchell and M. P. Collins, "Prestressed concrete structures," First Edit. Response Publications, Canada, 1997.

[42] R. M. Oinam, P. C. A. Kumar, and D. R. Sahoo, "Cyclic Performance of Steel Fiber-Reinforced Concrete Exterior Beam- Cyclic performance of steel fiber-reinforced concrete exterior beam-column joints," Earthq. Struct., vol. 16, no. 5, pp. 533–546, 2019.

[43] D. Dowrick, "Earthquake resistant design and risk reduction," Second Edi. Tauranga, New Zealand: JOHN WILEY AND SONS, INC., 2009.

APPENDIX A

The constitutive relationship for concrete

A.1 Popovics stress-strain relationship

$$f_{ci} = -\left(\frac{\varepsilon_{ci}}{\varepsilon_p}\right) f_p \left(\frac{n}{n-1+(\frac{\varepsilon_{ci}}{\varepsilon_p})^n}\right) \qquad for\ \varepsilon_{ci} < 0 \tag{1}$$

$$n = (\frac{E_c}{E_c - E_{sec}}) \tag{2}$$

$$E_{sec} = \frac{f_p}{/\varepsilon_p/} \tag{3}$$

Where f_p is peak concrete compressive stress, ε_p is strain corresponding to peak concrete compressive stress, n is curve fitting parameter, E_c is initial tangent stiffness and E_{sec} is secant stiffness.

A.2 Modified Park-Kent stress-strain relationship

$$f_{ci}^b = -\left[f_p + z_m f_p\left(\varepsilon_{ci} - \varepsilon_p\right)\right] < 0\ or - 0.2 f_p \qquad for\ \varepsilon_{ci} < \varepsilon_p < 0 \tag{4}$$

$$Z_m = \frac{0.5}{(\frac{3 + 0.29/f_c'/}{145/f_c'/-1000})(\frac{\varepsilon_0}{-0.002}) + (\frac{/f_{lat}/}{170})^{0.9} + \varepsilon_p} \tag{5}$$

$$f_c^i\ and\ f_{lat}\ in\ MPa$$

$$f_{lat} = f_{c1} + f_{c2} + f_{c3} - f_{ci} \leq 0 \qquad i = 1\ or\ 2 \tag{6}$$

Where f_{ci} is principal stress which acts transversally to the considered direction, f_c' is the concrete cylinder uniaxial compressive strength and ε_0 is concrete compressive strain corresponding to f_c'.

A.3 Hognestad (parabola) stress – strain relationship

$$f_{ci} = -f_p\{2(\frac{\varepsilon_{ci}}{\varepsilon_p}) - (\frac{\varepsilon_{ci}}{\varepsilon_p})^2\} < 0 \qquad for\ \varepsilon_{ci} < 0 \tag{7}$$

$$E_c = \frac{2f_p}{/\varepsilon_p/} \tag{8}$$

Where f_p is peak concrete compressive stress, ε_p is strain corresponding to peak concrete compressive stress and E_c is initial tangent stiffness.

A.4 Attard & Setunge stress-strain relationship

Stress-strain relationships in this model are computed at 3 points: peak, inflection point i and inflection point $2i$ as shown in Figure 4.5.

- **Confined peak stress (f_0)**

$$\frac{f_0}{f_c} = (\frac{f_r}{f_t} + 1)^k$$

$$k = 1.25\left[1 + 0.062\frac{f_r}{f_c}\right](f_c)^{-0.21} \qquad MPa$$

- **Strain at confined peak stress (ε_0)**

$$\frac{\varepsilon_0}{\varepsilon_c} = 1 + (17 - 0.06f_c)\left(\frac{f_r}{f_c}\right) \qquad MPa$$

- **Stress at point of inflection (f_i)**

$$\frac{f_i}{f_o} = \frac{\left(\frac{f_{ic}}{f_c} - 1\right)}{5.06(\frac{f_r}{f_c})^{0.57} + 1} + 1$$

- **Strain at point of inflection (ε_i)**

$$\frac{\varepsilon_i}{\varepsilon_o} = \frac{\left(\frac{\varepsilon_{ic}}{\varepsilon_c} - 2\right)}{5.06\left(\frac{f_r}{f_c}\right)^{0.57} + 1} + 2$$

- **Stress corresponding to strain of $\varepsilon_{2i} = 2\varepsilon_i$ - ε_o**

$$\frac{f_{2i}}{f_o} = \frac{\left(\frac{f_{2ic}}{f_c} - 1\right)}{6.35\left(\frac{f_r}{f_c}\right)^{0.62} + 1} + 1$$

Where f_0 is peak stress; f_c is uniaxial compressive stress of concrete; f_r is the confining pressure; f_t is the tensile strength of concrete, k is a parameter that reflects the effectiveness of confinement, ε_0 is strain at peak stress and ε_c is strain at uniaxial compressive stress of concrete.

APPENDIX B

The constitutive relationship for ductile steel reinforcement

$$f_s = \begin{cases} E_s \varepsilon_s & \text{for } \varepsilon_s \leq \varepsilon_y \\ f_y & \text{for } \varepsilon_y < \varepsilon_s \leq \varepsilon_{sh} \\ f_u + (f_y - f_u)\left(\frac{\varepsilon_u - \varepsilon_s}{\varepsilon_u - \varepsilon_{sh}}\right)^p & \text{for } \varepsilon_{sh} < \varepsilon_s \leq \varepsilon_u \\ 0 & \text{for } \varepsilon_u < \varepsilon_s \end{cases}$$

Where ε_s is reinforcement strain, ε_{sh} is strain hardening, ε_y is yield strain, ε_u is the ultimate strain, f_y yield strength, f_u is ultimate strength, E_s is elastic modulus and P is a parameter for strain hardening.

APPENDIX C

C.1 Longitudinal reinforcement stress distribution measured at the partially prestressed concrete exterior beam-column interface

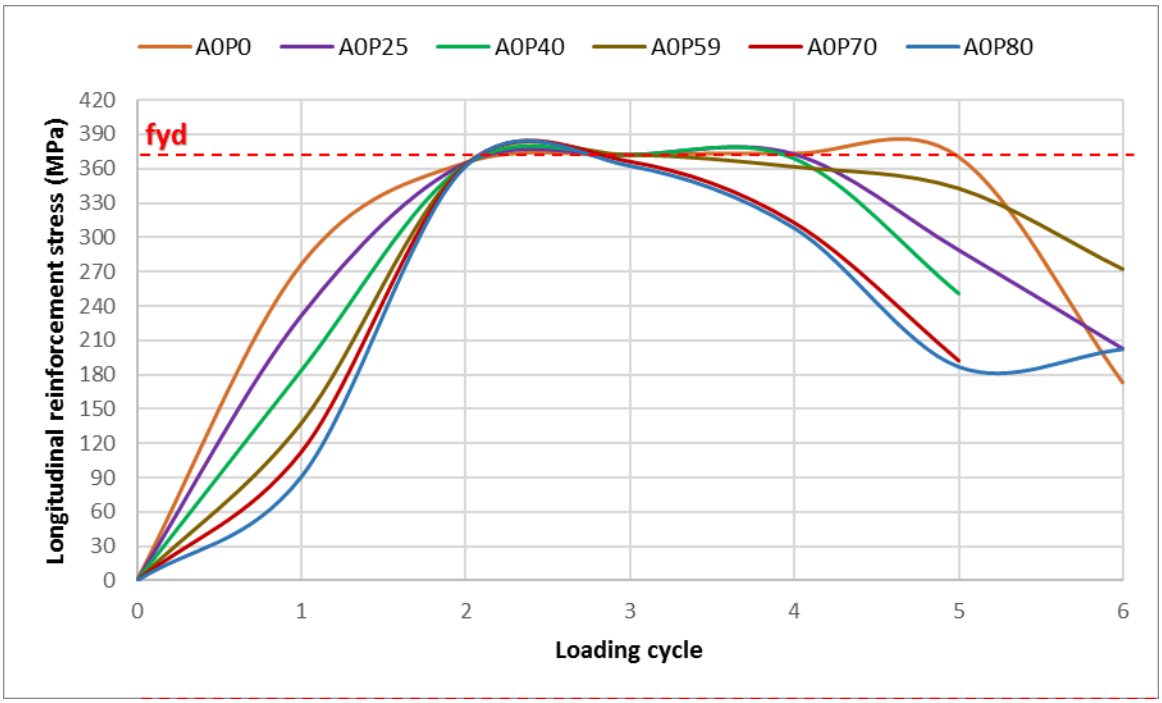

C.2 Distribution of transverse reinforcement yielding along with loading cycle at the partially prestressed concrete exterior beam-column joint

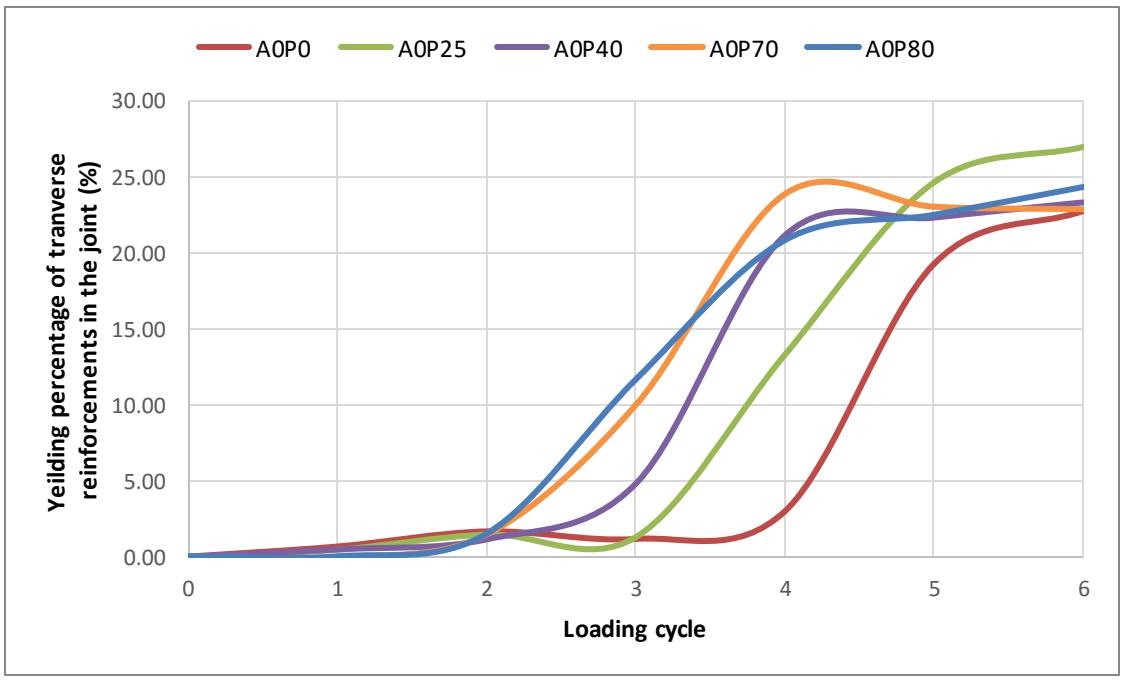

APPENDIX D

D.1 Shear strain distribution of concrete at the partially prestressed concrete exterior beam-column joint specimens at final storey displacement (positive and negative sign indicates compressive and tensile shear strain)

Specimen A0P0 Concrete shear strain $(\gamma_{xy}), 10^{-3}$

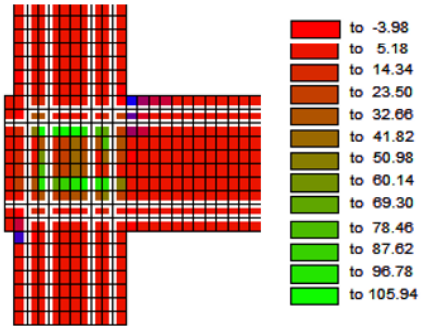

Specimen A0P25 Concrete shear strain $(\gamma_{xy}), 10^{-3}$

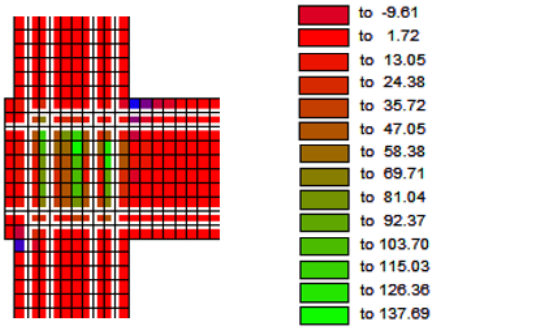

Specimen A0P40 Concrete shear strain $(\gamma_{xy}), 10^{-3}$

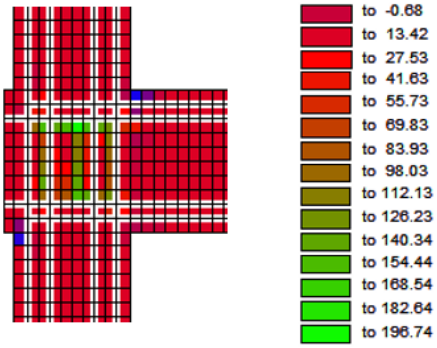

Specimen A0P59 Concrete shear strain $(\gamma_{xy}), 10^{-3}$

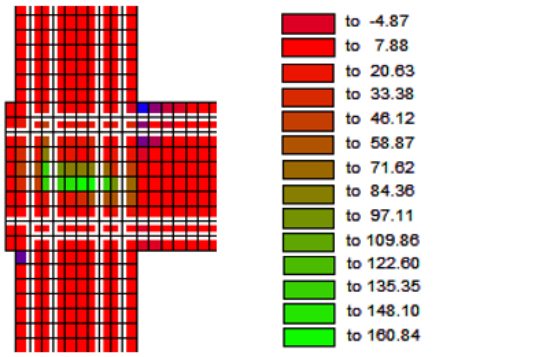

Specimen A0P70 Concrete shear strain $(\gamma_{xy}), 10^{-3}$

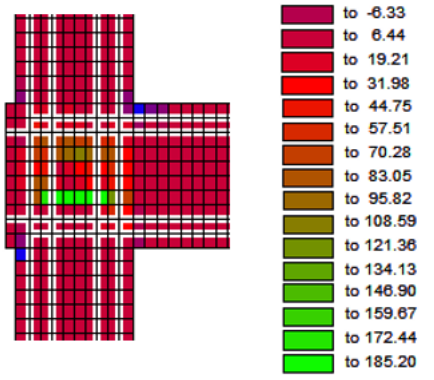

Specimen A0P80 Concrete shear strain $(\gamma_{xy}), 10^{-3}$

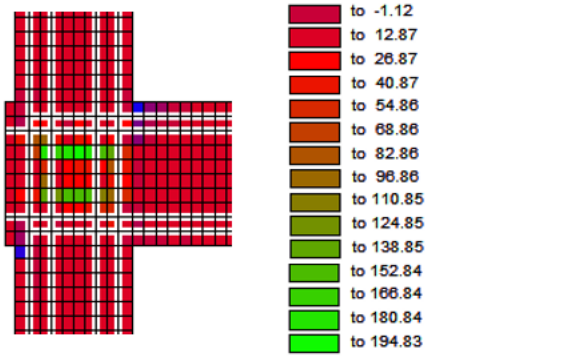

D.2 Failure crack pattern at final storey displacement of the partially prestressed concrete exterior beam-column joint specimens